

Nanotechnologies and Chemical Tools for Cell Biology

by

Xing Chen

B.S. (Tsinghua University) 2002

A dissertation submitted in partial satisfaction of the

requirements for the degree of

Doctor of Philosophy

in

Chemistry

in the

Graduate Division

of the

University of California, Berkeley

Committee in charge:

Professor Carolyn R. Bertozzi, Co-Chair

Professor Alexander K. Zettl, Co-Chair

Professor Peidong Yang

Professor Steven G. Louie

Fall 2007

The dissertation of Xing Chen is approved:

Co-Chair: Cy Bji Date 11/19/07

Co-Chair: Ray Witt Date 11/26/07

Steven G. Jovic Date 11/21/07

Jovic Date 11/21/07

University of California, Berkeley

Fall, 2007

Nanotechnologies and Chemical Tools for Cell Biology

© 2007

by Xing Chen

Abstract

Nanotechnologies and Chemical Tools for Cell Biology

by

Xing Chen

Doctor of Philosophy in Chemistry

University of California, Berkeley

Professor Carolyn R. Bertozzi, Co-Chair

Professor Alexander K. Zettl, Co-Chair

New technologies have historically facilitated the study of cell biology. The ability to probe cell functions with nanoscale precision and understand cellular processes at a molecular level is currently the key challenge in the field. The fields of nanoscience and chemical biology have added a whole new array of tools to the arsenal of cell biologists. This dissertation describes several nanotechnologies and chemical tools that I have developed to probe living cells.

Chapter one gives a brief overview on the current status of biomedical and biotechnological applications of carbon nanotubes (CNTs). CNTs are one-dimensional molecular wires with unique structural, electrical, and mechanical properties. One of the most exciting applications of CNTs is in the exploration of biological systems. In this chapter, strategies for functionalization of CNTs with emphasis on biological applications are reviewed. Representative developments in biosensing, bioimaging, intracellular

delivery, and tissue engineering are presented. Recent studies on toxicity of CNTs are also discussed.

Chapter two describes the development of a nanoscale cell injector for delivery of cargo to the interior of living cells without physiological harm. Technologies for introducing molecules into living cells are vital for probing the physical properties and biochemical interactions that govern the cell's behavior. The nanoinjector used CNTs to deliver cargo into cells. A CNT attached to an atomic force microscope tip was functionalized with cargo via a disulfide linker. Penetration of cell membranes with this "nanoneedle", followed by reductive cleavage of the disulfide bonds within the cell's interior, resulted in the release of cargo inside the cells. The capability of the nanoinjector was demonstrated by injection of protein-coated quantum dots into live human cells. Single-particle tracking was employed to characterize the diffusion dynamics of injected quantum dots in the cytosol. This new technique causes no discernible membrane or cell damage, and can deliver a discrete number of molecules to the cell's interior without the requirement of a carrier solvent.

Chapter three presents a biomimetic functionalization strategy for interfacing CNTs with biological systems. The potential biological applications of CNTs have been limited by their insolubility in aqueous environment and their intrinsic toxicity. We developed a biomimetic surface modification of CNTs using glycosylated polymers designed to mimic natural cell surface mucin glycoproteins. The polymers were end-functionalized with lipid tails for self-assembly on the CNT surface through hydrophobic

interactions. Mucin mimic-coated CNTs were soluble in water, resisted non-specific protein binding and bound specifically to biomolecules via receptor-ligand interactions. The functionalized CNTs were then bound to cell surfaces via specific carbohydrate receptors. Whereas unmodified CNTs induced cell death, the functionalized CNTs were found to be nontoxic. This strategy for biomimetic surface engineering provides a means to bridge nanomaterials and biological systems.

Chapter four further extends the biomimetic strategy for functionalization of CNTs to glycosylated dendrimers. Dendrimers are synthetic macromolecules with well-defined size and molecular structure. We developed a new class of amphiphilic bifunctional glycodendrimers that comprised carbohydrate units displayed in the periphery and a pyrene tail that bound to SWNT surface via π - π interactions. Mimicking the branched structure of cell-surface glycans, the dendrimer scaffold extended the pendent glycans well above the nanotube surface. The glycodendrimer-coated CNTs were soluble in water, and noncytotoxic. We also demonstrated that the coated CNTs could interface with biological systems including proteins and cells.

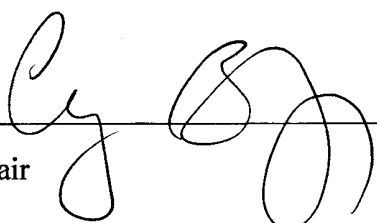
Chapter five presents a biosensing application of glycodendrimer-coated CNTs. The conductivity of CNTs is sensitive to their surrounding environment. We employed single-walled carbon nanotube network field-effect transistor (SWNTN-FET) devices to investigate glycan-lectin interactions. The SWNTs in SWNTN-FETs were first coated with glycodendrimers using the method described in the previous chapter. SWNTN-FETs coated with glycodendrimers were shown to specifically recognize target lectins.

This label-free electronic detection using SWNTN-FETs might be further explored for sensing of bacteria and viruses.

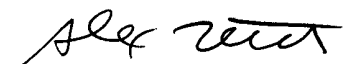
Chapter six describes the cytotoxicity studies of boron nitride nanotubes (BNNTs) and their biological applications. The inherent cytotoxicity of CNTs has imposed severe limitations on their use in living systems and therapeutic composites. The cytotoxicity of CNTs can be reduced by biocompatible surface functionalization, but the possibility of *in situ* desorption brings considerable risk to their use in living organisms. Here we report that boron nitride nanotubes (BNNTs), isosteres of CNTs with unique physical properties, are inherently noncytotoxic. Furthermore, BNNTs can be surface functionalized with biological epitopes that mediate protein and cell binding. Finally, we show that BNNTs can deliver DNA oligomers to the interior of cells with no apparent toxicity. This work suggests that BNNTs may be superior to CNTs as biological probes and nanomedicines.

Chapter seven presents a metabolic oligosaccharide engineering approach towards boron neutron capture therapy (BNCT). Selective targeting of boron-containing reagents to tumors is one of the key components of BNCT. Many tumor-associated carbohydrate antigens possess the monosaccharide sialic acid, and indeed, the overexpression of sialic acid has been correlated with many different types of cancers. Here we present a strategy for the selective delivery of BNCT reagents to tumor cells that exploits intrinsic differences in sialic acid expression. The approach capitalizes on the unnatural substrate tolerance of the enzymes in the sialoside biosynthetic pathway, which allows the

metabolic conversion of boron containing unnatural sialic acid into the corresponding sialosides in cells. A sialic acid analog containing carborane, a common moiety of BNCT agents, was synthesized and shown to be metabolically incorporated into cell surface glycoconjugates. This approach might find further applications in BNCT.



Co-Chair



Co-Chair

The dissertation is dedicated to my family for their enduring love and support.

Nanotechnologies and Chemical Tools for Cell Biology

Table of Contents

Chapter 1. Fuctionalization of carbon nanotubes for biological applications

Introduction.....	1
Fuctionalization of carbon nanotubes.....	4
Covalent functionalization.....	5
Non-covalent functionalization.....	7
Biological applications.....	10
Biosensing.....	10
Bioimaging.....	14
Intracellular delivery.....	14
Tissue engineering.....	20
Toxicity.....	21
<i>In vitro</i> toxicity.....	21
<i>In vivo</i> toxicity.....	23
Pharmacokinetics.....	25
Conclusions and outlooks.....	26
References.....	27

Chapter 2. A cell nanoinjector based on carbon nanotubes

Introduction.....	45
Results and discussion.....	46
Design and construction of a cell nanoinjector.....	46
Nanoinjection of quantum dots into HeLa cells.....	50
Cell viability after nanoinjection.....	56
Diffusion dynamics of injected quantum dots in the cytosol.....	60
Conclusions.....	61
Materials and methods.....	62
References.....	70

Chapter 3. Biomimetic functionalization of carbon nanotubes using cell surface mucin mimics

Introduction.....	72
Results and discussion.....	73
Design and synthesis of mucin mimic polymers.....	73
Coating CNTs with mucin mimic polymers.....	77
Specific binding of proteins to mucin mimic-coated CNTs.....	80
Interfacing mucin mimic-coated CNTs with living cells.....	83
Cytotoxicity studies of mucin mimic-coated CNTs.....	87
Conclusions.....	88

Materials and methods.....	89
References.....	99

Chapter 4. Development of glycosylated dendrimers for biomimetic functionalization of carbon nanotubes

Introduction.....	103
Results and discussion.....	107
Design and synthesis of glycosylated dendrimers.....	107
Functionalization of CNTs with glycosylated dendrimers.....	107
Specific binding of proteins to glycodendrimer-coated CNTs.....	110
Interfacing glycodendrimer-coated CNTs with living cells.....	113
Cytotoxicity studies of glycodendrimer-coated CNTs.....	115
Conclusions.....	117
Materials and methods.....	117
References.....	126

Chapter 5. Label-free detection of glycan-lectin interactions using carbon nanotube network field-effect transistors

Introduction.....	129
Results and discussion.....	132
Functionalization of SWNTN-FETs with glycodendrimers.....	132
Lectin detection on SWNTN-FETs.....	135

Conclusions.....	137
Materials and methods.....	137
References.....	140

Chapter 6. Boron nitride nanotubes are noncytotoxic and can be functionalized for interaction with proteins and cells

Introduction.....	142
Results and discussion.....	143
Synthesis of BNNTs.....	143
Cytotoxicity studies of BNNTs.....	145
Biomimetic functionalization of BNNTs with glycodendrimer.....	148
BNNTs as molecular transporters.....	157
Conclusions.....	159
Materials and methods.....	159
References.....	164

Chapter 7. A metabolic oligosaccharide engineering approach towards boron neutron capture therapy

Introduction.....	166
Results and discussion.....	167
Design and synthesis of carboranyl sialic acid.....	167

Evaluation of coboranyl sialic acid analogs in cells.....	171
Conclusions.....	175
Materials and methods.....	175
References.....	178

List of Figures

Figure 1.1.	A carbon nanotubes can be thought of as a sheet of graphite rolled into a cylinder.....	2
Figure 1.2.	Transmission electron microscopy images of SWNTs and MWNTs.....	3
Figure 1.3.	Two types of device architectures of field effect transistors with carbon nanotube conducting channels.....	12
Figure 1.4.	Functionalized CNTs were able to cross the cell membrane and deliver cargo into the cytoplasm or nucleus of fibroblasts.....	15
Figure 1.5.	Schematic of the nanoinjector.....	19
Figure 2.1.	Schematic of the nanoinjection procedure.....	46
Figure 2.2.	SEM and TEM images of a MWNT-AFM tip.....	47
Figure 2.3.	Functionalization of MWNT-AFM tips.....	49
Figure 2.4.	Control experiment: MWNT-AFM tips were incubated directly with QDot [®] Streptavidin without prior coating with linker 1	51
Figure 2.5.	Nanoinjection of QDot [®] Streptavidin conjugates into a target HeLa cell.....	53
Figure 2.6.	Functionalization of MWNT-AFM tips with QDot [®] Streptavidin conjugates via linker 2	54
Figure 2.7.	Control experiments: QDot [®] Streptavidin conjugates were loaded onto the MWNTs using linker 2	55
Figure 2.8.	Calcein AM assay.....	58

Figure 2.9.	Annexin V-FITC/PI assay for apoptosis.....	59
Figure 2.10.	Tracking the movement of a quantum dot cluster in the cytosol.....	61
Figure 3.1.	The structural features of native mucin and mucin mimic, and the synthesis of C ₁₈ - α -MM.....	75
Figure 3.2.	The model for the self-assembly of C ₁₈ -MMs on the surface of CNTs and the photographs of vials containing mucin mimic-coated CNT solutions.....	76
Figure 3.3.	AFM, SEM and TEM images of C ₁₈ - α -MM-SWNTs.....	79
Figure 3.4.	Specific binding of HPA to C ₁₈ - α -MM-coated nanotubes.....	82
Figure 3.5.	Schematic of interfacing CNTs on cell surfaces via carbohydrate-receptor binding.....	84
Figure 3.6.	Binding of C ₁₈ - α -MM-coated CNTs to Chinese hamster ovary (CHO) cells via HPA crosslinks.....	85
Figure 3.7.	The structures of C ₁₈ - α -MM/TR and C ₁₈ - β -MM/TR and the flow cytometry analysis of cells in pathway II of Figure 3.5.....	86
Figure 3.8.	Effects of glycopolymer-coated and unmodified CNTs on the growth of CHO cells.....	88
Figure 4.1.	Photographs of vials containing SWNT suspensions, and SEM and TEM images of G3Man-SWNTs.....	109
Figure 4.2.	Lectin binding to glycodendrimer-coated SWNTs.....	111

Figure 4.3.	Modulation of lectin bindings to SWNTs co-functionalized with two different glycodendrimers.....	112
Figure 4.4.	Interfacing glycodendrimer-coated SWNTs with live cells.....	114
Figure 4.5.	Effects of glycodendrimer-coated SWNTs on the proliferation of HEK 293 cells.....	116
Figure 5.1.	Schematic representation of the detection of lectins via SWNTN-FETs functionalized with glycodendrimers, and the structure of glycodendrimer.....	131
Figure 5.2.	Scanning electron microscopy image of the SWNTN-FET devices.....	132
Figure 5.3.	The <i>G-V_g</i> curves of SWNTN-FETs.....	134
Figure 6.1.	Structural characterization of pristine multiwalled BNNTs with high purity and high quality.....	144
Figure 6.2.	BNNTs do not inhibit cell proliferation.....	146
Figure 6.3.	BNNTs have no effect on cell viability.....	147
Figure 6.4.	The Structure of G2Man.....	149
Figure 6.5.	Photographs of vials containing BNNT suspensions.....	151
Figure 6.6.	The TEM image of G2Man-BNNTs.....	152
Figure 6.7.	Specific binding of ConA to G2Man-BNNTs.....	154
Figure 6.8.	Cell surface binding of G2Man-BNNTs.....	156
Figure 6.9.	Intracellular delivery of ssDNA using BNNTs as transporters.....	159

Figure 7.1.	Metabolism of Ac ₄ ManNAz was inhibited with compound 5 and natural sialic acid.....	174
Figure 7.2.	Metabolism of Ac ₄ ManNAz was inhibited with compound 6 with 20 fold higher efficiency than its unprotected counterpart.....	175

List of Schemes

Scheme 1.1.	General strategy for carboxylic acid derivatization of CNTs.....	6
Scheme 1.2.	General approach to non-covalent functionalization of CNTs.....	8
Scheme 2.1.	Synthesis of the linkers.....	66
Scheme 4.1.	Synthesis of generation 3 glycodendrimers.....	105
Scheme 4.2.	Synthesis of generation 2 glycodendrimers.....	106
Scheme 7.1.	Unnatural ManNAc and sialic acid can be metabolized by cell into cell surface sialosides.....	168
Scheme 7.2.	Synthesis of 9-carboranyl-NeuAc and its protected derivative.....	170

List of Tables

Table 2.1.	Trypan blue test of cells after nanoinjecton.....	57
-------------------	---	----

Acknowledgements

It is no doubt that having an excellent advisor is the most important thing for graduate school. I am more than lucky to have two! My utmost gratitude goes to my advisors, Professor Carolyn Bertozzi and Professor Alex Zettl, for their wonderful mentorship and friendship. Being a joint student between two totally different research groups, both scientifically and culturally, has been enormously challenging, enjoyable, and rewarding. The resources in their labs are second to none, and the way they conduct research has greatly expanded my vision of science. Carolyn and Alex are also amazing role models. Carolyn is always energetic and passionate about science. I still remember the excitement she showed for the collaborative research in our first meeting. Her enthusiasm influences me greatly when I pursue my own interests and projects. Alex has been a patient mentor and a superior teacher. He is always supportive, giving me freedom to explore my own interests while providing guidance throughout all challenges. His expertise in physics combined with his strong interest in chemistry and biology is truly exceptional. I learned a lot from him in our discussions. I am proud of the scientist I have become from my graduate study at Berkeley with Carolyn and Alex.

I am definitely thankful to all members (present and past) in the Bertozzi and Zettl groups. It is fortunate to be surrounded with colleagues and friends who are always willing to help. Particularly, I would like to thank Margot Paulick for teaching me how to make my first molecule. Jie Song was a great help in getting me oriented and started within Bertozzi group, especially at LBNL. Goo Soo Lee and David Rabuka were

wonderful collaborators on the mucin mimic project. I thank Jennifer Czlapinski for her help with fluorescent microscopy. I appreciate the advice and friendship from Seung-Wuk Lee. Peng Wu has been an amazing collaborator and a true friend. He has also been a continuous source of scientific advice, especially on organic synthesis. Zev Gartner is an expert in DNA and helped me on DNA wrapping of nanotubes. I give my warmest thank to William Mickelson for all his kind help. He helped me get orientated in Zettl group, helped me with TEM experiments, and even helped me pass my driving test. Chih-Wei Chang has helped me a lot on basic physics concepts and experiments. Weiqiang Han was able to synthesize all kinds of nanotubes I asked for. I thank Andras Kis whose AFM expertise is an essential for the nanoinjector project. Brian Kessler has fabricated the FET devices for our biosensor project. I thank Micheal Rousseas and David Okawa for making boron nitride nanotubes.

My special thanks go to Professor Peidong Yang, for his constant help and guidance throughout the development of this dissertation. I met Peidong in Beijing before coming to Berkeley. Since then, he has given me continuous support in my transition to the U.S., my graduate study at Berkeley, and my applications to postdoctoral fellowship.

I am also grateful to Professor Steve Louie for reading my dissertation on short notice. I thank Professor Carlos Bustamante for the help on nanoinjector project and the insightful discussions on biophysics. I thank Professor Matt Francis and Professor Jay Groves for the helpful discussions in NSET meetings.

I also thank several talented undergraduate students. Shaunt Oungoulian helped

with aligning carbon nanotubes on metal foil. I owe a special acknowledgement to Un Chong Tam, the most smart and hard-working undergraduate student who made a significant contribution to the research in this dissertation. The talent that Gautam Rangan has for scientific animation has made the publications and presentations more beautiful.

I want to acknowledge my undergraduate research advisor, Professor Yadong Li. I really appreciate the opportunity to work in his lab when I was a sophomore. Yadong was the one who made me, for the first time, think about what science really is and what a scientist should be like. He not only taught me how to run experiments but also helped me develop communication skills. Without him, my achievements would not be possible.

I appreciate the time and effort of Xiaoting Huang for proofreading my dissertation. I thank all of my friends, for phone calls, emails, and occasional gatherings. Their caring support helped me survive all the difficulties in this process.

Finally, and most importantly, I thank my grandma, parents, brothers, and sister, for their unfaltering faith and unconditional love. My achievements have been and will always be in debt to them. I dedicate this dissertation to my family. May their lives be full of joy.

Chapter 1: Fuctionalization of carbon nanotubes for biological applications

Introduction

Carbon nanotubes (CNTs) are a key ingredient in the field of nanoscience and nanotechnology because of their remarkable structural, electrical, and mechanical properties (1). As one of the forms of pure carbon, a CNT can be conceptually viewed as a sheet of graphite rolled into a perfectly seamless tube with nanometer diameter (Fig. 1.1). There are two types of CNTs: single-walled carbon nanotubes (SWNTs) that are comprised of a single graphene sheet and multi-walled carbon naotubes (MWNTs) that are comprised of multiple concentric cylindrical sheets of graphite (Fig 1.2). Since the discovery of CNTs (2, 3), hundreds of research groups from diverse scientific disciplines have joined the field, leading to numerous advances in the synthesis, physical property characterization, and applications of this amazing nanomaterial (4). CNTs have been considered for various technological applications including nanoelectronics, chemical sensors, field emission devices, and nanocomposites. These advances have been previously reviewed (4).

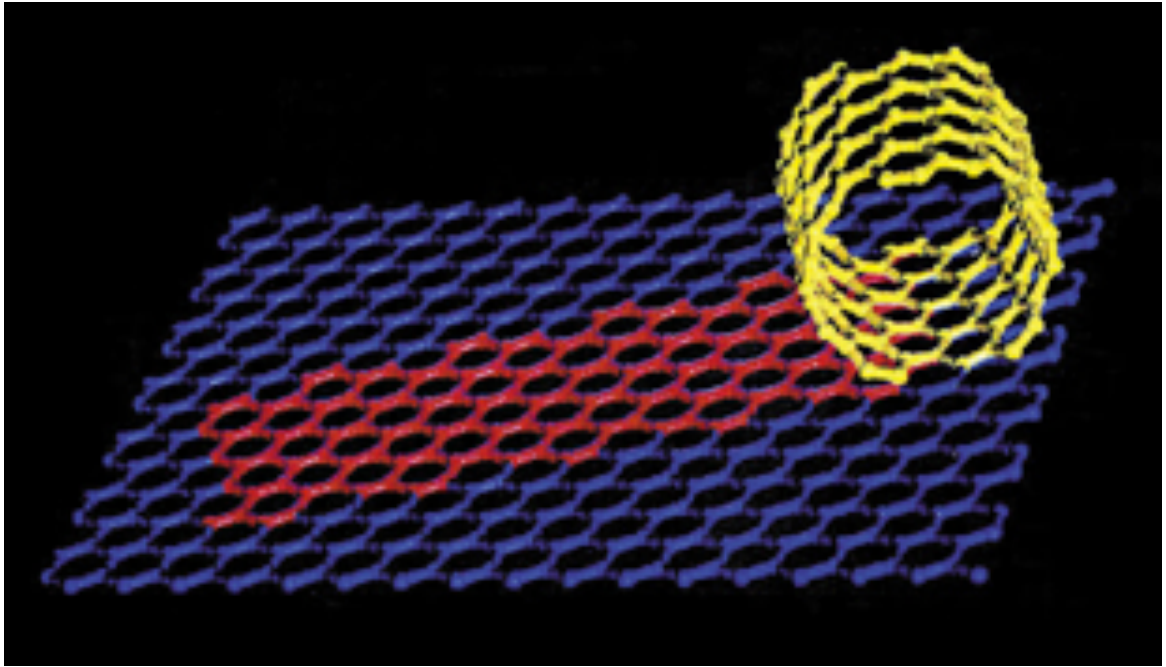


Figure 1.1. A carbon nanotube can be thought of as a sheet of graphite (a hexagonal lattice of carbon) rolled into a cylinder.

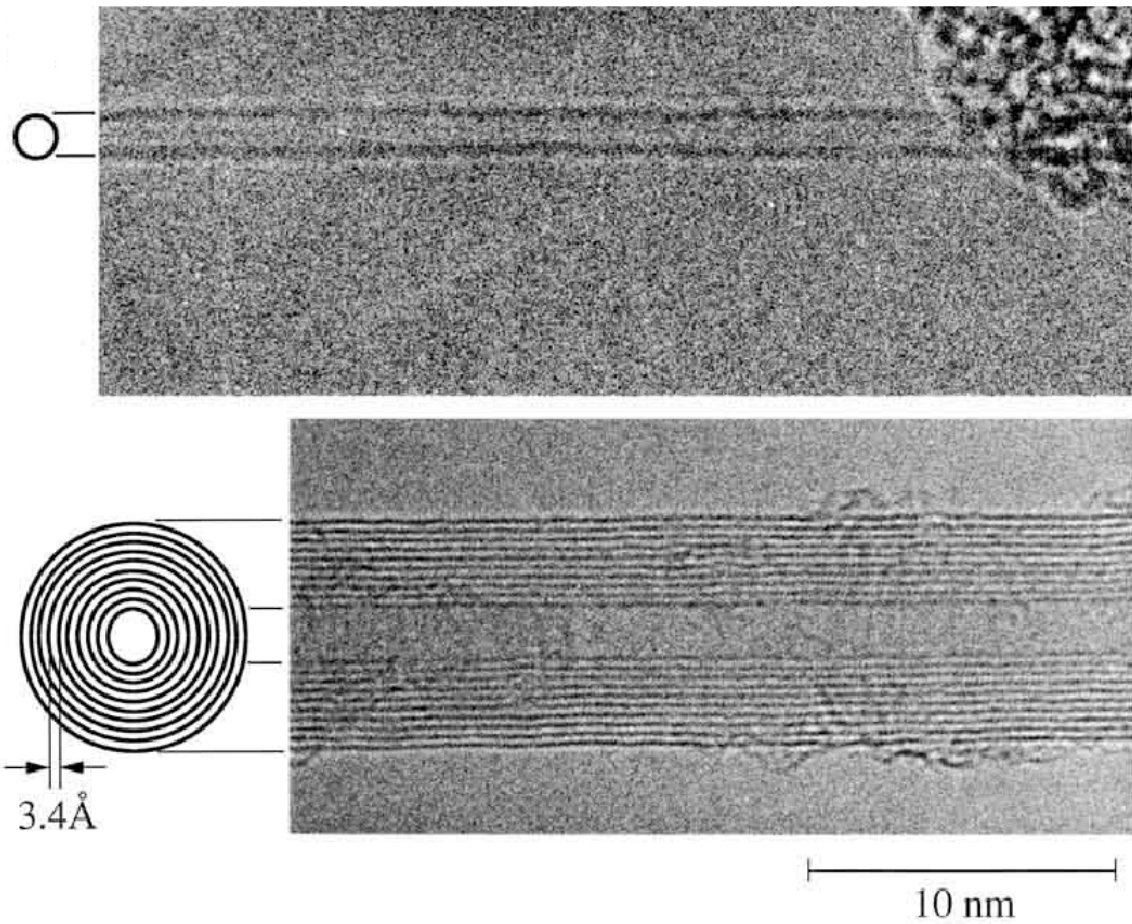


Figure 1.2. Transmission electron microscopy (TEM) images of SWNTs (top) and MWNTs (bottom). CNTs have a diameter of several nanometers, with a tube length that can be up to several millimeters, typically several micrometers. The interlayer distance in MWNTs is about 3.4 Å, which is slightly greater than the distance between graphene layers in graphite (approximately 3.35 Å).

In recent years, CNTs have also generated great interest in the field of biology (5-8). The ability to manipulate and probe biological materials at the nanoscale is becoming increasingly important for biophysical studies of single molecules, cells, and for biotechnology devices. The unique properties of CNTs offer great opportunities for biological applications including bioimaging, biosensing, intracellular delivery, and tissue engineering. In addition, the understanding of the chemical properties of CNTs and the development of functionalization strategies have made it feasible to integrate CNTs with biological systems (9). In this chapter, we first discuss some emerging methodologies for functionalization of CNTs with emphasis on biological applications. We then give some examples on recent biotechnological and biomedical applications of CNTs. Finally, the toxicity and pharmacokinetics of CNTs are discussed. It is not our intention to provide a comprehensive review. Instead, we focus on recent trends and emphasize some particularly promising technologies.

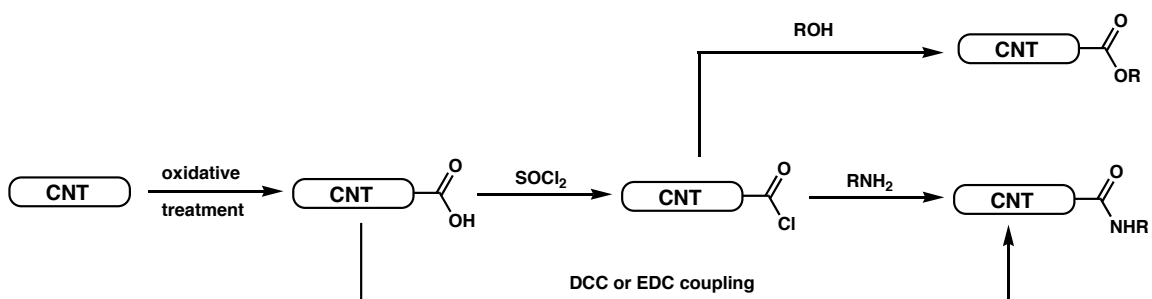
Functionalization of carbon nanotubes

The ability to functionalize nanotubes is crucial to many of the applications of CNTs. For example, the field emission properties (10-12) of a “bare” nanotube may be very different from a functionalized one, especially if a foreign chemical group is attached at the tip of the tube. Strategies for functionalizing both the ends and walls of CNTs have been extensively explored for tailoring the properties of these materials and engineering nanotube-based devices (9).

For biological applications, the insolubility of CNTs in aqueous environments has been a major barrier. Surface modification methods have been developed to solubilize CNTs in water, which made it possible to manipulate and process CNTs in solution phase (6). In addition, various biomolecules including DNA (13, 14), proteins (15, 16), and carbohydrates (17, 18) have been conjugated to CNTs. These biologically functionalized CNTs may be used for probing biological processes. The functionalization methods can be roughly divided into two categories: covalent functionalization and non-covalent functionalization.

Covalent functionalization. The most commonly used covalent modification has been oxidative treatment of CNTs to generate carboxylic groups on the nanotube surfaces. This procedure was originally developed to remove impurities produced during CNT synthesis such as amorphous carbon and metal catalysts (19). The purification process usually involved oxidative acid treatment, such as refluxing in nitric acid or sonication in a concentrated $\text{H}_2\text{SO}_4/\text{HNO}_3$ mixture (19). Along with eliminating the impurities, the treatment also shortened the nanotubes and created many carboxylic acid groups both on the ends and the walls of CNTs (19-21). The carboxylic acids can be further elaborated by coupling with amines or alcohols to attach a variety of molecules (Scheme 1.1). For example, long alkyl chains were attached to CNTs via the amidation of nanotube-bound carboxylic acid groups with alkylamines, and the functionalized CNTs were soluble in organic solvents (20). Oligomeric poly(ethylene glycol) was attached in a similar fashion to make CNTs soluble in water and more biologically

friendly (22, 23). Biologically useful molecules such as fluorescent dyes (24), nucleic acids (13), and carbohydrates (25) were also linked to CNTs by the carboxylic acid derivatization protocol.

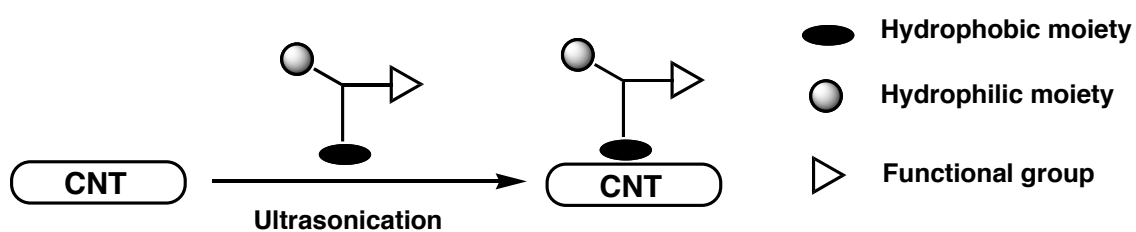


Scheme 1.1. General strategy for carboxylic acid derivatization of CNTs.

Apart from carboxylic acid derivatization, a number of other covalent modification methods that utilized the reactivity of the π conjugation system have been reported. Those reactions could be used to attach functional groups directly to the graphic surface of CNTs. Margrave and coworkers reported the fluorination of CNTs (26). Fluorinated CNTs were soluble in various organic solvents. More interestingly, fluorinated CNTs could be further derivatized chemically by reaction with organolithium reagents or Grignard reagents. These reactions and the applications of fluorinated CNTs have been recently reviewed (27). Another interesting methodology is the 1,3-dipolar addition reported by Prato and coworkers (28, 29). The walls of CNTs reacted with a α -amino acid and an aldehyde. This reaction has been used to solubilize CNTs and attach biomolecules such as peptides and nucleic acids (7). Other examples include the hydrogenation of CNTs via Birch reduction (30), addition of carbenes (31), reaction with diazonium reagents (32, 33), and nitrene addition (20, 34).

Non-covalent functionalization. The development of non-covalent modification methods was largely driven by the need to solubilize CNTs in aqueous solution. Most of the methods involve passive adsorption of an amphiphilic molecule or polymer (Scheme 1.2). The mechanism was suggested to be hydrophobic interactions or π - π stacking in water between the hydrophobic moieties and the CNT surface (35-40). The hydrophilic moieties then conferred water solubility to the CNTs. Reactive groups could also be incorporated into the amphiphilic molecules so that the functionalized CNTs could be

further elaborated with molecules of interest. The functionalization procedures were usually straightforward, requiring only ultrasonication of CNTs in an aqueous solution of the amphiphilic molecule. In addition, non-covalent CNT modification mostly preserves the intrinsic properties of CNTs, an advantage over covalent functionalization.



Scheme 1.2. General approach to non-covalent functionalization of CNTs. The hydrophobic moiety serves as an anchor via hydrophobic interaction or π - π stacking. The hydrophilic moiety renders solubility in water. The functional group can be used for attaching molecules of interest. It should be noted that the hydrophilic moiety sometimes can serve as a functional group for further elaboration.

Non-covalent functionalization of CNTs started with the use of various surfactants to disperse CNTs in water solution (19, 35, 36, 41-47). Sodium dodecyl sulfate (SDS) and Triton X-100 are the two most widely used surfactants. The solution properties of CNTs dispersed by these surfactants were well characterized (41). Weisman and coworkers used SDS to dissolve SWNTs and were able to characterize their near-infrared (NIR) fluorescence properties (36). They also acquired the structure-assigned optical spectra of SWNTs using such solutions (42). A careful TEM study performed by Mioskowski and coworkers visualized the adsorption of SDS and other

amphiphilic molecules with lipid chains (35). The mechanistic basis of the hydrophobic interaction and π - π stacking on CNT surface was revealed by experimental studies and computational simulations (35-40). Hydrophobic interactions were further explored to attach molecules of interest on CNT surface. For example, as described in Chapter 3, we designed and synthesized a glycosylated polymer bearing a C₁₈ lipid in order to coat CNTs with carbohydrates (17, 18). Dai and coworkers covalently linked U1A proteins to Tween-20 and then coated the CNT surface with the conjugates for antibody recognition (16). Another widely used strategy is to use pyrene-based anchors. Dai and coworkers reported the use of 1-pyrenebutanoic acid succinimide ester as a bifunctional linker to immobilize proteins on CNT surface (15). The pyrene moiety bound to CNT surface via π - π stacking, while the succinimidyl ester group at the other end of the bifunctional molecule could react with amines in the proteins. This method has since been adopted in various scenarios (48-57).

A variety of polymers have been used to make CNT-polymer composite materials (58). For water solubilization, polymers with polar and non-polar blocks could wrap CNTs and make them soluble in water (17, 18, 47, 59-70). For example, Wang and coworkers wrapped CNTs with a Nafion polymer bearing polar side chains (59). The wrapped CNTs were soluble in PBS buffer and were used as amperometric biosensors. A (PEO-PPO-PEO) triblock polymer was also able to wrap and solubilize CNTs (47). An interesting report by Wooley and coworkers showed the use of an amphiphilic diblock polymer to solubilize CNTs, followed by cross-linking the hydrophilic outer shell to

stabilize the wrapped CNTs in aqueous solution (62). SWNT dispersions that responded to temperature and pH changes in poly(*N*-isopropylacrylamide) and poly-L-lysine solutions were also reported (63).

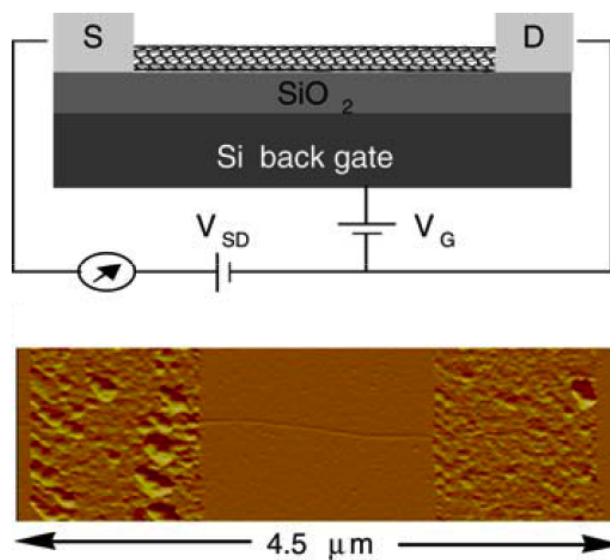
Some biomolecules can interact directly with CNT surfaces in a non-covalent fashion. Zheng and coworkers found that single-stranded DNA (ssDNA) could disperse CNTs in water and the DNA-wrapped CNTs can be sorted based on their structures (14, 71-74). In addition, double-stranded DNA (dsDNA) could also bind to CNT surfaces (75). Designed amphiphilic peptides could wrap CNTs to make them soluble via non-covalent interactions (76-80). Phage display (81) was used to identify peptide sequences with selective affinity for CNT surfaces (82, 83). Non-specific adsorption of proteins to CNT surfaces was believed to result from hydrophobic interaction (84-87). Polysaccharides such as starch (88, 89), Gum Arabic (45), chizophyllan, Curdlan (90), and cyclodextrin (91, 92) also wrap CNT surfaces via non-covalent interactions.

Biological applications

Biosensing. Research effort into CNT-based nanoelectronics, driven by the ultimate objective of further miniaturizing the current silicon-based microelectronics (93), has led to extensive exploration of field effect transistor using SWNTs as the conducting channel (SWNT-FET). The electronic characteristics of SWNT-FET devices have been well studied (94-96). Experimental and theoretical studies have indicated that the environment surrounding the CNTs can influence the electrical conductance. These

phenomena were originally explored to develop sensitive chemical sensors for various gases such as oxygen (97) and ammonia (98). Consequently, biosensing based on SWNT-FETs has attracted considerable attention (99). Two types of device architectures of SWNT-FETs have been used for biosensing. An SWNT-FET can be built using a single SWNT to connect the source and the drain (Fig. 1.3A). Alternatively, the device can contain a random array of SWNTs interconnected with the source and drain, called carbon nanotube network field-effect transistor (SWNTN-FET) (Fig. 1.3B). The basic detection scheme is to first immobilize biomolecules on the CNT surface such as a receptor for the analytes of interest. Ligand-receptor binding can then be detected by monitoring the changes in the device characteristics.

A



B

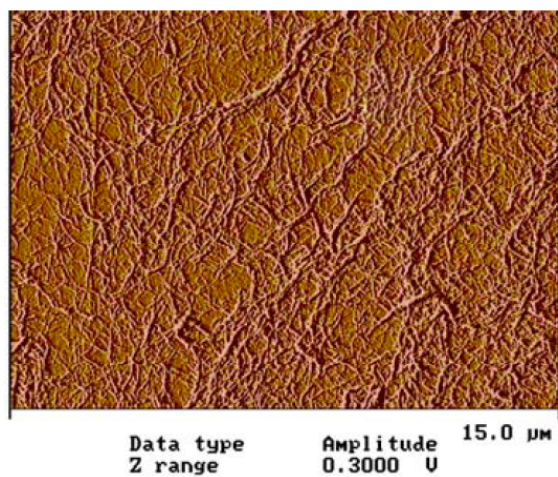


Figure 1.1. Two types of device architectures of field effect transistors with carbon nanotube conducting channels. **(A)** SWNT-FET uses a single semiconducting SWNT to connect the source and drain electrodes. **(B)** The configuration of SWNTN-FET is the same as SWNT-FET, with the difference that a SWNT network connects the source and drain. (Reprinted from ref. 99)

Various research groups have explored SWNT-FETs or SWNTN-FETs for sensing a range of biological events. In a very simple version, non-specific binding of proteins to unfunctionalized SWNT surfaces could be detected (85). Functionalizing the SWNT surface in the devices for detecting specific ligand-receptor interactions is of great importance. The biotin-streptavidin interaction has been widely used as a model system. For example, biotin could be non-covalently linked to SWNTs to serve as the recognition site for streptavidin. The binding of streptavidin could be detected by changes in the device characteristics (16, 100). Other ligand-receptor interactions have also been detected in a device setting. Several groups reported antibody-antigen recognition detection (57, 101, 102). For example, SWNT-FETs immobilized with antibodies were used to detect prostate-specific antigen (PSA) (57), a marker of prostate cancer. Mukasa and coworkers immobilized anti-hemagglutinin antibodies on SWNT-FETs to detect influenza virus particles (103). DNA aptamers were also immobilized to SWNT surface as molecular recognition elements for different proteins such as thrombin (104). Star and coworkers recently reported the label-free detection of DNA hybridization using SWNTN-FETs (105).

The optical properties of CNTs were explored for biosensing applications as well. Weismann, Smalley, and coworkers found that individual semiconducting SWNTs dispersed in solution could display distinctive NIR fluorescence arising from their electronic band gap (36, 42). Surface modification of SWNTs could change their fluorescence energy. For example, the conformational change of dsDNA on SWNT

surface could be detected via decrease in their NIR emission energy (75). A similar detection scheme has been used for detecting DNA hybridization (106) and for glucose sensing (107-109).

Bioimaging. Lieber and coworkers pioneered the early use of CNTs as atomic force microscopy (AFM) tips for imaging biomolecules (110, 111). The structural features of CNTs (small diameter and high aspect ratio) and mechanical robustness make them ideal AFM probes for imaging biomolecules with nanometer scale resolution. The CNT-AFM tips have been used to image antibodies (112, 113), DNA (114-117), and β -amyloid protofibrils (118).

Their NIR fluorescence properties (36) make CNTs attractive for optical imaging. NIR fluorescence is ideal for bioimaging because of greater tissue penetration and reduced auto-fluorescent background in thick tissue compared to visible dyes. NIR fluorescence spectroscopy of living cells (119, 120) and tissues (107) has been employed with CNT probes. Recently, Weisman and coworkers reported the fluorescence imaging of CNTs in *Drosophila melanogaster* (fruit flies) (121).

CNTs have also been used as scaffolds for imaging agents. For example, Scheinberg and coworkers labeled CNTs with Yttrium-86 for PET imaging in mice (122). Strano and coworkers reported CNTs functionalized with iron oxide nanoparticles for MRI and NIR fluorescence multimodal biomedical imaging (123).

Intracellular delivery. The development of new and efficient strategies for intracellular delivery is of fundamental importance in the fields of cell biology and

pharmacology (124). New materials such as dendrimers and nanoparticles have been studied for drug and gene delivery (125, 126). Recently, CNTs have emerged as a new intracellular delivery system for transporting a variety of biomolecules and therapeutic agents (7, 14, 24, 75, 120, 127-141). Cellular uptake of CNTs was first reported by Prato and coworkers (127). They functionalized CNTs with a fluorescent dye or a peptide using 1,3-dipolar addition. The functionalized CNTs were internalized into the cytoplasm or nucleus of fibroblasts (Fig. 1.4) (127). Shortly after, Dai and coworkers reported that oxidized CNTs covalently modified with fluorescein or biotin-streptavidin complexes could be taken up by cells (24). The cellular delivery of CNTs was visualized directly by TEM imaging (128). CNTs were observed mainly in the cytoplasm with some nanotubes observed in the cell membrane in the process of translocation. Weismann and coworkers demonstrated the use of NIR fluorescence to observe CNTs taken up by macrophage cells (120). The generality of this delivery system has been

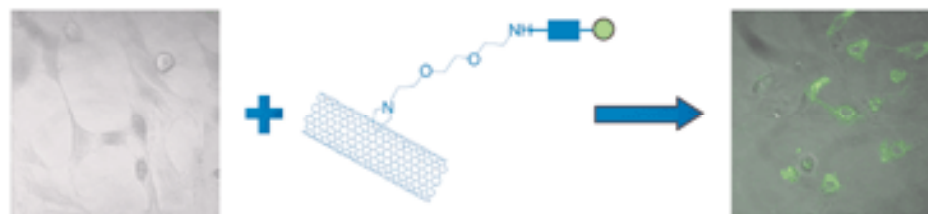


Figure 1.4. Functionalized CNTs were able to cross the cell membrane and deliver cargo into the cytoplasm or nucleus of fibroblasts. (Reprinted from ref. 127)

demonstrated with a range of biomolecules including proteins, DNA, and RNA in various mammalian cell types as well as yeast and bacterium (129, 130).

Since these pioneering studies, CNTs have been extensively explored as molecular transporters for various applications including gene delivery (132-135), cancer cell targeting (137, 138), and RNA interference (140, 141). Both ssDNA and dsDNA bind to CNT surfaces via π - π stacking (14). DNA-wrapped CNTs have been shown to be internalized into cells (75, 131). For gene delivery applications, plasmid DNA was electrostatically condensed onto CNTs functionalized with positive charges such as ammonium groups (128, 132). The potential of CNTs as gene transfer vectors has been explored by transfecting cells with plasmid DNA pCMV-Bgal expressing β -galactosidase (128), pCMV-Luc expressing luciferase (133), and the gene encoding GFP (134) with fairly good efficiency. Ren and coworkers developed a highly efficient technique based on the penetration of nickel-embedded CNTs into cells by magnetic field driving, called nanotube spearing (135). Unprecedented high efficiency was demonstrated with the transfection of various cells including primary B cells and neurons, which are traditionally difficult to transfect (135).

Functionalized CNTs have also been used as delivery vehicles for small drug-like molecules (24, 127). Praoto and coworkers developed a strategy for multiple functionalization of CNTs with different types of molecules—a fluorescein group for imaging and the antibiotic amphotericin B. This delivery particle was internalized by cells, and the antibiotic retained its activity against pathogens (136). An interesting study

by Hosmane and coworkers used CNTs to deliver carborane groups for boron neutron capture therapy (137). Instead of delivering therapeutic agents, Dai and coworkers targeted CNTs specifically to cancer cells, where the strong NIR absorbance of the CNTs was utilized to generate heat locally and trigger cell death (138). Dai and coworkers also reported the intracellular delivery of siRNA for RNA interference (140, 141). The CNT-siRNA conjugates triggered silencing more efficiently than commercial transfection agents. Although the pharmacokinetics of CNT delivery systems remains to be characterized, the ability of CNTs to penetrate cells offers promise for drug delivery *in vivo*.

The internalization pathway for CNTs has been studied, and two different mechanisms have been proposed. Dai and coworkers believed that CNT conjugates were taken up by cells via clathrin-mediated endocytosis (24, 129, 131, 138). However, Praoto and coworkers observed cellular uptake under endocytosis-inhibiting conditions and proposed an energy-independent mechanism (130). The discrepancy might be due to the difference in CNT sizes and functionalization strategies. It is more likely either mechanism could be true under specific circumstances.

Another promising application of CNTs in intracellular delivery is to use them as “nanoneedles” for single-cell injection (49). Traditionally, microinjection has been widely used to directly inject a solution into a single cell through a glass micropipette, but it suffers from the damage of cell membrane (142). As described in chapter 2, we recently developed a nanoscale cell injector based on CNTs for intracellular delivery

without membrane damage (49). This nanoinjection technique used a single MWNT attached to an AFM tip to deliver cargo that was attached on CNT surface via a disulfide linker. Penetration of cell membranes with this “nanoneedle” controlled by AFM, followed by reductive cleavage of the disulfide bonds within the cell’s interior, resulted in the release of cargo inside the cells (Figure 1.5). The capability of the nanoinjector was demonstrated by injecting protein-coated quantum dots into live human cells. Similarly, Kouklin and coworkers used MWNT bundles attached on AFM tips to deliver fluorescent dyes into cells (143). Moudgil and coworkers functionalized MWNT-AFM tips with gold nanoparticles and used them to penetrate cell membrane (144). While still in its infant stage, the nanoinjector provides a fundamentally new mechanism for delivering molecules into cells without the need for carrier solvent and with no apparent cell damage. The unique capabilities of the nanoinjector can be further exploited in a number of ways. Other biomolecules such as DNA and RNA, or synthetic structures such as polymers, dendrimers and nanoparticles can be delivered into cells in a similar fashion. In conjunction with organelle-specific optical probes, the nanoinjector concept might be extended to the delivery of cargo to specific subcellular compartments. In principle, cells such as bacteria that are too small for microinjection should be amenable to nanoinjection.

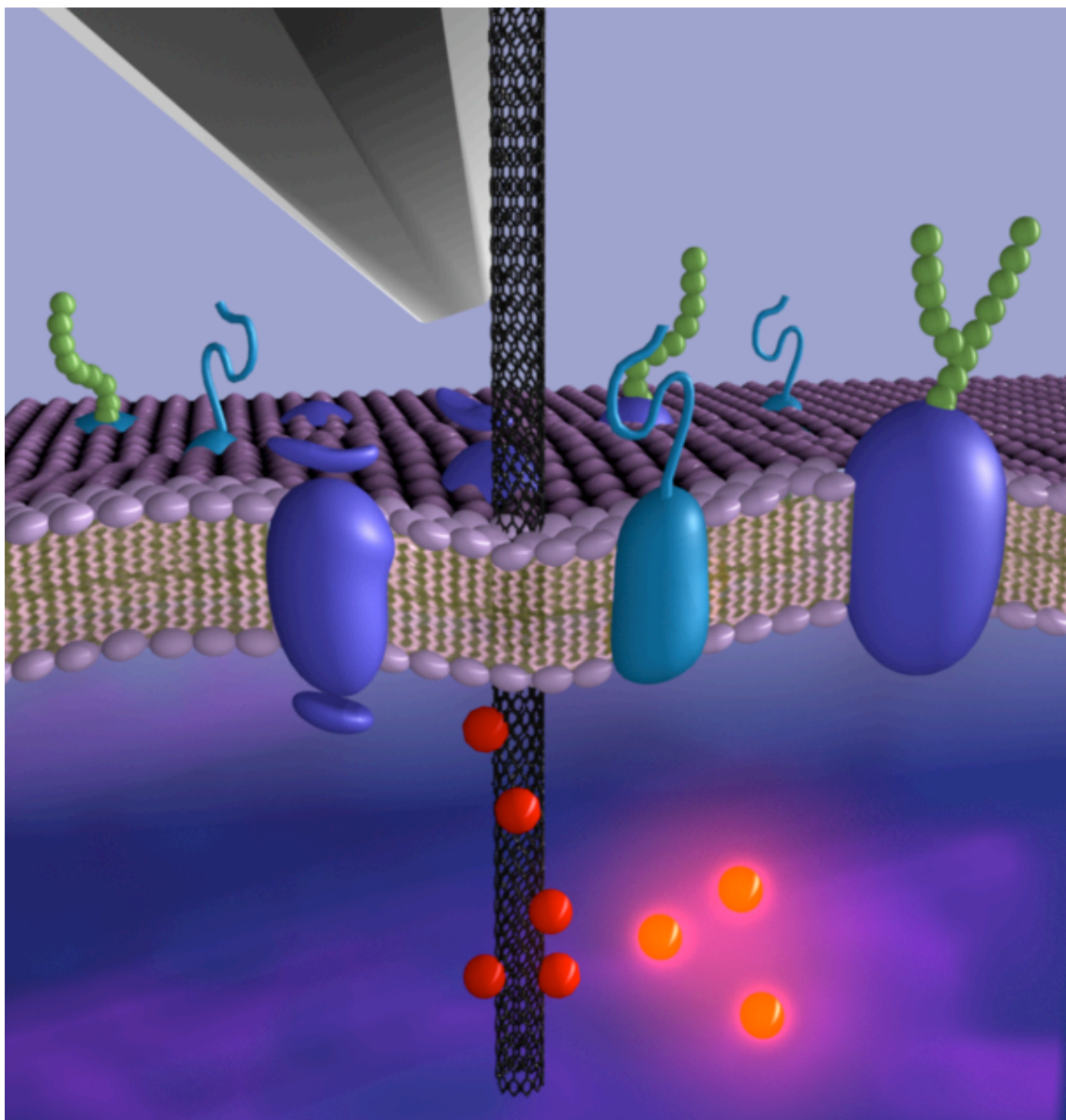


Figure 1.5. Schematic of the nanoinjector: A MWNT-AFM tip with cargo attached to the MWNT surface via a disulfide linker penetrates a cell membrane. After disulfide reduction within the cell's cytosol, the cargo is released into the cytosol.

Tissue engineering. Their excellent mechanical properties, electronic conductivity, and extremely large surface area make CNTs very attractive as tissue engineering scaffolds. Already, both unfunctionalized and functionalized CNTs have been considered for use as scaffolds for cell growth. One promising avenue is to use CNTs as scaffolds to guide nerve regeneration. Mattson and coworkers demonstrated that MWNTs covalently functionalized with 4-hydroxynonenal could serve as substrates for growing embryonic rat brain nerve cells (145). Chemical functionalization seemed to be necessary for neuronal cell growth on CNT surfaces (145). Haddon and coworkers studied the neuron growth on both SWNTs and MWNTs functionalized with different moieties (146, 147). They concluded that neuron growth was largely affected by the surface charges on the functionalized CNTs. Kotov and coworkers compared neuron growth on SWNT substrates and tissue culture dishes and found that higher neurite extension and branching occurred on the former. Gabay and coworkers reported the patterning of neural networks on CNT substrates, in which neurons formed self-organized aggregates on the CNT islands and then interconnected in neighboring islands to form neural networks (148). Recently, Kotov and coworkers showed successful differentiation of mouse neural stem cells into neurons, astrocytes, and oligodendrocytes with clear formation of neurites on SWNT composite substrates (149).

Bone tissue engineering is another area of interest for using CNT substrates as scaffolds. MacDonald and coworkers developed a collagen/SWNT composite as substrate for growing rat aortic smooth muscle cells (150). Mikos and coworkers

characterized the mechanical properties of SWNT-polymer composites for use as injectable reinforcing fillers in bone tissue engineering (151, 152). They also compared CNTs with other carbon nanostructures such as fullerenes (153). The application of CNTs in musculoskeletal and neural tissue engineering is still at an early stage. Much work remains to be done to assess the cell compatibility and CNT pharmacostability.

Toxicity

The success of CNTs for biological applications largely depends on their biocompatibility. People have been concerned about the harmful interactions of nanomaterials including CNTs with biological systems and the environment, and their potential to generate toxicity (154-157). Human exposure to CNTs is likely to increase in the coming years due to the wider use of CNTs. Therefore, studies on the toxicity of CNTs are of great importance (158-161).

***In vitro* toxicity.** Various groups have recently observed that CNTs (both SWNTs and MWNTs) possess toxicity towards a range of cell lines (162-179). Shvedova and coworkers reported the cell viability loss of human epidermal keratinocytes (HaCaT) when cultured with SWNTs for 18 h (162). The toxicity was proposed to be due to oxidative stress induced by SWNTs. This mechanism was later confirmed by Ramesh and coworkers in more detailed studies in keratinocytes (167) and human BJ Foreskin cells (176). The residual catalyst particles such as iron might be important in determining redox-dependent responses (174, 180). Cui and coworkers

reported that SWNTs decreased cell adhesion, inhibited cell proliferation, and induced apoptosis in a dose- and time-dependent manner in cultured human HEK 293 cells (164). MWNTs were also observed to induce T lymphocyte apoptosis (168). Chen and coworkers did a careful mechanistic study on the cytotoxicity of MWNTs and found that exposing cells to MWCNTs at cytotoxic doses induced cell cycle arrest and increased apoptosis/necrosis (169). Gene array analysis indicated that multiple cellular pathways are perturbed after exposure to MWNTs. Monteiro-Riviere and coworkers found that MWNTs localized within cytoplasmic vacuoles of the human epidermal keratinocytes (HEK) and initiated an irritation response in a time-dependent manner (163).

Zhao and coworkers compared the cytotoxicity of SWNTs, MWNTs, and C₆₀ in alveolar macrophages (AM) and found that SWNTs showed more profound cytotoxicity than MWNTs, while no significant toxicity was observed for C₆₀, which suggested that the toxicity of CNTs was geometry-dependent (165). Margrez and coworkers also observed that the cytotoxicity of CNTs is size-dependent by comparing different carbon-based nanomaterials (181). Another report by Sato and coworkers showed on the cytotoxicity of MWNTs was influenced by length (170). However, no significant difference in cytotoxicity between SWNTs and MWNTs was observed by Soto and coworkers when tested with a murine macrophage cell line (166). Other factors like cell culture medium (182, 183), surface area (175), and agglomeration (184) were also studied.

The observed cytotoxicity of CNTs imposed limitations on their biological applications. Accordingly, significant effort has been directed at curbing the cytotoxicity of CNTs by surface functionalization. Simple acid treatment was found to increase toxicity of CNTs, probably due to increased solubility and better contact with cells (168, 181). Ausman and coworkers found that as the degree of sidewall functionalization increased, the SWNT became less cytotoxic (185). In fact, various groups have functionalized CNTs covalently or non-covalently to make them water-soluble, and in many cases, the functionalized CNTs showed reduced cytotoxicity (24, 29, 127, 131, 186).

In vivo toxicity. Initially, large-scale production of CNTs promoted discussion of exposure risk to workers. Maynard and coworkers studied the release of SWNTs into air and the exposure of workers (187). They found an airborne concentration of 53 $\mu\text{g}/\text{m}^3$ and glove deposition of 0.2-6 mg per hand. A series of studies by Huczko and coworkers in humans, rabbits, and guinea pigs indicated that exposure to CNTs did not cause skin irritation or allergy, but could induce pathologies in lung tissues (188-190).

Several studies regarding pulmonary toxicity of CNTs have been performed. Lam and coworkers studied SWNTs in mouse lung tissue and reported that SWNTs induced epithelial granulomas and interstitial inflammation in a time-dependent manner (191). A more detailed study by Shvedova and coworkers revealed the dose- and time-dependence of pulmonary toxicity in mice upon pharyngeal aspiration of SWNTs (192). Warheit and coworkers performed a similar study in rats via intratracheal instillation of SWNTs (193).

They observed a mortality rate of 15% upon 5mg/kg instillation, and found that the lung tissue exhibited granuloma formation and inflammation. MWNTs induced similar responses in rats as observed by Lison and coworkers (194). The *in vivo* toxicity of CNTs can depend on various factors. For example, longer CNTs were found to induce more severe inflammation response than shorter ones (170). Li and coworkers also demonstrated a difference in mouse pathological lesions induced by MWNTs administered by different procedures: intratracheal instillation and inhalation (195).

Endo and coworkers evaluated the biological responses to CNTs by measuring T cells in peripheral blood and by the histopathological study of tissues (196). They found that SWNTs activated the major histocompatibility complex (MHC) class I pathway of antigen presentation. Simeonova and coworkers reported the cardiovascular effects of pulmonary exposure to SWNTs in mice (197). Radomsky and coworkers showed that platelets were targeted and activated by CNTs followed by the acceleration of the development of carotid artery thrombosis (198).

The toxicity of CNTs has been reasonably well studied both *in vitro* and *in vivo*. However, the results were sometimes conflicting. Furthermore, the mechanism of CNT toxicity remains unclear, although some proposed pathways have been examined. Differences in CNT synthesis procedures and experimental approaches may account for these discrepancies. A reference material is desired for standardizing toxicity assays. It was also suggested that two or more independent test systems should be necessary for CNT toxicity tests (199).

Pharmacokinetics

Studies on biodistribution and pharmacokinetics of CNTs are relatively few. The size, shape, aggregation, and surface properties of CNTs might largely determine their pharmacokinetics (154). Wang and coworkers labeled the SWNTs with radioactive Iodine-125 atoms, and then the tracer was used to study the distribution of SWNTs introduced via intraperitoneal administration into mice (200). They found that SWNTs moved easily among the compartments and tissues of the body and no tissue damage was observed. Most of the SWNTs (about 94%) were excreted into the urine. Li and coworkers reported similar results for MWNTs, using ⁹⁹Techetium-labeled water-soluble MWNTs (201). Kostarelos and coworkers functionalized CNTs with diethylenetriaminepentaacetic (DTPA) and radiolabeled them with Indium-111, then studied their biodistribution and blood circulation half-lives in mice via intravenous route of administration (202). The CNTs showed affinities for various organs and blood 30 min after administration. They also reported CNTs were rapidly cleared from all tissues and had a maximum blood circulation half-life of 3.5 h. The characteristic NIR fluorescence of SWNTs was also utilized to study their biodistribution. Weisman and coworkers intravenously administered surfactant-coated SWNTs to rabbits and monitored them by NIR fluorescence imaging (203). They found that blood proteins displaced the nanotube coating of synthetic surfactant molecules within seconds. The nanotube concentration in the blood serum decreased exponentially with a half-life of 1 h and significant concentrations of SWNTs were found only in the liver after 24 h. Recently,

Dai and coworkers investigated the biodistribution of radiolabelled SWNTs in mice by positron emission tomography (PET) and Raman spectroscopy (204). They found that SWNTs functionalized with phospholipids bearing polyethylene-glycol (PEG) were very stable *in vivo* and exhibited relatively long blood circulation time and low uptake by the reticuloendothelial system.

These studies afforded initial quantitative analysis of CNTs accumulated in animal tissues and provided useful data for their development in the biomedical field. It is especially encouraging that no acute toxicity was observed for functionalized CNTs. More studies remain to be performed using different CNTs and different protocols.

Conclusions and outlooks

Our understanding of the structural, chemical, electronic, and mechanical properties of CNTs, combined with readily available functionalization methodologies, has motivated extensive efforts towards biological applications of CNTs. Some promising techniques based on CNTs have been developed, although the current body of work has been largely limited to proof-of-concept. It is likely that CNTs will become useful in clinical applications in the coming years. However, more work is needed to further understand the biological properties of functionalized CNTs, such as toxicity and pharmacokinetics.

References

1. R. Saito, G. Dresselhaus, M. S. Dresselhaus, Physical Properties of Carbon Nanotubes. (Imperial College Press, London, UK, 1998).
2. A. Oberlin, M. Endo, T. Koyama, Filamentous Growth of Carbon through Benzene Decomposition. *J. Cryst. Growth* **32**, 335-349 (1976).
3. S. Iijima, Helical Microtubules of Graphitic Carbon. *Nature* **354**, 56-58 (1991).
4. M. Terrones, Science and technology of the twenty-first century: Synthesis, properties and applications of carbon nanotubes. *Annu. Rev. Mater. Res.* **33**, 419-501 (2003).
5. C. R. Martin, P. Kohli, The emerging field of nanotube biotechnology. *Nat. Rev. Drug Discovery* **2**, 29-37 (2003).
6. Y. Lin *et al.*, Advances toward bioapplications of carbon nanotubes. *J. Mater. Chem.* **14**, 527-541 (2004).
7. A. Bianco, K. Kostarelos, M. Prato, Applications of carbon nanotubes in drug delivery. *Curr. Opin. Chem. Biol.* **9**, 674-679 (2005).
8. W. Wei, A. Sethuraman, C. Jin, N. A. Monteiro-Riviere, R. J. Narayan, Biological properties of carbon nanotubes. *J. Nanosci. Nanotechnol.* **7**, 1284-1297 (2007).
9. Y. P. Sun, K. F. Fu, Y. Lin, W. J. Huang, Functionalized carbon nanotubes: Properties and applications. *Acc. Chem. Res.* **35**, 1096-1104 (2002).
10. W. A. Deheer, A. Chatelain, D. Ugarte, A Carbon Nanotube Field-Emission Electron Source. *Science* **270**, 1179-1180 (1995).
11. P. G. Collins, A. Zettl, A simple and robust electron beam source from carbon nanotubes. *Appl. Phys. Lett.* **69**, 1969-1971 (1996).
12. K. A. Dean, B. R. Chalamala, Current saturation mechanisms in carbon nanotube field emitters. *Appl. Phys. Lett.* **76**, 375-377 (2000).

13. K. A. Williams, P. T. M. Veenhuizen, B. G. de la Torre, R. Eritja, C. Dekker, Nanotechnology - Carbon nanotubes with DNA recognition. *Nature* **420**, 761-761 (2002).
14. M. Zheng *et al.*, DNA-assisted dispersion and separation of carbon nanotubes. *Nat. Mater.* **2**, 338-342 (2003).
15. R. J. Chen, Y. G. Zhang, D. W. Wang, H. J. Dai, Noncovalent sidewall functionalization of single-walled carbon nanotubes for protein immobilization. *J. Am. Chem. Soc.* **123**, 3838-3839 (2001).
16. R. J. Chen *et al.*, Noncovalent functionalization of carbon nanotubes for highly specific electronic biosensors. *Proc. Natl. Acad. Sci. USA* **100**, 4984-4989 (2003).
17. X. Chen, G. S. Lee, A. Zettl, C. R. Bertozzi, Biomimetic engineering of carbon nanotubes by using cell surface mucin mimics. *Angew. Chem. Int. Ed.* **43**, 6111-6116 (2004).
18. X. Chen *et al.*, Interfacing carbon nanotubes with living cells. *J. Am. Chem. Soc.* **128**, 6292-6293 (2006).
19. J. Liu *et al.*, Fullerene pipes. *Science* **280**, 1253-1256 (1998).
20. J. Chen *et al.*, Solution properties of single-walled carbon nanotubes. *Science* **282**, 95-98 (1998).
21. D. B. Mawhinney *et al.*, Surface defect site density on single walled carbon nanotubes by titration. *Chem. Phys. Lett.* **324**, 213-216 (2000).
22. K. F. Fu *et al.*, Defunctionalization of functionalized carbon nanotubes. *Nano Lett.* **1**, 439-441 (2001).
23. W. J. Huang, S. Fernando, L. F. Allard, Y. P. Sun, Solubilization of single-walled carbon nanotubes with diamine-terminated oligomeric poly(ethylene glycol) in different functionalization reactions. *Nano Lett.* **3**, 565-568 (2003).
24. N. W. S. Kam, T. C. Jessop, P. A. Wender, H. J. Dai, Nanotube molecular transporters: Internalization of carbon nanotube-protein conjugates into mammalian cells. *J. Am. Chem. Soc.* **126**, 6850-6851 (2004).

25. L. R. Gu *et al.*, Single-walled carbon nanotubes displaying multivalent ligands for capturing pathogens. *Chem. Commun.*, 874-876 (2005).
26. E. T. Mickelson *et al.*, Fluorination of single-wall carbon nanotubes. *Chem. Phys. Lett.* **296**, 188-194 (1998).
27. V. N. Khabashesku, W. E. Billups, J. L. Margrave, Fluorination of single-wall carbon nanotubes and subsequent derivatization reactions. *Acc. Chem. Res.* **35**, 1087-1095 (2002).
28. V. Georgakilas *et al.*, Organic functionalization of carbon nanotubes. *J. Am. Chem. Soc.* **124**, 760-761 (2002).
29. V. Georgakilas *et al.*, Amino acid functionalisation of water soluble carbon nanotubes. *Chem. Commun.*, 3050-3051 (2002).
30. S. Pekker, J. P. Salvetat, E. Jakab, J. M. Bonard, L. Forro, Hydrogenation of carbon nanotubes and graphite in liquid ammonia. *J. Phys. Chem. B* **105**, 7938-7943 (2001).
31. H. Hu *et al.*, Sidewall functionalization of single-walled carbon nanotubes by addition of dichlorocarbene. *J. Am. Chem. Soc.* **125**, 14893-14900 (2003).
32. J. L. Bahr *et al.*, Functionalization of carbon nanotubes by electrochemical reduction of aryl diazonium salts: A bucky paper electrode. *J. Am. Chem. Soc.* **123**, 6536-6542 (2001).
33. M. S. Strano *et al.*, Electronic structure control of single-walled carbon nanotube functionalization. *Science* **301**, 1519-1522 (2003).
34. M. Holzinger *et al.*, Sidewall functionalization of carbon nanotubes. *Angew. Chem. Int. Ed.* **40**, 4002-4005 (2001).
35. C. Richard, F. Balavoine, P. Schultz, T. W. Ebbesen, C. Mioskowski, Supramolecular self-assembly of lipid derivatives on carbon nanotubes. *Science* **300**, 775-778 (2003).
36. M. J. O'connell *et al.*, Band gap fluorescence from individual single-walled carbon nanotubes. *Science* **297**, 593-596 (2002).

37. M. S. Strano *et al.*, The role of surfactant adsorption during ultrasonication in the dispersion of single-walled carbon nanotubes. *J. Nanosci. Nanotechnol.* **3**, 81-86 (2003).
38. S. Gotovac *et al.*, Effect of nanoscale curvature of single-walled carbon nanotubes on adsorption of polycyclic aromatic hydrocarbons. *Nano Lett.* **7**, 583-587 (2007).
39. Y. H. Zhang *et al.*, Direct measurements of the interaction between pyrene and graphite in aqueous media by single molecule force spectroscopy: Understanding the pi-pi interactions. *Langmuir* **23**, 7911-7915 (2007).
40. E. J. Wallace, M. S. P. Sansom, Carbon nanotube/detergent interactions via coarse-grained molecular dynamics. *Nano Lett.* **7**, 1923-1928 (2007).
41. M. F. Islam, E. Rojas, D. M. Bergey, A. T. Johnson, A. G. Yodh, High weight fraction surfactant solubilization of single-wall carbon nanotubes in water. *Nano Lett.* **3**, 269-273 (2003).
42. S. M. Bachilo *et al.*, Structure-assigned optical spectra of single-walled carbon nanotubes. *Science* **298**, 2361-2366 (2002).
43. S. Bandow *et al.*, Purification of single-wall carbon nanotubes by microfiltration. *J. Phys. Chem. B* **101**, 8839-8842 (1997).
44. K. B. Shelimov, R. O. Esenaliev, A. G. Rinzler, C. B. Huffman, R. E. Smalley, Purification of single-wall carbon nanotubes by ultrasonically assisted filtration. *Chem. Phys. Lett.* **282**, 429-434 (1998).
45. R. Bandyopadhyaya, E. Nativ-Roth, O. Regev, R. Yerushalmi-Rozen, Stabilization of individual carbon nanotubes in aqueous solutions. *Nano Lett.* **2**, 25-28 (2002).
46. N. Nakashima, Y. Tomonari, H. Murakami, Water-soluble single-walled carbon nanotubes via noncovalent sidewall-functionalization with a pyrene-carrying ammonium ion. *Chem. Lett.*, 638-639 (2002).
47. V. C. Moore *et al.*, Individually suspended single-walled carbon nanotubes in various surfactants. *Nano Lett.* **3**, 1379-1382 (2003).

48. K. Besteman, J. O. Lee, F. G. M. Wiertz, H. A. Heering, C. Dekker, Enzyme-coated carbon nanotubes as single-molecule biosensors. *Nano Lett.* **3**, 727-730 (2003).
49. X. Chen, A. Kis, A. Zettl, C. R. Bertozzi, A cell nanoinjector based on carbon nanotubes. *Proc. Natl. Acad. Sci. USA* **104**, 8218-8222 (2007).
50. P. G. Holder, M. B. Francis, Integration of a self-assembling protein scaffold with water-soluble single-walled carbon nanotubes. *Angew. Chem. Int. Ed.* **46**, 4370-4373 (2007).
51. L. W. Qu *et al.*, Interactions of functionalized carbon nanotubes with tethered pyrenes in solution. *J. Chem. Phys.* **117**, 8089-8094 (2002).
52. L. S. Fifield *et al.*, Noncovalent functionalization of carbon nanotubes with molecular anchors using supercritical fluids. *J. Phys. Chem. B* **108**, 8737-8741 (2004).
53. V. Georgakilas, V. Tzitzios, D. Gournis, D. Petridis, Attachment of magnetic nanoparticles on carbon nanotubes and their soluble derivatives. *Chem. Mater.* **17**, 1613-1617 (2005).
54. H. Paloniemi *et al.*, Water-soluble full-length single-wall carbon nanotube polyelectrolytes: Preparation and characterization. *J. Phys. Chem. B* **109**, 8634-8642 (2005).
55. K. Narimatsu, J. Nishioka, H. Murakami, N. Nakashima, Design, synthesis, and characterization of carbon nanotube solubilizers carrying a reactive group. *Chem. Lett.* **35**, 892-893 (2006).
56. D. Wang, W. X. Ji, Z. C. Li, L. W. Chen, A biomimetic "polysoap" for single-walled carbon nanotube dispersion. *J. Am. Chem. Soc.* **128**, 6556-6557 (2006).
57. C. Li *et al.*, Complementary detection of prostate-specific antigen using In(2)O(3) nanowires and carbon nanotubes. *J. Am. Chem. Soc.* **127**, 12484-12485 (2005).
58. M. Moniruzzaman, K. I. Winey, Polymer nanocomposites containing carbon nanotubes. *Macromolecules* **39**, 5194-5205 (2006).

59. J. Wang, M. Musameh, Y. H. Lin, Solubilization of carbon nanotubes by Nafion toward the preparation of amperometric biosensors. *J. Am. Chem. Soc.* **125**, 2408-2409 (2003).
60. M. J. O'connell *et al.*, Reversible water-solubilization of single-walled carbon nanotubes by polymer wrapping. *Chem. Phys. Lett.* **342**, 265-271 (2001).
61. D. Li *et al.*, Dispersion of carbon nanotubes in aqueous solutions containing poly(diallyldimethylammonium chloride). *J. Mater. Sci. Lett.* **22**, 253-255 (2002).
62. H. Y. Huang, T. Kowalewski, E. E. Remsen, R. Gertzmann, K. L. Wooley, Hydrogel-coated glassy nanospheres: A novel method for the synthesis of shell cross-linked knedels. *J. Am. Chem. Soc.* **119**, 11653-11659 (1997).
63. D. Wang, L. W. Chen, Temperature and pH-responsive single-walled carbon nanotube dispersions. *Nano Lett.* **7**, 1480-1484 (2007).
64. Y. Dror, W. Pyckhout-Hintzen, Y. Cohen, Conformation of polymers dispersing single-walled carbon nanotubes in water: A small-angle neutron scattering study. *Macromolecules* **38**, 7828-7836 (2005).
65. D. Baskaran, J. W. Mays, M. S. Bratcher, Noncovalent and nonspecific molecular interactions of polymers with multiwalled carbon nanotubes. *Chem. Mater.* **17**, 3389-3397 (2005).
66. B. Zhao, H. Hu, A. P. Yu, D. Perea, R. C. Haddon, Synthesis and characterization of water soluble single-walled carbon nanotube graft copolymers. *J. Am. Chem. Soc.* **127**, 8197-8203 (2005).
67. V. A. Sinani *et al.*, Aqueous dispersions of single-wall and multiwall carbon nanotubes with designed amphiphilic polycations. *J. Am. Chem. Soc.* **127**, 3463-3472 (2005).
68. J. Zhu, M. Yudasaka, M. F. Zhang, S. Iijima, Dispersing carbon nanotubes in water: A noncovalent and nonorganic way. *J. Phys. Chem. B* **108**, 11317-11320 (2004).
69. S. H. Qin, D. Q. Qin, W. T. Ford, D. E. Resasco, J. E. Herrera, Functionalization of single-walled carbon nanotubes with polystyrene via grafting to and grafting from methods. *Macromolecules* **37**, 752-757 (2004).

70. J. C. Grunlan, A. R. Mehrabi, M. V. Bannon, J. L. Bahr, Water-based single-walled-nanotube-filled polymer composite with an exceptionally low percolation threshold. *Adv. Mater.* **16**, 150-153 (2004).
71. M. Zheng, E. D. Semke, Enrichment of single chirality carbon nanotubes. *J. Am. Chem. Soc.* **129**, 6084-6085 (2007).
72. G. Dukovic *et al.*, Racemic single-walled carbon nanotubes exhibit circular dichroism when wrapped with DNA. *J. Am. Chem. Soc.* **128**, 9004-9005 (2006).
73. S. G. Chou *et al.*, Optical characterization of DNA-wrapped carbon nanotube hybrids. *Chem. Phys. Lett.* **397**, 296-301 (2004).
74. M. Zheng *et al.*, Structure-based carbon nanotube sorting by sequence-dependent DNA assembly. *Science* **302**, 1545-1548 (2003).
75. D. A. Heller *et al.*, Optical detection of DNA conformational polymorphism on single-walled carbon nanotubes. *Science* **311**, 508-511 (2006).
76. G. R. Dieckmann *et al.*, Controlled assembly of carbon nanotubes by designed amphiphilic peptide helices. *J. Am. Chem. Soc.* **125**, 1770-1777 (2003).
77. M. Reches, E. Gazit, Formation of closed-cage nanostructures by self-assembly of aromatic dipeptides. *Nano Lett.* **4**, 581-585 (2004).
78. H. Xie *et al.*, Peptide cross-linking modulated stability and assembly of peptide-wrapped single-walled carbon nanotubes. *J. Mater. Chem.* **15**, 1734-1741 (2005).
79. A. B. Dalton *et al.*, Hierarchical self-assembly of peptide-coated carbon nanotubes. *Adv. Funct. Mater.* **14**, 1147-1151 (2004).
80. M. J. Pender, L. A. Sowards, J. D. Hartgerink, M. O. Stone, R. R. Naik, Peptide-mediated formation of single-wall carbon nanotube composites. *Nano Lett.* **6**, 40-44 (2006).
81. U. Kriplani, B. K. Kay, Selecting peptides for use in nanoscale materials using phagedisplayed combinatorial peptide libraries. *Curr. Opin. Biotechnol.* **16**, 470-475 (2005).
82. S. Q. Wang *et al.*, Peptides with selective affinity for carbon nanotubes. *Nat. Mater.* **2**, 196-200 (2003).

83. Z. D. Su, T. Leung, J. F. Honek, Conformational selectivity of peptides for single-walled carbon nanotubes. *J. Phys. Chem. B* **110**, 23623-23627 (2006).
84. F. Balavoine *et al.*, Helical crystallization of proteins on carbon nanotubes: A first step towards the development of new biosensors. *Angew. Chem. Int. Ed.* **38**, 1912-1915 (1999).
85. S. Boussaad, N. J. Tao, R. Zhang, T. Hopson, L. A. Nagahara, In situ detection of cytochrome c adsorption with single walled carbon nanotube device. *Chem. Commun.*, 1502-1503 (2003).
86. B. R. Azamian, J. J. Davis, K. S. Coleman, C. B. Bagshaw, M. L. H. Green, Bioelectrochemical single-walled carbon nanotubes. *J. Am. Chem. Soc.* **124**, 12664-12665 (2002).
87. Y. Lin, L. F. Allard, Y. P. Sun, Protein-affinity of single-walled carbon nanotubes in water. *J. Phys. Chem. B* **108**, 3760-3764 (2004).
88. A. Star, D. W. Steuerman, J. R. Heath, J. F. Stoddart, Starched carbon nanotubes. *Angew. Chem. Int. Ed.* **41**, 2508-2512 (2002).
89. O. K. Kim *et al.*, Solubilization of single-wall carbon nanotubes by supramolecular encapsulation of helical amylose. *J. Am. Chem. Soc.* **125**, 4426-4427 (2003).
90. M. Numata *et al.*, Inclusion of cut and as-grown single-walled carbon nanotubes in the helical superstructure of schizophyllan and curdlan (ss-1,3-glucans). *J. Am. Chem. Soc.* **127**, 5875-5884 (2005).
91. J. Chen, M. J. Dyer, M. F. Yu, Cyclodextrin-mediated soft cutting of single-walled carbon nanotubes. *J. Am. Chem. Soc.* **123**, 6201-6202 (2001).
92. T. Ogoshi, Y. Takashima, H. Yamaguchi, A. Harada, Chemically-responsive sol-gel transition of supramolecular single-walled carbon nanotubes (SWNTs) hydrogel made by hybrids of SWNTs and cyclodextrins. *J. Am. Chem. Soc.* **129**, 4878-+ (2007).
93. R. H. Baughman, A. A. Zakhidov, W. A. de Heer, Carbon nanotubes - the route toward applications. *Science* **297**, 787-792 (2002).

94. A. Bachtold, P. Hadley, T. Nakanishi, C. Dekker, Logic circuits with carbon nanotube transistors. *Science* **294**, 1317-1320 (2001).
95. R. Martel, T. Schmidt, H. R. Shea, T. Hertel, P. Avouris, Single- and multi-wall carbon nanotube field-effect transistors. *Appl. Phys. Lett.* **73**, 2447-2449 (1998).
96. P. Avouris, Molecular electronics with carbon nanotubes. *Acc. Chem. Res.* **35**, 1026-1034 (2002).
97. P. G. Collins, K. Bradley, M. Ishigami, A. Zettl, Extreme oxygen sensitivity of electronic properties of carbon nanotubes. *Science* **287**, 1801-1804 (2000).
98. J. Kong *et al.*, Nanotube molecular wires as chemical sensors. *Science* **287**, 622-625 (2000).
99. G. Gruner, Carbon nanotube transistors for biosensing applications. *Anal. Bioanal. Chem.* **384**, 322-335 (2006).
100. A. Star, J. C. P. Gabriel, K. Bradley, G. Gruner, Electronic detection of specific protein binding using nanotube FET devices. *Nano Lett.* **3**, 459-463 (2003).
101. H. R. Byon, H. C. Choi, Network single-walled carbon nanotube-field effect transistors (SWNT-FETs) with increased Schottky contact area for highly sensitive biosensor applications. *J. Am. Chem. Soc.* **128**, 2188-2189 (2006).
102. R. J. Chen *et al.*, An investigation of the mechanisms of electronic sensing of protein adsorption on carbon nanotube devices. *J. Am. Chem. Soc.* **126**, 1563-1568 (2004).
103. S. Takeda *et al.*, Detection of influenza virus hemagglutinin with randomly immobilized anti-hemagglutinin antibody on a carbon nanotube sensor. *J. Nanosci. Nanotechnol.* **7**, 752-756 (2007).
104. H. M. So *et al.*, Single-walled carbon nanotube biosensors using aptamers as molecular recognition elements. *J. Am. Chem. Soc.* **127**, 11906-11907 (2005).
105. A. Star *et al.*, Label-free detection of DNA hybridization using carbon nanotube network field-effect transistors. *Proc. Natl. Acad. Sci. USA* **103**, 921-926 (2006).

106. E. S. Jeng, A. E. Moll, A. C. Roy, J. B. Gastala, M. S. Strano, Detection of DNA hybridization using the near-infrared band-gap fluorescence of single-walled carbon nanotubes. *Nano Lett.* **6**, 371-375 (2006).
107. P. W. Barone, S. Baik, D. A. Heller, M. S. Strano, Near-infrared optical sensors based on single-walled carbon nanotubes. *Nat. Mater.* **4**, 86-92 (2005).
108. P. W. Barone, R. S. Parker, M. S. Strano, In vivo fluorescence detection of glucose using a single-walled carbon nanotube optical sensor: Design, fluorophore properties, advantages, and disadvantages. *Anal. Chem.* **77**, 7556-7562 (2005).
109. P. W. Barone, M. S. Strano, Reversible control of carbon nanotube aggregation for a glucose affinity sensor. *Angew. Chem. Int. Ed.* **45**, 8138-8141 (2006).
110. A. T. Woolley, C. L. Cheung, J. H. Hafner, C. M. Lieber, Structural biology with carbon nanotube AFM probes. *Chem. Biol.* **7**, R193-R204 (2000).
111. J. H. Hafner, C. L. Cheung, A. T. Woolley, C. M. Lieber, Structural and functional imaging with carbon nanotube AFM probes. *Prog. Biophys. Mol. Biol.* **77**, 73-110 (2001).
112. J. H. Hafner, C. L. Cheung, C. M. Lieber, Growth of nanotubes for probe microscopy tips. *Nature* **398**, 761-762 (1999).
113. C. L. Cheung, J. H. Hafner, C. M. Lieber, Carbon nanotube atomic force microscopy tips: Direct growth by chemical vapor deposition and application to high-resolution imaging. *Proc. Natl. Acad. Sci. USA* **97**, 3809-3813 (2000).
114. H. Nishijima *et al.*, Carbon-nanotube tips for scanning probe microscopy: Preparation by a controlled process and observation of deoxyribonucleic acid. *Appl. Phys. Lett.* **74**, 4061-4063 (1999).
115. J. Li, A. M. Cassell, H. J. Dai, Carbon nanotubes as AFM tips: Measuring DNA molecules at the liquid/solid interface. *Surf. Interface Anal.* **28**, 8-11 (1999).
116. A. T. Woolley, C. Guillemette, C. L. Cheung, D. E. Housman, C. M. Lieber, Direct haplotyping of kilobase-size DNA using carbon nanotube probes. *Nat. Biotechnol.* **18**, 760-763 (2000).

117. S. Carnally *et al.*, Ultra-resolution imaging of a self-assembling biomolecular system using robust carbon nanotube AFM probes. *Langmuir* **23**, 3906-3911 (2007).
118. S. S. Wong, J. D. Harper, P. T. Lansbury, C. M. Lieber, Carbon nanotube tips: High-resolution probes for imaging biological systems. *J. Am. Chem. Soc.* **120**, 603-604 (1998).
119. D. A. Heller, S. Baik, T. E. Eurell, M. S. Strano, Single-walled carbon nanotube spectroscopy in live cells: Towards long-term labels and optical sensors. *Adv. Mater.* **17**, 2793-2799 (2005).
120. P. Cherukuri, S. M. Bachilo, S. H. Litovsky, R. B. Weisman, Near-infrared fluorescence microscopy of single-walled carbon nanotubes in phagocytic cells. *J. Am. Chem. Soc.* **126**, 15638-15639 (2004).
121. T. K. Leeuw *et al.*, Single-walled carbon nanotubes in the intact organism: near-IR imaging and biocompatibility studies in *Drosophila*. *Nano Lett.* **7**, 2650-2654 (2007).
122. M. R. McDevitt *et al.*, PET Imaging of Soluble Yttrium-86-Labeled Carbon Nanotubes in Mice. *PLoS ONE* **2**, e907 (2007).
123. J. H. Choi *et al.*, Multimodal biomedical imaging with asymmetric single-walled carbon nanotube/iron oxide nanoparticle complexes. *Nano Lett.* **7**, 861-867 (2007).
124. D. A. Smith, H. van de Waterbeemd, Pharmacokinetics and metabolism in early drug discovery. *Curr. Opin. Chem. Biol.* **3**, 373-378 (1999).
125. Y. Y. Liu, H. Miyoshi, M. Nakamura, Nanomedicine for drug delivery and imaging: A promising avenue for cancer therapy and diagnosis using targeted functional nanoparticles. *Int. J. Cancer* **120**, 2527-2537 (2007).
126. C. C. Lee, J. A. MacKay, J. M. J. Frechet, F. C. Szoka, Designing dendrimers for biological applications. *Nat. Biotechnol.* **23**, 1517-1526 (2005).
127. D. Pantarotto, J. P. Briand, M. Prato, A. Bianco, Translocation of bioactive peptides across cell membranes by carbon nanotubes. *Chem. Commun.*, 16-17 (2004).

128. D. Pantarotto *et al.*, Functionalized carbon nanotubes for plasmid DNA gene delivery. *Angew. Chem. Int. Ed.* **43**, 5242-5246 (2004).
129. N. W. S. Kam, H. J. Dai, Carbon nanotubes as intracellular protein transporters: Generality and biological functionality. *J. Am. Chem. Soc.* **127**, 6021-6026 (2005).
130. K. Kostarelos *et al.*, Cellular uptake of functionalized carbon nanotubes is independent of functional group and cell type. *Nat. Nanotechol.* **2**, 108-113 (2007).
131. N. W. S. Kam, Z. A. Liu, H. J. Dai, Carbon nanotubes as intracellular transporters for proteins and DNA: An investigation of the uptake mechanism and pathway. *Angew. Chem. Int. Ed.* **45**, 577-581 (2006).
132. R. Singh *et al.*, Binding and condensation of plasmid DNA onto functionalized carbon nanotubes: Toward the construction of nanotube-based gene delivery vectors. *J. Am. Chem. Soc.* **127**, 4388-4396 (2005).
133. Y. Liu *et al.*, Polyethylenimine-grafted multiwalled carbon nanotubes for secure noncovalent immobilization and efficient delivery of DNA. *Angew. Chem. Int. Ed.* **44**, 4782-4785 (2005).
134. L. Z. Gao *et al.*, Carbon nanotube delivery of the GFP gene into mammalian cells. *Chembiochem* **7**, 239-242 (2006).
135. D. Cai *et al.*, Highly efficient molecular delivery into mammalian cells using carbon nanotube spearing. *Nat. Methods* **2**, 449-454 (2005).
136. W. Wu *et al.*, Targeted delivery of amphotericin B to cells by using functionalized carbon nanotubes. *Angew. Chem. Int. Ed.* **44**, 6358-6362 (2005).
137. Z. Yinghuai *et al.*, Substituted carborane-appended water-soluble single-wall carbon nanotubes: New approach to boron neutron capture therapy drug delivery. *J. Am. Chem. Soc.* **127**, 9875-9880 (2005).
138. N. W. S. Kam, M. O'Connell, J. A. Wisdom, H. J. Dai, Carbon nanotubes as multifunctional biological transporters and near-infrared agents for selective cancer cell destruction. *Proc. Natl. Acad. Sci. USA* **102**, 11600-11605 (2005).

139. N. W. S. Kam, H. J. Dai, Single walled carbon nanotubes for transport and delivery of biological cargos. *Phys. Status Solidi B* **243**, 3561-3566 (2006).
140. N. W. S. Kam, Z. Liu, H. J. Dai, Functionalization of carbon nanotubes via cleavable disulfide bonds for efficient intracellular delivery of siRNA and potent gene silencing. *J. Am. Chem. Soc.* **127**, 12492-12493 (2005).
141. Z. Liu, M. Winters, M. Holodniy, H. J. Dai, siRNA delivery into human T cells and primary cells with carbon-nanotube transporters. *Angew. Chem. Int. Ed.* **46**, 2023-2027 (2007).
142. D. J. Stephens, R. Pepperkok, The many ways to cross the plasma membrane. *Proc. Natl. Acad. Sci. USA* **98**, 4295-4298 (2001).
143. N. A. Kouklin, W. E. Kim, A. D. Lazareck, J. M. Xu, Carbon nanotube probes for single-cell experimentation and assays. *Appl. Phys. Lett.* **87**, 173901-173903 (2005).
144. I. U. Vakarelski, S. C. Brown, K. Higashitani, B. M. Moudgil, Penetration of living cell membranes with fortified carbon nanotube tips. *Langmuir* **23**, 10893-10896 (2007).
145. M. P. Mattson, R. C. Haddon, A. M. Rao, Molecular functionalization of carbon nanotubes and use as substrates for neuronal growth. *J. Mol. Neurosci.* **14**, 175-182 (2000).
146. H. Hu, Y. C. Ni, V. Montana, R. C. Haddon, V. Parpura, Chemically functionalized carbon nanotubes as substrates for neuronal growth. *Nano Lett.* **4**, 507-511 (2004).
147. H. Hu *et al.*, Polyethyleneimine functionalized single-walled carbon nanotubes as a substrate for neuronal growth. *J. Phys. Chem. B* **109**, 4285-4289 (2005).
148. T. Gabay, E. Jakobs, E. Ben-Jacob, Y. Hanein, Engineered self-organization of neural networks using carbon nanotube clusters. *Physica A* **350**, 611-621 (2005).
149. E. Jan, N. A. Kotov, Successful differentiation of mouse neural stem cells on layer-by-layer assembled single-walled carbon nanotube composite. *Nano Lett.* **7**, 1123-1128 (2007).

150. R. A. MacDonald, B. F. Laurenzi, G. Viswanathan, P. M. Ajayan, J. P. Stegemann, Collagen-carbon nanotube composite materials as scaffolds in tissue engineering. *J. Biomed. Mater. Res. Part A* **74A**, 489-496 (2005).
151. X. F. Shi *et al.*, Rheological behaviour and mechanical characterization of injectable poly(propylene fumarate)/single-walled carbon nanotube composites for bone tissue engineering. *Nanotechnology* **16**, S531-S538 (2005).
152. X. F. Shi *et al.*, Injectable nanocomposites of single-walled carbon nanotubes and biodegradable polymers for bone tissue engineering. *Biomacromolecules* **7**, 2237-2242 (2006).
153. B. Sitharaman *et al.*, Injectable in situ cross-linkable nanocomposites of biodegradable polymers and carbon nanostructures for bone tissue engineering. *J. Biomater. Sci., Polym. Ed.* **18**, 655-671 (2007).
154. A. Nel, T. Xia, L. Madler, N. Li, Toxic potential of materials at the nanolevel. *Science* **311**, 622-627 (2006).
155. G. Oberdorster, E. Oberdorster, J. Oberdorster, Nanotoxicology: An emerging discipline evolving from studies of ultrafine particles. *Environ. Health Perspectives* **113**, 823-839 (2005).
156. J. Muller, F. Huaux, D. Lison, Respiratory toxicity of carbon nanotubes: How worried should we be? *Carbon* **44**, 1048-1056 (2006).
157. S. Lanone, J. Boczkowski, Biomedical applications and potential health risks of nanomaterials: Molecular mechanisms. *Curr. Mol. Med.* **6**, 651-663 (2006).
158. C. W. Lam, J. T. James, R. McCluskey, S. Arepalli, R. L. Hunter, A review of carbon nanotube toxicity and assessment of potential occupational and environmental health risks. *Crit. Rev. Toxicol.* **36**, 189-217 (2006).
159. K. Donaldson *et al.*, Carbon nanotubes: A review of their properties in relation to pulmonary toxicology and workplace safety. *Toxicol. Sci.* **92**, 5-22 (2006).
160. L. Lacerda, A. Bianco, M. Prato, K. Kostarelos, Carbon nanotubes as nanomedicines: From toxicology to pharmacology. *Adv. Drug Deliv. Rev.* **58**, 1460-1470 (2006).

161. A. Helland, P. Wick, A. Koehler, K. Schmid, C. Som, Reviewing the environmental and human health knowledge base of carbon nanotubes. *Environ. Health Perspectives* **115**, 1125-1131 (2007).
162. A. A. Shvedova *et al.*, Exposure to carbon nanotube material: Assessment of nanotube cytotoxicity using human keratinocyte cells. *J. Toxicol. Environ. Health, Part A* **66**, 1909-1926 (2003).
163. N. A. Monteiro-Riviere, R. J. Nemanich, A. O. Inman, Y. Y. Y. Wang, J. E. Riviere, Multi-walled carbon nanotube interactions with human epidermal keratinocytes. *Toxicol. Lett.* **155**, 377-384 (2005).
164. D. X. Cui, F. R. Tian, C. S. Ozkan, M. Wang, H. J. Gao, Effect of single wall carbon nanotubes on human HEK293 cells. *Toxicol. Lett.* **155**, 73-85 (2005).
165. G. Jia *et al.*, Cytotoxicity of carbon nanomaterials: Single-wall nanotube, multi-wall nanotube, and fullerene. *Environ. Sci. Technol.* **39**, 1378-1383 (2005).
166. K. F. Soto, A. Carrasco, T. G. Powell, K. M. Garza, L. E. Murr, Comparative in vitro cytotoxicity assessment of some manufactured nanoparticulate materials characterized by transmission electron microscopy. *J. Nanoparticle Res.* **7**, 145-169 (2005).
167. S. K. Manna *et al.*, Single-walled carbon nanotube induces oxidative stress and activates nuclear transcription factor-kappa B in human keratinocytes. *Nano Lett.* **5**, 1676-1684 (2005).
168. M. Bottini *et al.*, Multi-walled carbon nanotubes induce T lymphocyte apoptosis. *Toxicol. Lett.* **160**, 121-126 (2006).
169. L. H. Ding *et al.*, Molecular characterization of the cytotoxic mechanism of multiwall carbon nanotubes and nano-onions on human skin fibroblast. *Nano Lett.* **5**, 2448-2464 (2005).
170. Y. Sato *et al.*, Influence of length on cytotoxicity of multi-walled carbon nanotubes against human acute monocytic leukemia cell line THP-I in vitro and subcutaneous tissue of rats in vivo. *Mol. BioSyst.* **1**, 176-182 (2005).
171. S. Garibaldi, C. Brunelli, V. Bavastrello, G. Ghigliotti, C. Nicolini, Carbon nanotube biocompatibility with cardiac muscle cells. *Nanotechnology* **17**, 391-397 (2006).

172. S. Fiorito, A. Serafino, F. Andreola, P. Bernier, Effects of fullerenes and single-wall carbon nanotubes on murine and human macrophages. *Carbon* **44**, 1100-1105 (2006).
173. A. V. Liopo, M. P. Stewart, J. Hudson, J. M. Tour, T. C. Pappas, Biocompatibility of native and functionalized single-walled carbon nanotubes for neuronal interface. *J. Nanosci. Nanotechnol.* **6**, 1365-1374 (2006).
174. V. E. Kagan *et al.*, Direct and indirect effects of single walled carbon nanotubes on RAW 264.7 macrophages: Role of iron. *Toxicol. Lett.* **165**, 88-100 (2006).
175. F. R. Tian, D. X. Cui, H. Schwarz, G. G. Estrada, H. Kobayashi, Cytotoxicity of single-wall carbon nanotubes on human fibroblasts. *Toxicol. in Vitro* **20**, 1202-1212 (2006).
176. S. Sarkar *et al.*, Analysis of stress responsive genes induced by single-walled carbon nanotubes in BJ foreskin cells. *J. Nanosci. Nanotechnol.* **7**, 584-592 (2007).
177. D. M. Brown *et al.*, An in vitro study of the potential of carbon nanotubes and nanofibres to induce inflammatory mediators and frustrated phagocytosis. *Carbon* **45**, 1743-1756 (2007).
178. M. Davoren *et al.*, In vitro toxicity evaluation of single walled carbon nanotubes on human A549 lung cells. *Toxicol. in Vitro* **21**, 438-448 (2007).
179. P. M. V. Raja *et al.*, Impact of carbon nanotube exposure, dosage and aggregation on smooth muscle cells. *Toxicol. Lett.* **169**, 51-63 (2007).
180. K. Pulskamp, S. Diabate, H. F. Krug, Carbon nanotubes show no sign of acute toxicity but induce intracellular reactive oxygen species in dependence on contaminants. *Toxicol. Lett.* **168**, 58-74 (2007).
181. A. Magrez *et al.*, Cellular toxicity of carbon-based nanomaterials. *Nano Lett.* **6**, 1121-1125 (2006).
182. Y. Zhu, T. C. Ran, Y. G. Li, J. X. Guo, W. X. Li, Dependence of the cytotoxicity of multi-walled carbon nanotubes on the culture medium. *Nanotechnology* **17**, 4668-4674 (2006).

183. A. Casey *et al.*, Probing the interaction of single walled carbon nanotubes within cell culture medium as a precursor to toxicity testing. *Carbon* **45**, 34-40 (2007).
184. P. Wick *et al.*, The degree and kind of agglomeration affect carbon nanotube cytotoxicity. *Toxicol. Lett.* **168**, 121-131 (2007).
185. C. M. Sayes *et al.*, Functionalization density dependence of single-walled carbon nanotubes cytotoxicity in vitro. *Toxicol. Lett.* **161**, 135-142 (2006).
186. H. Dumortier *et al.*, Functionalized carbon nanotubes are non-cytotoxic and preserve the functionality of primary immune cells. *Nano Lett.* **6**, 1522-1528 (2006).
187. A. D. Maynard *et al.*, Exposure to carbon nanotube material: Aerosol release during the handling of unrefined single-walled carbon nanotube material. *J. Toxicol. Environ. Health, Part A* **67**, 87-107 (2004).
188. A. Huczko, H. Lange, Carbon nanotubes: Experimental evidence for a null risk of skin irritation and allergy. *Fullerene Sci. Technol.* **9**, 247-250 (2001).
189. A. Huczko, H. Lange, E. Calko, H. Grubek-Jaworska, P. Droszcz, Physiological testing of carbon nanotubes: Are they asbestos-like? *Fullerene Sci. Technol.* **9**, 251-254 (2001).
190. A. Huczko *et al.*, Pulmonary toxicity of 1-D nanocarbon materials. *Fullerenes, Nanotubes, Carbon Nanostruct.* **13**, 141-145 (2005).
191. C. W. Lam, J. T. James, R. McCluskey, R. L. Hunter, Pulmonary toxicity of single-wall carbon nanotubes in mice 7 and 90 days after intratracheal instillation. *Toxicol. Sci.* **77**, 126-134 (2004).
192. A. A. Shvedova *et al.*, Unusual inflammatory and fibrogenic pulmonary responses to single-walled carbon nanotubes in mice. *Am. J. Physiol.* **289**, L698-L708 (2005).
193. D. B. Warheit *et al.*, Comparative pulmonary toxicity assessment of single-wall carbon nanotubes in rats. *Toxicol. Sci.* **77**, 117-125 (2004).
194. J. Muller *et al.*, Respiratory toxicity of multi-wall carbon nanotubes. *Toxicol. Appl. Pharmacol.* **207**, 221-231 (2005).

195. J. G. Li *et al.*, Comparative study of pathological lesions induced by multiwalled carbon nanotubes in lungs of mice by intratracheal instillation and inhalation. *Environ. Toxicol.* **22**, 415-421 (2007).
196. S. Koyama *et al.*, Role of systemic T-cells and histopathological aspects after subcutaneous implantation of various carbon nanotubes in mice. *Carbon* **44**, 1079-1092 (2006).
197. Z. Li *et al.*, Cardiovascular effects of pulmonary exposure to single-wall carbon nanotubes. *Environ. Health Perspectives* **115**, 377-382 (2007).
198. A. Radomski *et al.*, Nanoparticle-induced platelet aggregation and vascular thrombosis. *Br. J. Pharmacol.* **146**, 882-893 (2005).
199. J. M. Worle-Knirsch, K. Pulskamp, H. F. Krug, Oops they did it again! Carbon nanotubes hoax scientists in viability assays. *Nano Lett.* **6**, 1261-1268 (2006).
200. H. Wang *et al.*, Biodistribution of carbon single-wall carbon nanotubes in mice. *J. Nanosci. Nanotechol.* **4**, 1019-1024 (2004).
201. J. Guo, X. Zhang, Q. Li, W. Li, Biodistribution of functionalized multiwall carbon nanotubes in mice. *Nucl. Med. Biol.* **34**, 579-583 (2007).
202. R. Singh *et al.*, Tissue biodistribution and blood clearance rates of intravenously administered carbon nanotube radiotracers. *Proc. Natl. Acad. Sci. USA* **103**, 3357-3362 (2006).
203. P. Cherukuri *et al.*, Mammalian pharmacokinetics of carbon nanotubes using intrinsic near-infrared fluorescence. *Proc. Natl. Acad. Sci. USA* **103**, 18882-18886 (2006).
204. Z. Liu *et al.*, In vivo biodistribution and highly efficient tumour targeting of carbon nanotubes in mice. *Nat. Nanotechol.* **2**, 47-52 (2007).

Chapter 2: A cell nanoinjector based on carbon nanotubes*

Introduction

Technologies for introducing molecules into living cells are vital for probing the physical properties and biochemical interactions that govern the cell's behavior. The major challenge is to overcome the barrier imposed by the plasma membrane. This has been accomplished in a variety of ways, such as permeabilization of the membrane with lipids, electric currents, or pore-forming toxins, and physical penetration with a micropipette (i.e., microinjection) or microprojectile (*I*). Each method has its advantages and disadvantages, but one common liability is physical damage to the cell membrane.

To overcome this problem, we sought to develop an alternative method of intracellular delivery that combines the microinjection concept with emerging tools from nanotechnology. We envisioned a “nanoinjector” that would penetrate cell membranes with minimal perturbation, delivering cargo to the cell's interior with high spatial resolution (at the nanometer scale). The proposed technology comprised three essential components: a needle with nanoscale diameter, a manipulator with nanoscale resolution, and controllable loading and releasing of cargo. Here we report the construction and successful operation of a cell nanoinjector in which a single multi-walled carbon

* Andras Kis contributed to the work described in this chapter.

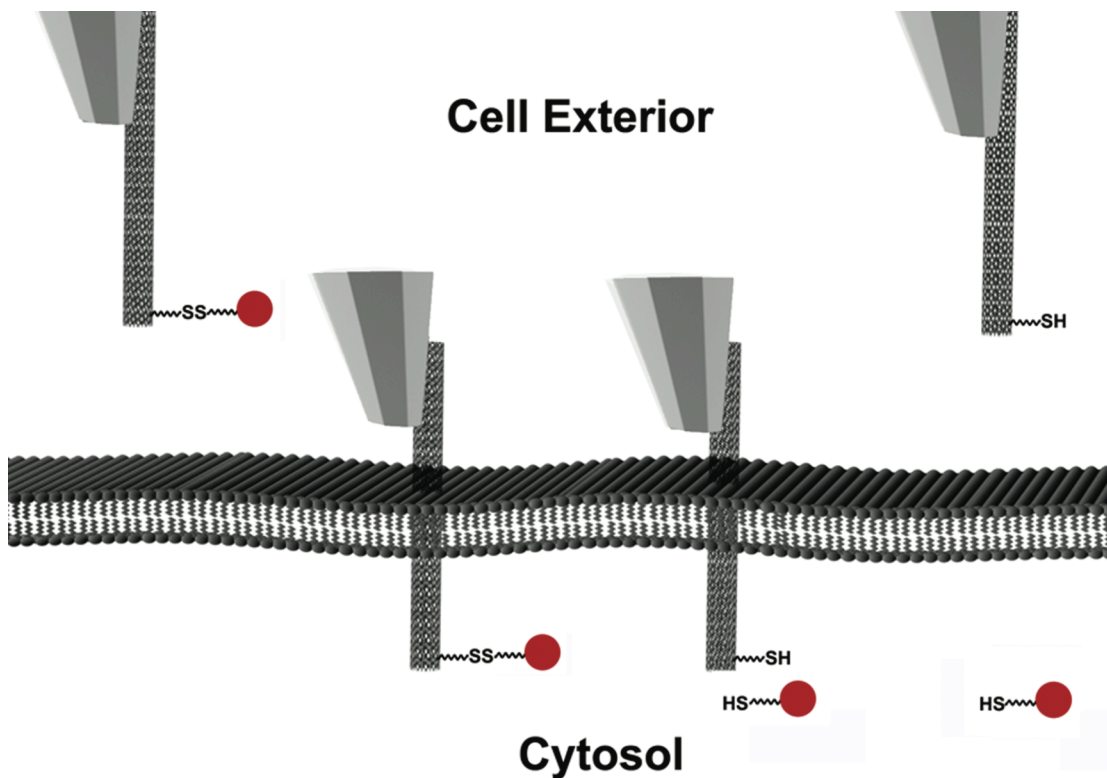


Figure 2.1. Schematic of the nanoinjection procedure: A MWNT-AFM tip with cargo attached to the MWNT surface via a disulfide linker penetrates a cell membrane. After disulfide reduction within the cell’s cytosol, the cargo is released and the nanoneedle is retracted.

nanotube (MWNT) attached to an atomic force microscope (AFM) tip served as the “nanoneedle” and an AFM integrated with an inverted fluorescence microscope served as the nanomanipulator (Fig. 2.1).

Results and discussion

Design and construction of a cell nanoinjector

With needle-like geometry, large Young’s modulus and high tensile strength (2, 3), carbon nanotubes (CNTs) are ideal nanoscale needles for this purpose. Their

diameters can be selected from a range of 1-20 nm, a scale that allows physical penetration of a cell's membrane without significant disruption of the cell's macrostructure. Indeed, such a piercing, which is on the scale of a single protein's diameter, should readily heal by lipid diffusion without perturbation of the cytoskeleton (4). Already, CNTs have demonstrated utility as cell transfection reagents and membrane penetrating delivery vehicles (5-8).

The nanomanipulation system was based on a commercially available AFM (MFP-3D-BIO™, Asylum Research, Santa Barbara, CA) that integrates an inverted fluorescence microscope (Nikon Eclipse TE2000-U). The AFM platform was ideal for this application, as it offers control of nanoneedle displacement at nanometer scale resolution and the ability to apply and monitor forces on the cell membrane. Thus, the AFM enabled precise positioning of the nanoneedle and high sensitivity monitoring of the membrane-piercing event.

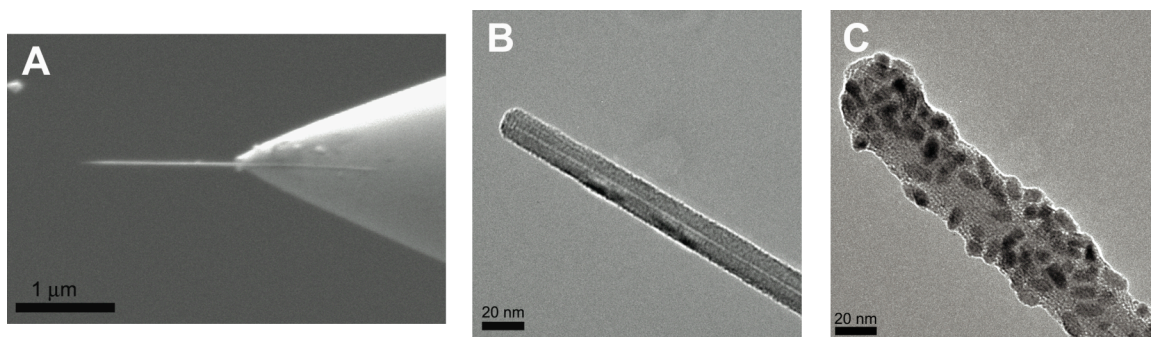


Figure 2.2. (A) SEM image of a MWNT-AFM tip. (B) TEM image of the tip region of (A). (C) TEM image of a MWNT-AFM tip coated with linker 1 and conjugated with QDot® Streptavidin.

The MWNT-AFM tips used in this work were fabricated as described previously (9). In brief, an individual MWNT of 10-20 nm in diameter was retrieved from a metal foil by the AFM tip using a nanomanipulator inside a scanning electron microscope (SEM). The MWNT was then cut to the desired length (0.5-1.5 μm) using an electron beam or electrical current. SEM and transmission electron microscopy (TEM) images of one representative MWNT-AFM tip are shown in Figures 2.2A and 2.2B, respectively.

For the controlled loading and release of cargo, we aimed to design a system that would obviate the need for a carrier solvent and, accordingly, the addition of excess volume to the cell's cytosol during the injection process. Toward this end, we exploited established chemical methods for CNT surface modification (10) and the intrinsic difference in redox potential between the intracellular and extracellular environments (11). Compound **1** (Fig. 2.3) fulfilled the functions of cargo loading and release as follows. Its pyrene moiety binds strongly to CNT surfaces via π - π stacking (12). Compound **1** is also endowed with a biotin moiety, separated from the pyrene group via a disulfide bond. In the relatively oxidizing environment of the cell's exterior, the disulfide is stable. However, once exposed to the reducing environment of the cytosol, the disulfide is cleaved, liberating attached cargo. The kinetics of disulfide bond cleavage within mammalian cells has been extensively studied, allowing prediction of release rates during the nanoinjection process (11, 13, 14).

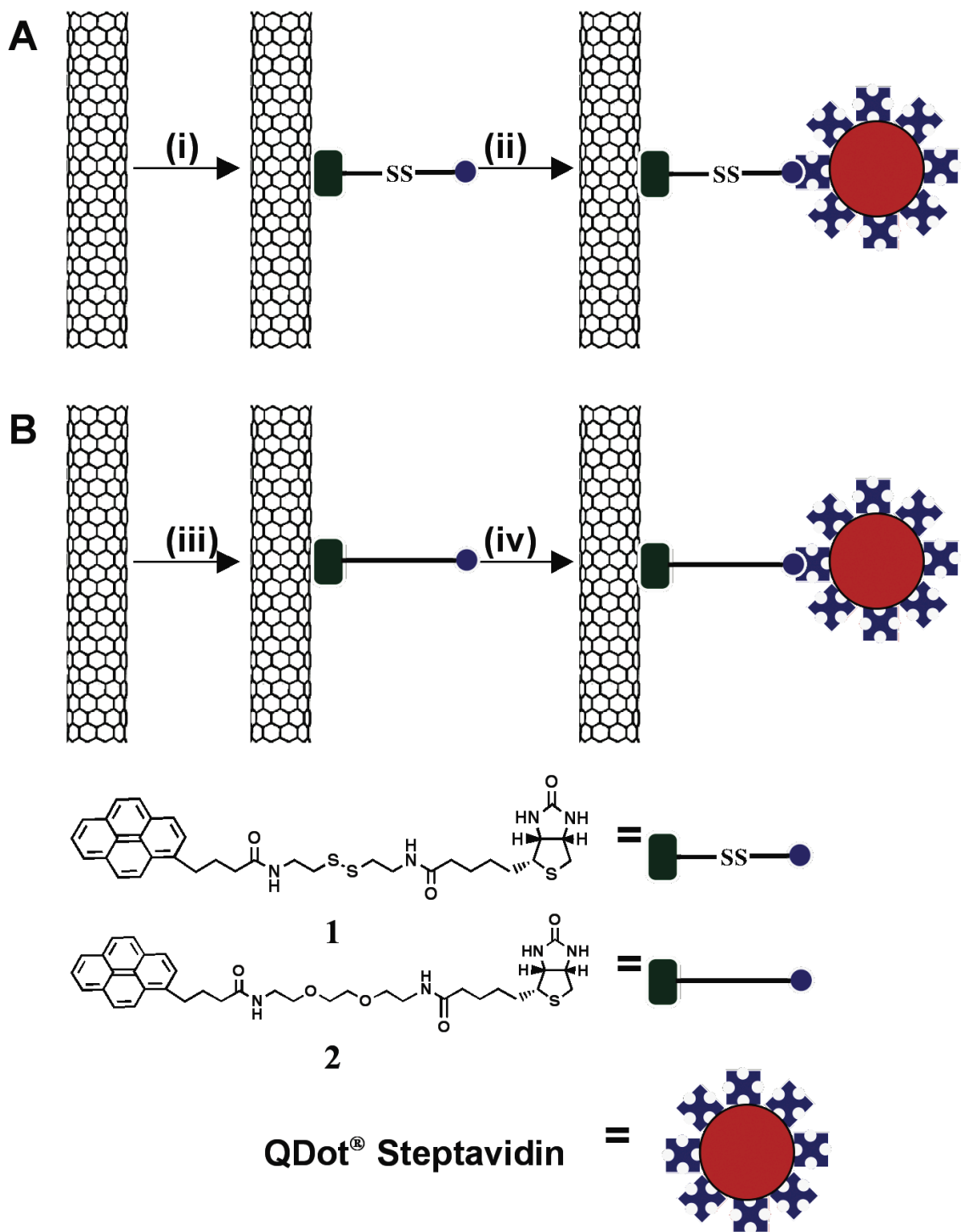


Figure 2.3. Functionalization of MWNT-AFM tips. **(A)** QDot® Streptavidin was attached to the MWNT surface through linker **1** containing a disulfide bond: (i) **1**, MeOH; (ii) QDot® Streptavidin, borate buffer. **(B)** QDot® Streptavidin was attached to the MWNT surface through linker **2** containing no disulfide bond: (iii) **2**, MeOH; (iv) QDot® Streptavidin, borate buffer.

Nanoinjection of quantum dots into HeLa cells

To demonstrate the function of the nanoinjector, we sought to deliver quantum dots to the cell's cytosol without concomitant membrane and cell damage, effects that are hard to avoid with conventional delivery technologies (1). Quantum dots have emerged as powerful optical probes for single particle and single molecule studies in cellular systems (15). Their bright fluorescence and resistance to photobleaching have enabled single-particle tracking of membrane proteins on the cell surface (16) and vesicles within cells (17). Without a delivery vehicle, quantum dots cannot access the cell's cytosol and nuclei. Accordingly, processes therein have been refractory to study using quantum dot technology.

We coated the MWNT-AFM tip with compound **1** by co-incubation in methanol. The tip was then loaded with streptavidin-coated quantum dots (QDot[®] Streptavidin, Invitrogen) via non-covalent complexation of streptavidin with biotin in borate buffer (Fig. 2.3A). The loaded MWNT-AFM tips were characterized by TEM. As shown in Fig. 2.2C, multiple QDot[®] Streptavidin conjugates were successfully loaded onto a single MWNT functionalized with compound **1** (up to several hundred per 1- μ M tip). In a control experiment, MWNT-AFM tips were incubated directly with QDot[®] Streptavidin without prior coating with compound **1**. In this case, no QDot[®] Streptavidin conjugates were observed on the MWNT surface (Fig. 2.4).

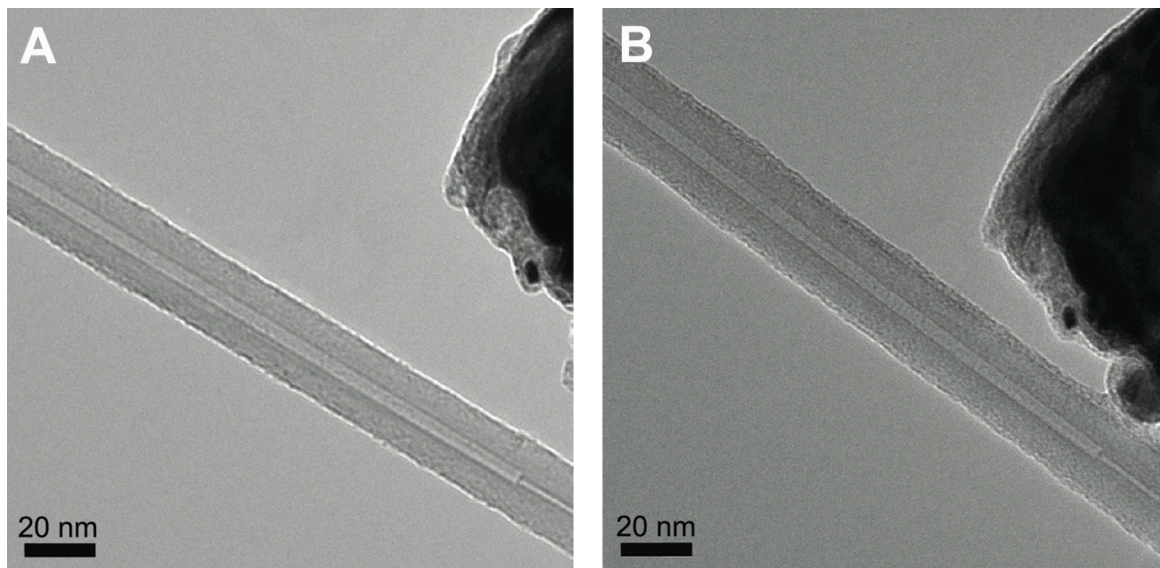


Figure 2.4. Control experiment: MWNT-AFM tips were incubated directly with QDot[®] Streptavidin without prior coating with linker **1**. **(A)** TEM image of a MWNT-AFM tip before incubation with QDot[®] Streptavidin conjugates. **(B)** TEM image of the MWNT-AFM tip after incubation with QDot[®] Streptavidin conjugates. In this case, no QDot[®] Streptavidin conjugates were observed on the MWNT surface. The dark shape is the AFM tip.

The nanoinjection experiments were then carried out using cultured HeLa cells, a human cervical epithelial cancer cell line. A target cell within the field of the optical microscope was identified, as indicated by the arrow in Figure 2.5B. The cantilever was then positioned on top of the target cell and the scan size was set to 0 nm. The deflection of the cantilever was measured with a photodiode to monitor the displacement of the nanoneedle as the MWNT-AFM tip approached the cell surface. After the MWNT came into contact with the cell, the cantilever was further lowered so that the MWNT nanoneedle penetrated the membrane. The MWNT nanoneedle was then maintained

inside the cell for various periods of time to allow reductive cleavage of disulfide bonds and release of QDot[®] Streptavidin conjugates. After injection, the cantilever was retracted and the cell was imaged by fluorescence microscopy.

As shown in Figure 2.5, fluorescence intensity inside the target cell indicated the release of quantum dots. QDot[®] Streptavidin conjugates were never observed in neighboring cells. We confirmed that the released quantum dots were within the cell's interior by video microscopy analysis. Their mobility was limited to the confines of the cell, where they exhibited slow diffusion and eventual immobilization, perhaps due to interactions with organelle membranes or cytoskeletal fibers.

In a typical experiment, a 15 to 30-minute incubation of the nanoneedle inside the cell was sufficient for release of a detectable number of quantum dots (Fig. 2.5). This observation is consistent with published disulfide reduction rates. Each quantum dot possesses ~15 streptavidin molecules and each streptavidin molecule can bind four biotin moieties. Therefore, the quantum dots are likely bound to MWNT surfaces via multiple disulfide bonds. The complete reduction of four disulfides within a protein molecule requires 15 minutes to 1 hour (13, 14), consistent with the release kinetics that we observe *in situ*. Based on fluorescence intensity calibration experiments using free quantum dots in solution, and the sensitivity of our fluorescence microscope, we estimate that the fluorescence intensity in Fig. 2.5 represents small clusters of quantum dots with a diameter of 50-100 nm (i.e., 5-50 quantum dots depending on their arrangement).

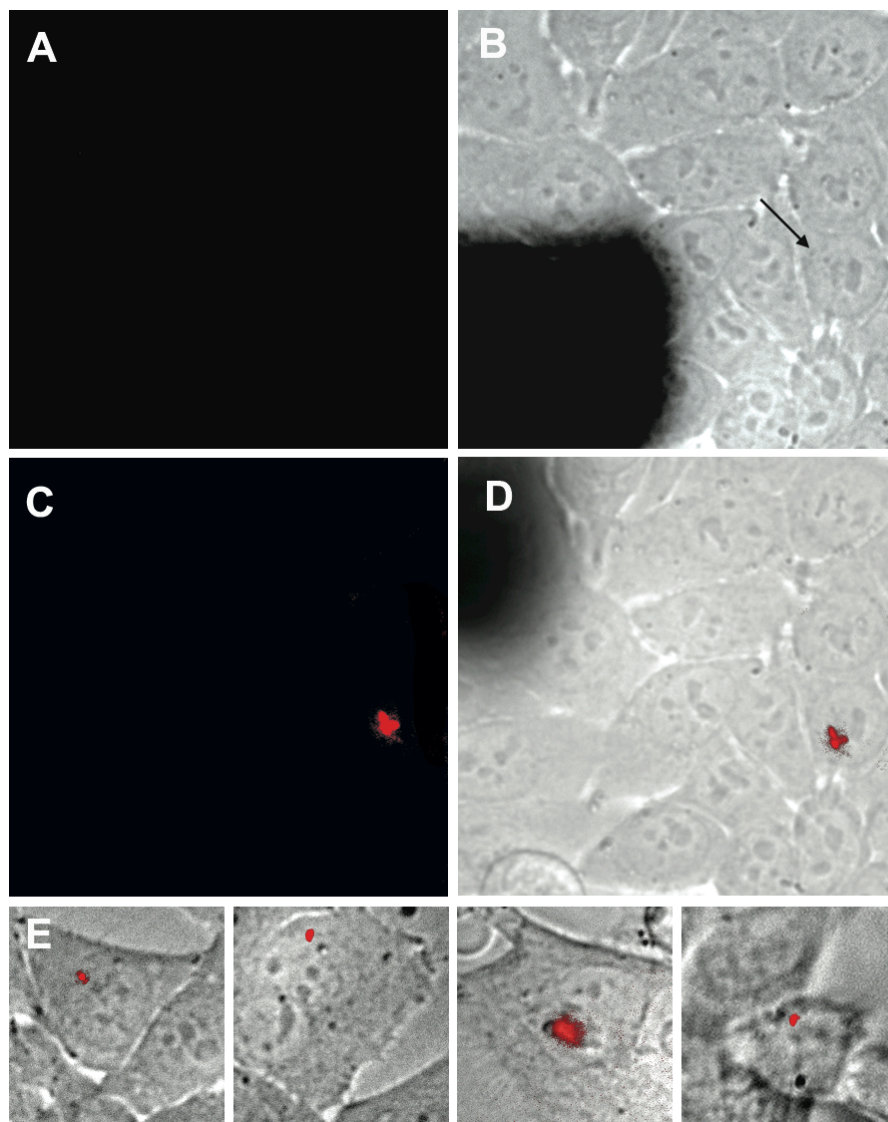


Figure 2.5. Nanoinjection of QDot[®] Streptavidin conjugates into a target HeLa cell. **(A)** Fluorescence image of the cells before nanoinjection. **(B)** Combined bright-field and fluorescence image of the cells before nanoinjection. The inserted arrow indicates the target cell. The dark shape in the lower left corner is the AFM cantilever. **(C)** Fluorescence image of the cells after the nanoinjection, showing fluorescent QDot[®] Streptavidin conjugates released inside the target cell. **(D)** Combined bright-field and fluorescence image of the cells after the nanoinjection. The QDot[®] Streptavidin conjugates are shown in red. The dark shape in the upper left corner is the retracted AFM cantilever. **(E)** Combined bright-field and fluorescence image of another four examples of HeLa cells after nanoinjection of QDot[®] Streptavidin. In all cases, fluorescence images were acquired with $\lambda_{\text{ex}} = 415 \text{ nm}$ and data collection with a 655 nm filter. Images are $70 \times 70 \mu\text{m}$ in (A)–(D) and $30 \times 30 \mu\text{m}$ in (E).

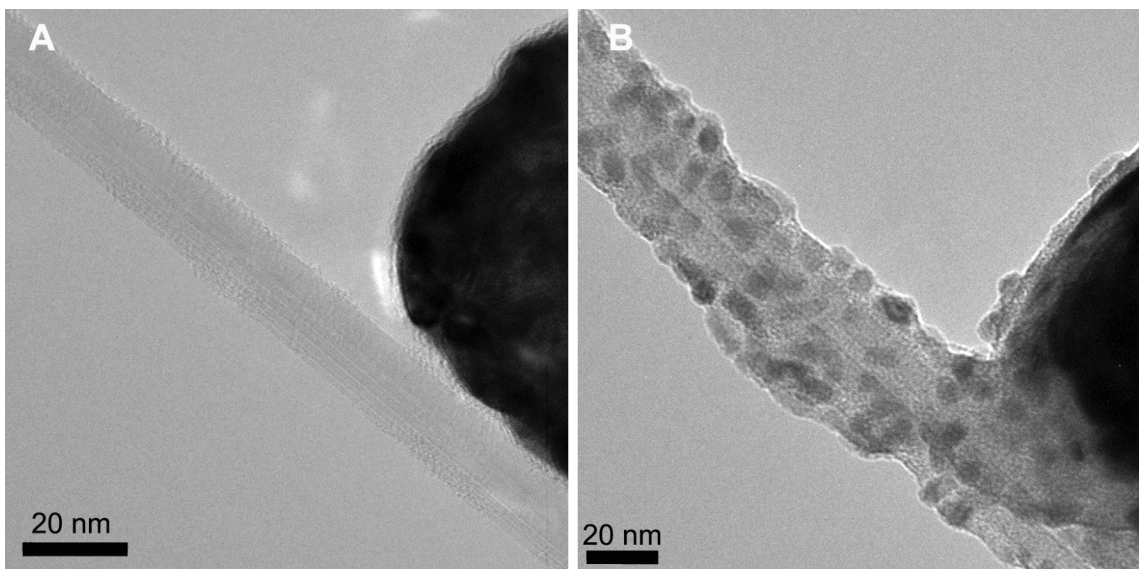


Figure 2.6. Functionalization of MWNT-AFM tips with QDot® Streptavidin conjugates via linker **2**. **(A)** TEM image of a MWNT-AFM tip before functionalization. **(B)** TEM image of the MWNT-AFM tip after functionalization with **2** and then conjugated with QDot® Streptavidin. The resulting MWNT-AFM tip appeared similar to MWNT-AFM tips bearing the disulfide-bound conjugates. The dark shape is the AFM tip.

To rule out the possibility that release of the QDot® Streptavidin conjugates occurred by desorption of the pyrene moiety from the MWNT surface rather than disulfide cleavage, we loaded cargo onto the MWNTs using control compound **2** (Fig. 2.3B). This linker possesses pyrene and biotin moieties, but replaces the disulfide bond with a polyethylene glycol (PEG) spacer separating the MWNT and streptavidin binding elements. We functionalized MWNT-AFM tips with **2** and then loaded QDot® Streptavidin conjugates onto the nanoneedle. The modified MWNT-AFM tips were analyzed by TEM and were similar to MWNT-AFM tips bearing the disulfide-bound conjugates (Fig. 2.6).

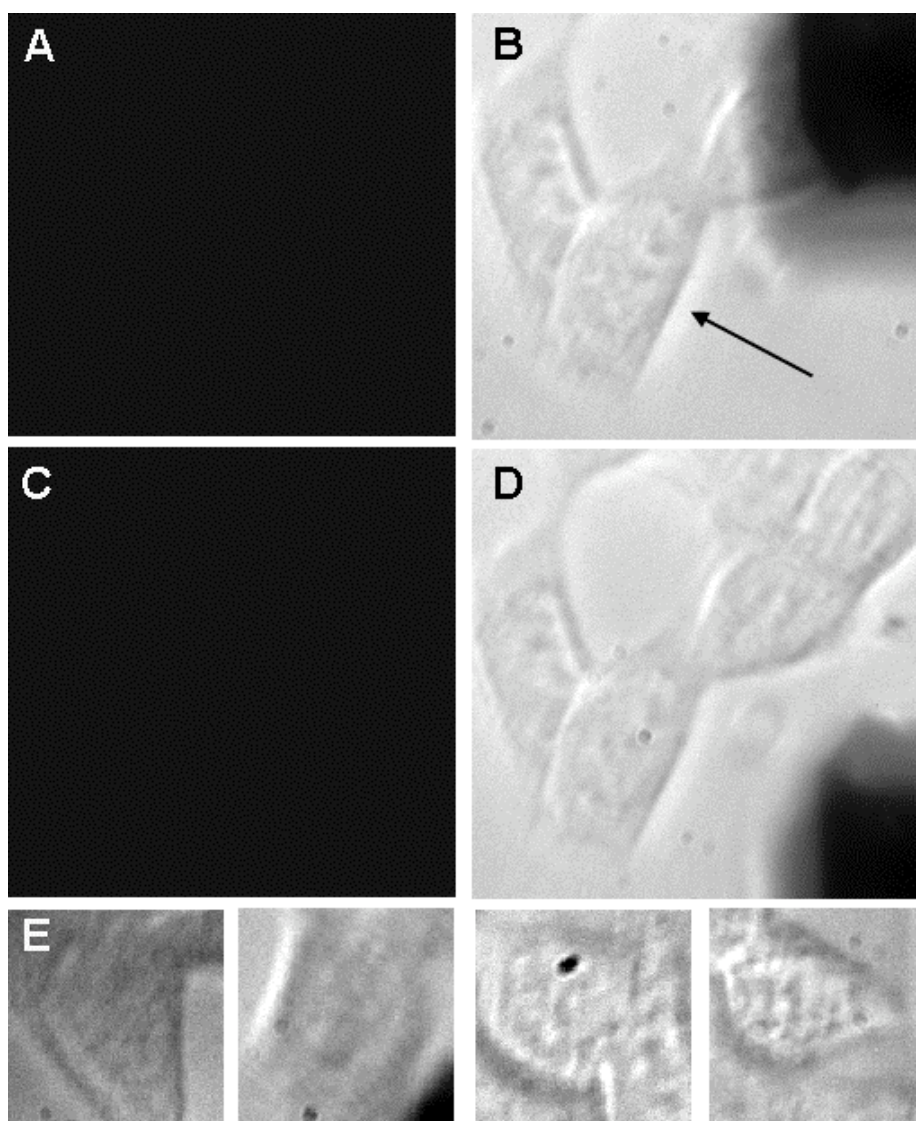


Figure 2.7. Control experiments: QDot[®] Streptavidin conjugates were loaded onto the MWNTs using linker **2**, which possesses pyrene and biotin moieties but lacks a disulfide bond. **(A)** Fluorescence image of the cells before nanoinjection. **(B)** Combined bright-field and fluorescence image of the cells before nanoinjection. The inserted arrow indicates the target cell. The dark shape in the upper right corner is the AFM cantilever. **(C)** Fluorescence image of the cells after the nanoinjection, showing no fluorescent QDot[®] Streptavidin conjugates released inside the target cell. **(D)** Combined bright-field and fluorescence image of the cells after the nanoinjection. No released QDot[®] Streptavidin conjugates were observed. The dark shape in the lower right corner is the retracted AFM cantilever. **(E)** Combined bright-field and fluorescence image of another four examples of HeLa cells after nanoinjection of QDot[®] Streptavidin, in none of which fluorescent QDot[®] Streptavidin conjugates were released. In all cases, fluorescence images were acquired with $\lambda_{\text{ex}} = 415 \text{ nm}$ and data collection with a 655 nm filter. Images are $70 \times 70 \mu\text{m}$ in (A)–(D) and $30 \times 30 \mu\text{m}$ in (E).

Similar nanoinjection experiments were carried out using HeLa cells but in this case no QDot[®] Streptavidin conjugates were released (with >5 different MWNT-AFM tips in >10 injection experiments) (Fig. 2.7). These results have two important implications. First, the release mechanism is dependent on disulfide bond cleavage and is therefore not simply due to desorption of the pyrene moiety from the MWNT surface. Second, the requirement of disulfide cleavage confirms that cargo release occurred within the reducing environment of the cytosol.

Cell viability after nanoinjection

A limitation of many intracellular delivery technologies is the harmful effects they exert on membranes and cells. Therefore, we probed the effects of nanoinjection on membrane integrity and cell viability using three assays: (i) the trypan blue exclusion assay (18), (ii) the Calcein AM assay (19), and (iii) the Annexin V-FITC/propidium iodide (PI) assay for apoptosis (20). In the trypan blue assay, the dye was added immediately after cell nanoinjection and the cells were monitored for 10 hours thereafter. No trypan blue inclusion or reduction in cell viability was observed during this time period (Table 2.1). In the Calcein AM assay, the cells were loaded with the fluorescent dye immediately prior to nanoinjection. Similar to the previous results, we saw no evidence of compromised membrane integrity for up to 10 hours (Fig. 2.8). Finally, nanoinjected cells showed no detectable staining with Annexin V-FITC or PI up to 10 hours after the event (Fig. 2.9). Thus, nanoinjection does not appear to induce apoptotic

pathways in the cells. In some experiments we held the nanoneedle inside the cell for > 1 hour without any visible effect on membrane integrity and cell viability. By contrast, a microinjection needle must typically be retracted within seconds of injection in order to avoid cell damage (21). Notably, the biocompatibility of nanoinjection should allow for exploration of a broad range of release chemistries that occur over extended time periods.

	Trypan blue test results
Cells after nanoinjection of the QDot [®] Streptavidin conjugates	Unstained (alive)
Cells penetrated with nanoneedle without loading of cargo	Unstained (alive)
Cells penetrated with nanoneedle loaded with QDot [®] Streptavidin conjugates using linker 2	Unstained (alive)
Positive control: cells penetrated with AFM tips with micron scale tip	Stained (dead)

Table 2.1. Trypan blue test of cells after nanoinjecton.

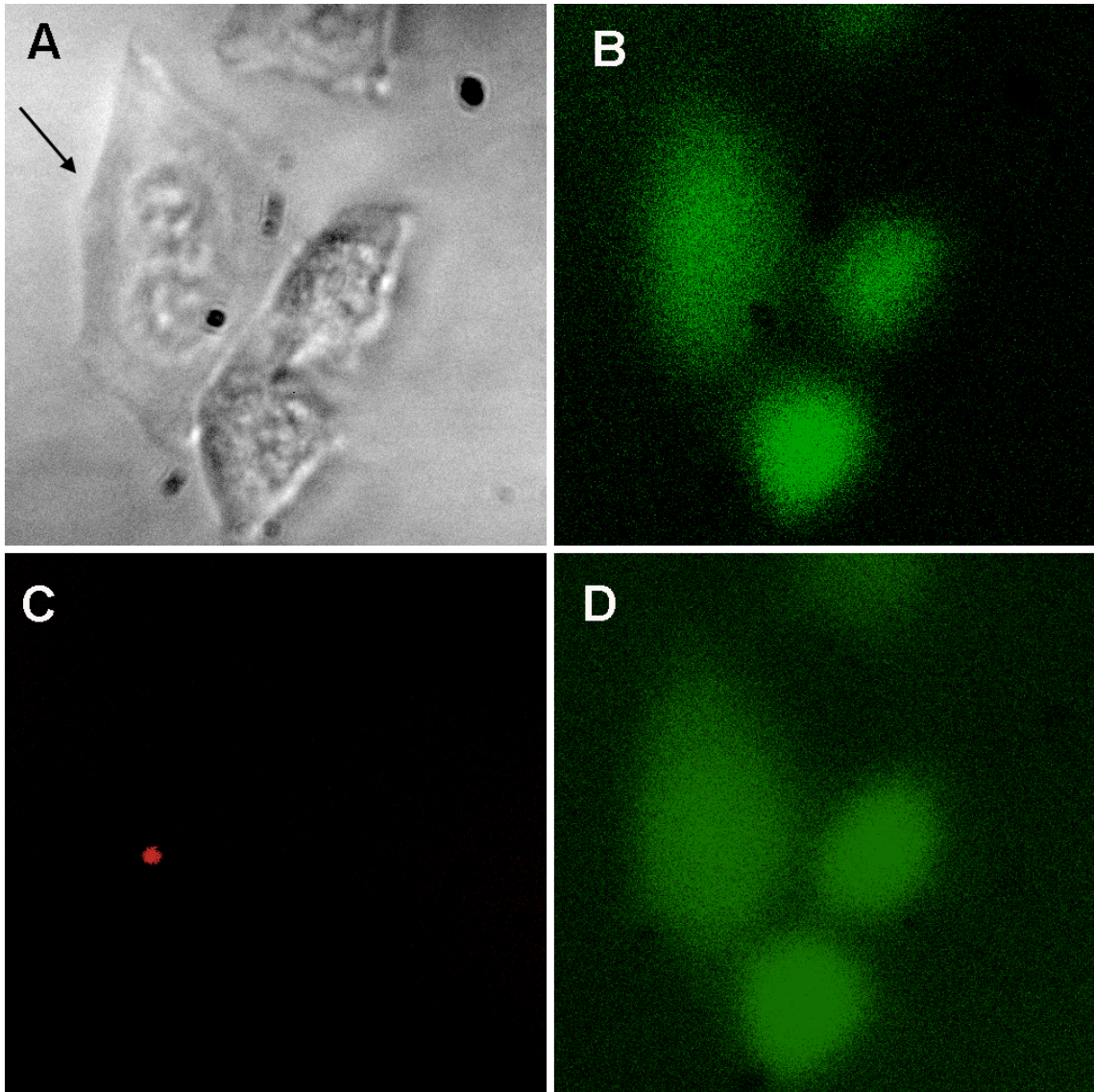


Figure 2.8. Calcein AM assay. **(A)** Bright-field image of the cells before nanoinjection. The inserted arrow indicates the target cell. **(B)** Fluorescence image (FITC filter set) of the cells before nanoinjection. The cells were loaded with Calcein AM and the green fluorescence indicates the viable cells. **(C)** Fluorescence image (Qdot-655 filter set) of the cells after the nanoinjection, showing fluorescent QDot[®] Streptavidin released inside the target cell. **(D)** Fluorescence image (FITC filter set) of the cells after the nanoinjection, in which no detectable loss in fluorescence was observed up to 10 hours after the injection.

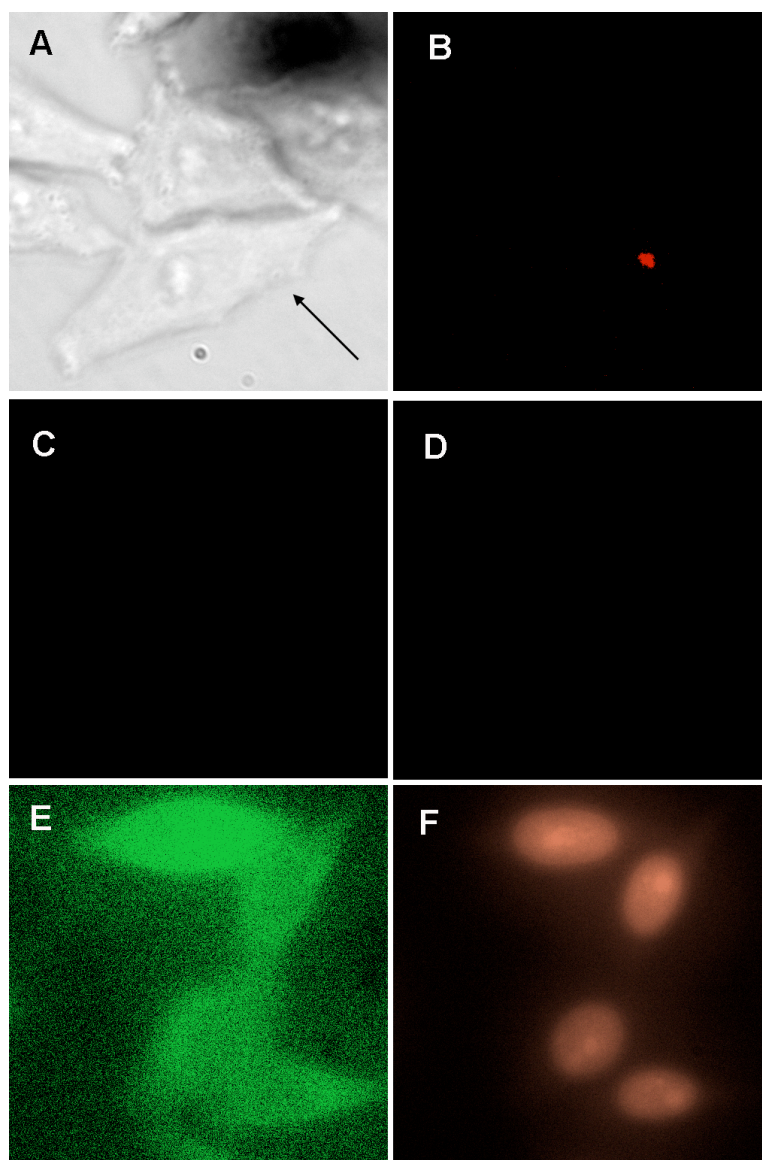


Figure 2.9. Annexin V-FITC/PI assay for apoptosis. **(A)** Bright-field image of the cells before nanoinjection. The inserted arrow indicates the target cell. **(B)** Fluorescence image (Qdot-655 filter set) of the cells after the nanoinjection, showing fluorescent QDot® Streptavidin released inside the target cell. **(C)** Fluorescence image (FITC filter set) of the cells before nanoinjection. The cell after nanoinjection did not stain with Annexin V-FITC, indicating nanoinjection did not induce apoptosis. **(D)** Fluorescence image (Rhodamine filter set) of the cells after the nanoinjection. No PI staining was observed up to 10 hours after the injection, indicating nanoinjection does not induce apoptosis. **(E)** and **(F)** Positive control: Apoptosis was induced by incubation with 5% ethanol for 60 min (E, F: FITC and Rhodamine filter sets, respectively).

Diffusion dynamics of injected quantum dots in the cytosol

The ability to deliver quantum dots to the cell's cytoplasm provides a platform for numerous studies of intracellular processes. As an example, we used the single-particle tracking technique (16, 17, 22) to characterize the diffusion dynamics of injected quantum dots in the cytosol, which has been previously studied using methods that can harm cells (23). After nanoinjection, the diffusion dynamics of cytosolic quantum dots were characterized by analyzing the mean square distance (Δr^2) and traveling time (Δt) for an injected quantum dot cluster (Fig. 2.10). The slope of the best-fit line afforded a diffusion coefficient of $0.3 \mu\text{m}^2/\text{sec}$. This value is approximately 10-fold lower than diffusion coefficients measured in pure water, which is consistent with previous measurements (23). A major advantage of the biocompatible nanoinjection technology is that the process can be performed repeatedly, or in tandem with other measurements, throughout the normal life cycle of the cell.

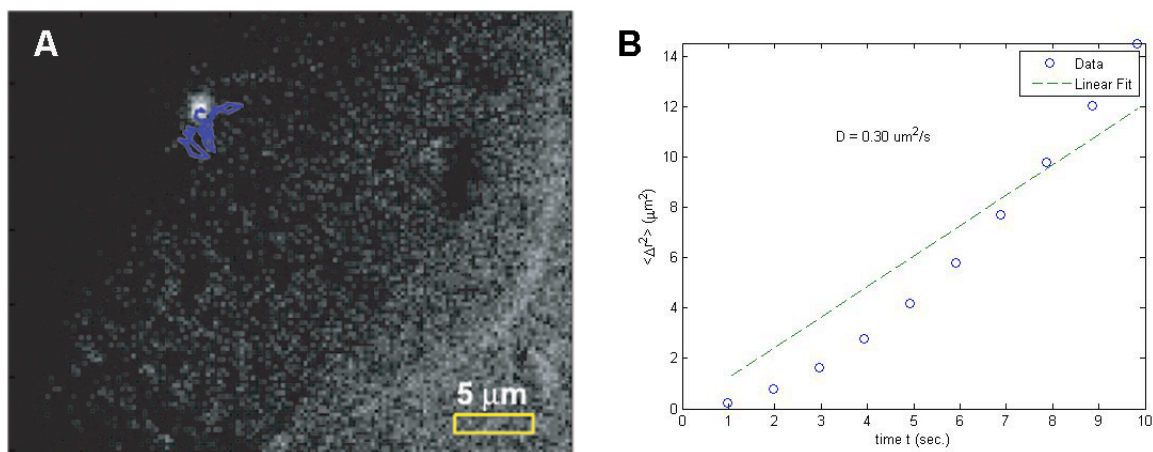


Figure 2.10. Tracking the movement of a quantum dot cluster in the cytosol. **(A)** A combined bright-field and fluorescence image of part of a HeLa cell with the trajectory of a quantum dot cluster indicated in blue. **(B)** The measured mean-square displacement versus time. The line is best fit to $\langle \Delta r^2 \rangle = 4D\Delta t$, where D is the diffusion coefficient.

Conclusions

In summary, the nanoinjector provides a fundamentally new mechanism for delivering a discrete, small number of molecules into cells without need for carrier solvent and with no apparent cell damage. The unique capabilities of the nanoinjector can be further exploited in a number of ways. Other biomolecules such as DNA and RNA, or synthetic structures such as polymers, dendrimers and nanoparticles can be delivered into cells in a similar fashion. In conjunction with organelle-specific optical probes, the nanoinjector concept might be extended to the delivery of cargo to specific subcellular compartments. In principle, cells such as bacteria that are too small for microinjection should be amenable to nanoinjection. Notably, the architecture of the nanoinjector allows the use of AFM to identify a target cell and position the nanoneedle, and is therefore not limited by the resolution of light microscopy.

Materials and methods

Fabrication of MWNT-AFM tips

The fabrication of MWNT-AFM tips was carried out in an FEI Sirion XL 30 SEM, equipped with a home-made manipulator. The procedure was described in detail in a previous publication (9).

SEM and TEM characterization

SEM images of MWNT-AFM tips were obtained on an FEI Sirion XL 30 SEM operated at 5 keV. TEM images of unfunctionalized and functionalized MWNT-AFM tips were obtained on a JEOL 2011 microscope operating at an electron energy of 100 keV. A homemade holder was used for loading MWNT-AFM tips.

Functionalization of MWNT-AFM tips

QDot[®] 655 Streptavidin conjugates (1 μ M solution, purchased from Invitrogen) were centrifuged at $5,000 \times g$, reserving the supernatant, prior to use. The MWNT-AFM tips were incubated with linker **1** or **2** (1 μ M, MeOH) at rt for 1 h, followed by washing 3 times with methanol and borate buffer (50 mM, pH = 8.3), respectively. The MWNT-AFM tips functionalized with **1** or **2** were then incubated with blocking buffer (borate buffer containing 1% BSA) for 30 min. The blocked MWNT-AFM tips were then transferred to a solution of QDot[®] 655 Streptavidin conjugates (1:25 dilution) in borate buffer and incubated at rt for 30 min, followed by washing with borate buffer for 3 times.

The functionalized MWNT-AFM tips were then used directly for nanoinjection experiments or dried under N₂ for TEM characterization. In a control experiment, the MWNT-AFM tips were incubated with blocking buffer for 30 min. The blocked MWNT-AFM tips were then transferred to a solution of QDot[®] 655 Streptavidin conjugates (1:25 dilution) in borate buffer and incubated at rt for 30 min, followed by washing 3 times with borate buffer. The MWNT-AFM tips were then dried under N₂ for TEM characterization.

Cell culture conditions

HeLa cells were grown in DMEM supplemented with penicillin (100 unit/mL), streptomycin (0.1 mg/mL), and 10% FCS and maintained in a 5% CO₂, water-saturated atmosphere at 37 °C.

Cell Viability Studies

The HeLa cells after nanoinjection were studied using three cell viability assays: trypan blue exclusion assay, Calcein AM assay, and Annexin V-FITC/propidium iodide assay. Trypan blue stain solution (0.4% in PBS buffer) was purchased from Invitrogen. Trypan blue is a vital dye. It is a negatively charged chromophore that only penetrates cells with damaged membranes. Immediately after nanoinjection, or penetration with nanoneedles, the cells were washed with serum-free medium. The dye was then added (0.08% in medium) and the cells were monitored for 10 hours thereafter.

Calcien acetoxymethylester (calcein AM) was purchased from Invitrogen. Calcein AM is the acetoxymethyl ester derivative of the fluorescent indicator calcein. Calcein AM is membrane-permeant and thus can be introduced into cells via co-incubation in media. Once inside the cells, calcein AM is hydrolyzed by endogenous esterases into the highly negatively charged green fluorescent dye calcein, which is retained in the cytoplasm. HeLa cells were incubated with calcein AM (2 μ M, PBS, 1% FBS) at room temperature for 1 hour. After washing with buffer, the cells were imaged by fluorescence microscopy. Nanoinjection was then performed on the target cell with calcien retained inside and the fluorescence was monitored during the injection and afterwards.

The annexin V-FITC/propidium iodide apoptosis detection kit was obtained from BD Biosciences. Cells undergoing apoptosis stain positively with annexin V-FITC but not with the vital dye propidium iodide (PI), whereas dead or necrotic cells stain with both annexin V-FITC and propidium iodide (PI). Immediately after nanoinjection or 2 hours after nanoinjection, the cells were incubated in the dark in 300 μ l of binding buffer containing 60 μ l of annexin V-FITC stock solution and 60 μ l of PI stock solution. The cells were monitored for 10 hours thereafter. In a positive control experiment, apoptosis was intentionally induced by incubation with 5% ethanol for 60 minutes.

Synthesis of new compounds

All chemical reagents were of analytical grade, obtained from commercial suppliers and used without further purification. Flash chromatography was performed using Merck 60Å 230-400 mesh silica gel. Analytical TLC was performed on Analtech Uniplate silica gel plates and visualized by staining with ceric ammonium molybdate or by absorbance of UV light at 254nm. ^1H NMR, and ^{13}C NMR spectra were obtained with Bruker AMX-400 or Bruker DRX-500 MHz spectrometers. ^1H and ^{13}C chemical shifts (δ) are reported in parts per million (ppm) referenced to TMS (0 ppm) and were measured relative to the residual solvent peak. Coupling constants (J) are reported in hertz (Hz). High-resolution fast atom bombardment (FAB) mass spectra were obtained at the UC Berkeley Mass Spectrometry Laboratory.

***N*-((pyren-1-yl)butanoyl)cystamine (3).** To a solution of cystamine dihydrochloride (1.00 g, 4.40 mmol) and 1-pyrenebutyric acid (1.27 g, 4.40 mmol) in 40 mL of anhydrous MeOH were added TBTU (2.80 g, 8.80 mmol), HOBt (0.890 g, 6.60 mmol), and triethylamine (1.82 mL, 13.2 mmol). The reaction mixture was stirred at rt overnight. The solvent was evaporated, and 1 M NaH₂PO₄ was added (10 mL, pH = 4.2). The aqueous was washed with ether. The aqueous solution was then basified to pH = 9 by 10 M NaOH and extracted with EtOAc (5 mL x 6). The combined organic phases were dried over MgSO₄, filtered, and concentrated. The resulting residue was purified by silica gel chromatography eluted with MeOH:CH₂Cl₂ (1:4) to give the product (950 mg, 51%). R_f = 0.40 (MeOH:CH₂Cl₂ = 1:4). ¹H NMR (CD₃OD, 400 MHz) δ 8.13 (d, *J* = 9.3 Hz, 1 H), 8.02 (d, *J* = 7.5 Hz, 2H), 7.94 (d, *J* = 8.4 Hz, 2 H), 7.84-7.76 (m, 3 H), 7.70 (d, *J* = 7.8 Hz, 1 H), 3.43 (t, *J* = 6.6 Hz, 2 H), 3.20 (t, *J* = 7.5 Hz, 2 H), 2.8 (t, *J* = 6.3 Hz, 2 H), 2.71 (t, *J* = 6.6 Hz, 2 H), 2.65 (t, *J* = 6.3 Hz, 2 H), 2.25 (t, *J* = 7.2 Hz, 2 H), 2.10-1.98 (m, 2 H). ¹³C NMR (CD₃OD, 100 MHz) δ 176.0, 137.3, 132.8, 132.3, 131.3, 129.9, 128.6, 128.5, 128.4, 127.7, 127.0, 126.2, 126.1, 126.0, 125.8, 124.4, 41.8, 41.2, 39.6, 38.6, 36.8, 33.8, 29.0. FAB-HRMS calcd for C₂₄H₂₇N₂OS₂ [MH]⁺: *m/z* 423.1565; found 423.1562.

***N*-((pyren-1-yl)butanoyl)-*N'*-(biotinyl)cystamine (1).** To a solution of biotin *N*-hydroxysuccinimide (290 mg, 0.850 mmol) in 4 mL of DMF were added *N*-((pyren-1-yl)butanoyl)cystamine (360 mg, 0.850 mmol), and triethylamine (0.350 mL, 2.55 mmol). The reaction mixture was stirred at rt for 7 h. DMF was then removed under high

vacuum. The resulting residue was purified by silica gel column chromatography eluting with MeOH:CH₂Cl₂ (1:9) to give the product (520 mg, 94%). R_f = 0.64 (MeOH:CH₂Cl₂ = 1:4). ¹H NMR (CDCl₃ + CD₃OD₃, 500 MHz) δ 8.14 (d, *J* = 9.0 Hz, 1 H), 8.04-7.98 (m, 2 H), 7.96 (d, *J* = 8.0 Hz, 2 H), 7.89-7.81 (m, 3 H), 7.72 (d, *J* = 7.5, 1 H), 4.22-4.17 (m, 1 H), 3.99-3.93 (m, 1 H), 3.37 (t, *J* = 6.5 Hz, 2 H), 3.33 (t, *J* = 6.6 Hz, 2 H), 3.27-3.23 (m, 2H), 2.82-2.77 (m, 1 H), 2.68-2.63 (m, 4 H), 2.61 (dd, *J* = 12.5, 4.5 Hz, 1 H), 2.50 (d, *J* = 12.5 Hz, 1 H), 2.22 (t, *J* = 7.5 Hz, 2 H), 2.11-1.98 (m, 4 H), 1.49-1.35 (m, 4 H), 1.21-1.09 (m, 2 H). ¹³C NMR (CDCl₃ + CD₃OD, 125 MHz) δ 174.5, 174.2, 164.0, 135.9, 131.3, 130.8, 129.9, 128.6, 127.4, 127.3, 126.7, 125.9, 125.0, 124.8(9), 124.8(6), 124.8, 124.7, 123.3, 62.0, 60.3, 55.4, 53.4, 40.1, 38.4, 38.3, 37.7, 37.5, 35.8, 35.5, 32.8, 28.2, 27.9, 27.5, 25.4. FAB-HRMS calcd for C₃₄H₄₁N₄O₃S₃ [MH]⁺: *m/z* 649.2341; found 649.2323.

***N*-(pyren-1-yl)butanoyl-*N'*-biotinyl-3,6-dioxaoctane-1,8-diamine (2).** To a solution of 1-pyrenebutyric acid *N*-hydroxysuccinimide (55.0 mg, 0.140 mmol) in 2 mL of DMF were added EZ-Link[®] Biotin-PEG₂-Amine (Pierce, IL) (50.0 mg, 0.130 mmol), and triethylamine (20.0 μL, 0.140 mmol). The reaction mixture was stirred at rt for 5 h. DMF was then removed under high vacuum. The resulting residue was purified by silica gel column chromatography eluting with MeOH:CH₂Cl₂ (15:85) to give the product (75.0 mg, 89%). R_f = 0.62 (MeOH:CH₂Cl₂ = 1:4). ¹H NMR (CDCl₃, 400 MHz) δ 8.25 (d, *J* = 9.2 Hz, 1 H), 8.11 (dd, *J* = 7.6, 2.4 Hz, 2 H), 8.05 (d, *J* = 8.8 Hz, 2 H), 7.97-7.92 (m, 3 H), 7.81 (d, *J* = 7.6, 1 H), 6.67 (br, 2 H, NH), 6.57 (br, 1 H, NH), 5.72 (br, 1 H, NH), 4.21-4.18 (m, 1 H), 3.96-3.93 (m, 1 H), 3.50-3.27 (m, 14 H), 2.84-2.78 (m, 1 H), 2.63

(dd, $J = 12.8, 4.4$ Hz, 1 H), 2.56 (d, $J = 11.6$ Hz, 1 H), 2.28 (t, $J = 7.2$, 2 H), 2.19-2.13 (m, 2 H), 2.08 (t, $J = 7.2$, 2 H), 1.58-1.43 (m, 4 H), 1.28-1.17 (m, 2 H). ^{13}C NMR (CDCl_3 , 100 MHz) δ 173.6, 173.3, 164.4, 136.2, 131.5, 131.0, 130.0, 128.9, 127.7, 127.6, 127.5, 126.8, 126.1, 125.2, 125.1, 125.0, 125.9, 123.6, 70.2, 70.1, 70.0, 69.9, 61.8, 60.3, 55.7, 50.8, 40.5, 39.4, 39.2, 36.0, 32.9, 28.3, 28.1, 27.6, 25.7. FAB-HRMS calcd for $\text{C}_{36}\text{H}_{45}\text{N}_4\text{O}_5\text{S}$ $[\text{MH}]^+$: m/z 645.3111; found 645.3092.

References

1. D. J. Stephens, R. Pepperkok, The many ways to cross the plasma membrane. *Proc. Natl. Acad. Sci. USA* **98**, 4295-4298 (2001).
2. M. F. Yu, B. S. Files, S. Arepalli, R. S. Ruoff, Tensile loading of ropes of single wall carbon nanotubes and their mechanical properties. *Phys. Rev. Lett.* **84**, 5552-5555 (2000).
3. M. F. Yu *et al.*, Strength and breaking mechanism of multiwalled carbon nanotubes under tensile load. *Science* **287**, 637-640 (2000).
4. G. Vereb *et al.*, Dynamic, yet structured: The cell membrane three decades after the Singer-Nicolson model. *Proc. Natl. Acad. Sci. USA* **100**, 8053-8058 (2003).
5. D. Pantarotto *et al.*, Functionalized carbon nanotubes for plasmid DNA gene delivery. *Angew. Chem. Int. Ed.* **43**, 5242-5246 (2004).
6. D. Cai *et al.*, Highly efficient molecular delivery into mammalian cells using carbon nanotube spearing. *Nat. Methods* **2**, 449-454 (2005).
7. N. W. S. Kam, M. O'Connell, J. A. Wisdom, H. J. Dai, Carbon nanotubes as multifunctional biological transporters and near-infrared agents for selective cancer cell destruction. *Proc. Natl. Acad. Sci. USA* **102**, 11600-11605 (2005).
8. N. A. Kouklin, W. E. Kim, A. D. Lazareck, J. M. Xu, Carbon nanotube probes for single-cell experimentation and assays. *Appl. Phys. Lett.* **87**, 173901-173903 (2005).
9. J. Martinez *et al.*, Length control and sharpening of atomic force microscope carbon nanotube tips assisted by an electron beam. *Nanotechnology* **16**, 2493-2496 (2005).
10. Y. Lin *et al.*, Advances toward bioapplications of carbon nanotubes. *J. Mater. Chem.* **14**, 527-541 (2004).
11. G. Saito, J. A. Swanson, K. D. Lee, Drug delivery strategy utilizing conjugation via reversible disulfide linkages: role and site of cellular reducing activities. *Adv. Drug Deliv. Rev.* **55**, 199-215 (2003).

12. R. J. Chen, Y. Zhang, D. Wang, H. Dai, Noncovalent sidewall functionalization of single-walled carbon nanotubes for protein immobilization. *J. Am. Chem. Soc.* **123**, 3838-3839 (2001).
13. M. Z. Atassi, A. F. Habeeb, L. Rydstedt, Lack of immunochemical cross-reaction between lysozyme and alpha-lactalbumin and comparison of their conformations. *Biochim. Biophys. Acta* **200**, 184-187 (1970).
14. K. S. Iyer, W. A. Klee, Direct Spectrophotometric Measurement of Rate of Reduction of Disulfide Bonds - Reactivity of Disulfide Bonds of Bovine Alpha-Lactalbumin. *J. Biol. Chem.* **248**, 707-710 (1973).
15. X. Michalet *et al.*, Quantum dots for live cells, in vivo imaging, and diagnostics. *Science* **307**, 538-544 (2005).
16. M. Dahan *et al.*, Diffusion dynamics of glycine receptors revealed by single-quantum dot tracking. *Science* **302**, 442-445 (2003).
17. X. L. Nan, P. A. Sims, P. Chen, X. S. Xie, Observation of individual microtubule motor steps in living cells with endocytosed quantum dots. *J. Phys. Chem. B* **109**, 24220-24224 (2005).
18. A. P. Arrigo *et al.*, Cytotoxic effects induced by oxidative stress in cultured mammalian cells and protection provided by Hsp27 expression. *Methods* **35**, 126-138 (2005).
19. D. Bratosin, L. Mitrofan, C. Paliu, J. Estaquier, J. Montreuil, Novel fluorescence assay using calcein-AM for the determination of human erythrocyte viability and aging. *Cytometry A* **66**, 78-84 (2005).
20. A. Moore, C. J. Donahue, K. D. Bauer, J. P. Mather, Simultaneous measurement of cell cycle and apoptotic cell death. *Methods Cell Biol.* **57**, 265-278 (1998).
21. J. C. Lacal, R. Perona, J. Feramisco, *Microinjection* (Birkhauser Verlag, 1999).
22. H. P. Babcock, C. Chen, X. W. Zhuang, Using single-particle tracking to study nuclear trafficking of viral genes. *Biophys. J.* **87**, 2749-2758 (2004).
23. K. Luby-Phelps, Cytoarchitecture and physical properties of cytoplasm: volume, viscosity, diffusion, intracellular surface area. *Int. Rev. Cytol.* **192**, 189-221 (2000).

Chapter 3: Biomimetic functionalization of carbon nanotubes using cell surface mucin mimics*

Introduction

One of the most exciting applications of nanoscale science and technology is in the exploration of biological systems (1, 2). Already, novel nanomaterials such as nanocrystals (3-8), nanowires (9, 10), and nanotubes (11-13) have proven capable of biological sensing and imaging. Because of their unique structural, mechanical, and electrical properties, carbon nanotubes (CNTs) have shown the potential for biosensing (14-16), imaging (17), intracellular delivering (18-20), and cancer cell targeting (21). However, two major roadblocks in these efforts have been the insolubility of CNTs in aqueous environment and their intrinsic toxicity. The aqueous environment required of biological materials cannot be inhabited by unfunctionalized CNTs. The surface of CNTs is hydrophobic and prone to non-specific bioadsorption, with biological components such as cells and proteins. Moreover, the inherent cytotoxicity of CNTs has imposed severe limitations on their use in biological systems (22-27).

In Nature, cells are faced with the similar challenge of resisting non-specific biomolecule interactions while engaging in specific molecular recognition. These

* Goo Soo Lee, Un Chong Tam, Jennifer L. Czapinski, and David Rabuka contributed to the work described in this chapter.

functions can be simultaneously fulfilled by mucin glycoproteins, defined by their dense clusters of *O*-linked glycans (28, 29). Here we describe a biomimetic surface modification of CNTs using glycosylated polymers designed to mimic natural cell surface mucins. The mucin mimic polymer contained a C₁₈ lipid tail for binding to CNT surface via hydrophobic interaction. The mucin mimic-coated CNTs were soluble in water, resisted non-specific protein binding, and bound specifically to biomolecules via receptor-ligand interactions. Furthermore, the coated CNTs were capable of interfacing with living cells via specific carbohydrate receptors. Whereas unmodified CNTs induced cell death, the functionalized CNTs were found to be nontoxic. This strategy for biomimetic surface engineering provides a means to bridge nanomaterials and biological systems.

Results and discussion

Design and synthesis of mucin mimic polymers

Mucins coat the surfaces of numerous cell types (28) and present epitopes for receptor-mediated cell-cell recognition (29). Their dense glycosylation confers rigidity to the polypeptide backbone and thereby extends the mucin polymer well above the cell surface (30). In addition, the glycans provide for strong hydration and passivation against biofouling. We have recently developed glycosylated polymers that share many properties with natural mucins (Fig. 3.1) (31). In native mucins, the clustered peptide-proximal α -*N*-acetylgalactosamine (α -GalNAc) residues are the major contributors to

peptide backbone rigidification. Although the core α -GalNAc residue is usually elaborated with additional sugars, removal of those sugars does not affect mucin architecture (32, 33). The importance of the α -GalNAc residue for mucin structure has also been suggested by NMR analysis of synthetic glycopeptides (34). Accordingly, we designed a synthetically tractable mucin mimic in which α -GalNAc residues were linked via an oxime bond to a poly(methyl vinyl ketone) [poly(MVK)] backbone (Fig. 3.1A). The synthesis involved chemoselective ligation of poly(MVK) with an aminoxy-functionalized GalNAc analog (35). Light scattering analysis indicated that the α -GalNAc-conjugated polymers adopt a rigid extended structure in water, similar to native mucin, whereas the unconjugated polymers adopt a more conventional globular structure (31).

In this work, we introduced a C_{18} lipid at one end of a mucin mimic polymer of molecular weight $\sim 75,000$ g/mol to enable surface modification of CNTs (Fig. 3.1B). The hydrated diameter of the lipid-terminated mucin mimic was determined by light scattering analysis to be ~ 54 nm. Lipids are known to self-assemble on the surface of CNTs via hydrophobic interactions in the presence of water (36). In addition, lipid-functionalized glycopolymers have been shown to form ordered arrays on graphite surfaces (37).

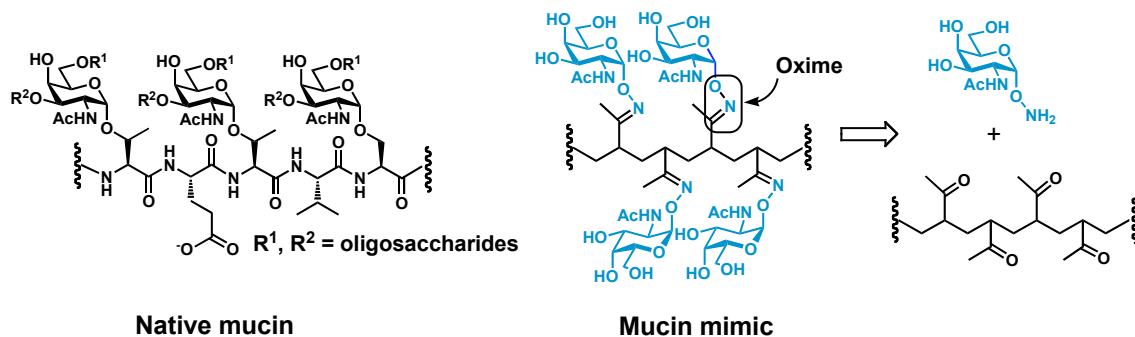
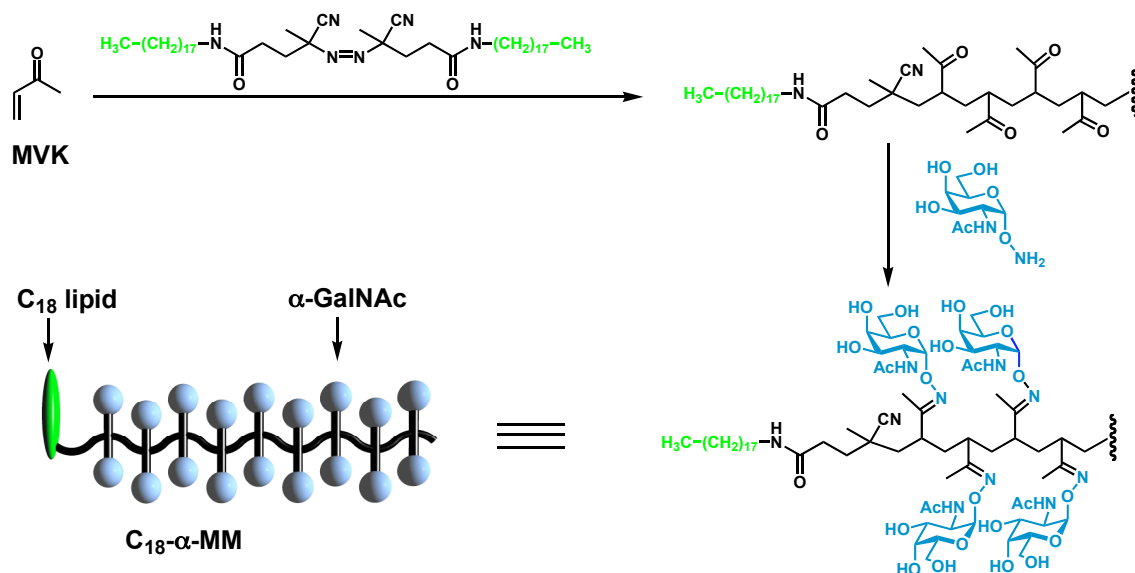
A**B**

Figure 3.1. (A) The structural features of native mucin (left) and designed and synthesized mucin mimic (right). Nature mucins are characterized by dense clusters of *O*-linked glycans bound to Ser/Thr residues of the polypeptide. The α -GalNAc residues attached to the Ser/Thr residues are elaborated with additional sugars but only the initial GalNAc residues are required for mucin structure. (B) Synthesis of C₁₈- α -MM. The C₁₈ lipid was conjugated to ACPA (4,4'-azobis(4-cyanopentanoic acid)) and the amide-linked product was used to initiate radical polymerization of MVK to produce C₁₈-poly(MVK). C₁₈- α -MM was obtained by chemoselective ligation of C₁₈-poly(MVK) with aminoxy-GalNAc.

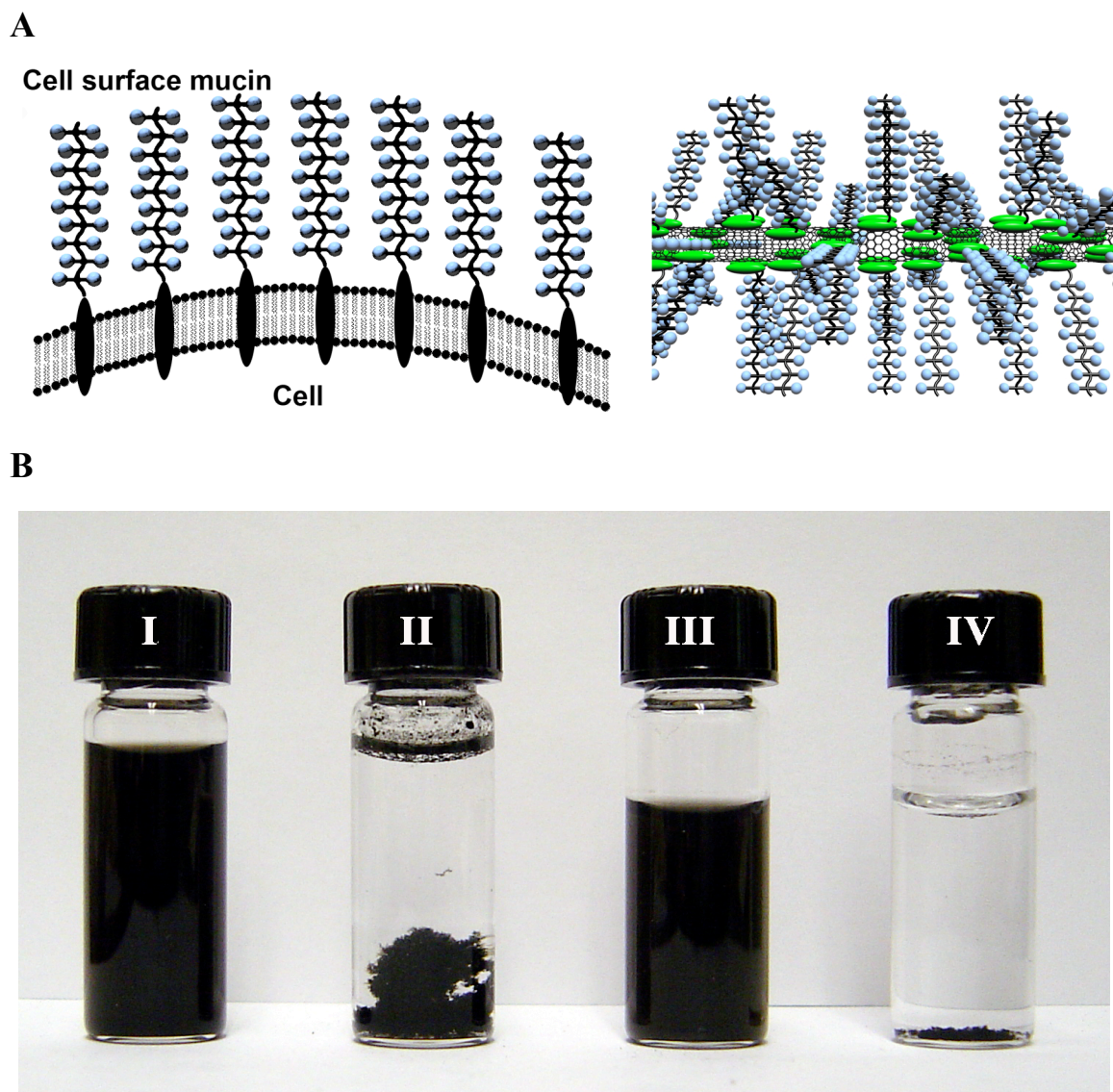


Figure 3.2. (A) The model for the self-assembly of C_{18} -MMs on the surface of carbon nanotubes (right), which is similar to the proposed arrangement of cell surface mucins (left). (B) Photographs of vials containing: (I) stable suspension of C_{18} - α -MM-SWNTs in H_2O after more than 3 months, (II) as-produced SWNTs in H_2O , which precipitate quickly in several hours, (III) stable suspension of C_{18} - α -MM-MWNTs in H_2O after more than 3 months, and (IV) as-produced MWNTs in H_2O , which precipitate quickly in several hours.

Coating CNTs with mucin mimic polymers

We envisioned that lipid-functionalized mucin mimics could assemble on CNTs similarly to the organization of native mucins in the cell membrane, with the glycosylated polymers projecting into the aqueous milieu (Fig. 3.2A). We first subjected single-walled carbon nanotubes (SWNTs) to ultrasonication in the presence of an aqueous solution of the C₁₈-functionalized mucin mimic bearing α -GalNAc residues (C₁₈- α -MM, Fig. 3.1B). The SWNTs were fully solubilized during the procedure (Fig. 3.2B-I), suggesting the formation of a hydrophilic surface coating. A similar procedure was applied to multi-walled carbon nanotubes (MWNTs) with the same outcome (Fig. 3.2B-III). The suspensions of C₁₈- α -MM-functionalized CNTs were stable for more than 3 months, while unfunctionalized CNTs precipitated very quickly (within hours) in aqueous solutions (Fig. 3.2B-II and 3.2B-IV). The C₁₈ lipid on the mucin mimic polymer was essential for CNT-solubilizing activity. CNTs rapidly precipitated from solutions of mucin mimic polymers lacking the lipid tail (not shown). These observations are consistent with a model in which C₁₈- α -MMs coat the CNTs as shown in Figure 3.2A.

The mucin mimic-coated CNTs (C₁₈- α -MM-SWNTs as representation) were directly characterized by atomic force microscopy (AFM), scanning electron microscopy (SEM), and transmission electron microscopy (TEM). As produced, SWNTs usually exist as bundles that are heavily entangled with one another to form three-dimensional (3D) networks. After functionalization with C₁₈- α -MM, the entangled SWNT bundles dissociated to form much finer bundles and even individual nanotubes, as observed by all

three imaging techniques. AFM permitted analysis of the modified tubes at ambient pressure and in hydrated form, which is important for maintaining the structure of the mucin coating. As shown in Figure 3.3A, tapping mode AFM images using a silicon substrate revealed C₁₈- α -MM-SWNTs with fairly uniform diameters of 65-70 nm. The idealized model shown in Figure 3.2A would predict a diameter on the order of 100 nm, roughly twice that of the mucin mimic polymer (the SWNT itself is only ~2 nm in diameter). However, distortions to the soft mucin coating imposed by the AFM tip or substrate, or a non-perpendicular angle of projection of the mucin polymer from the SWNT surface could account for the discrepancy.

SEM analysis of C₁₈- α -MM-SWNTs also provided evidence of the mucin coating. Exposure to the 5 keV electron beam led to visible sites of damage along the SWNT surface, as indicated by the arrows in Figure 3.3B. This was expected based on the sensitivity of organic species to electron beam-induced decomposition. The electron beam-induced damage increased with longer exposure times, culminating in near-complete destruction of the coating after 15 minutes. By contrast, unmodified CNTs are fairly stable under the electron beam, showing no visible change in surface morphology after prolonged exposure.

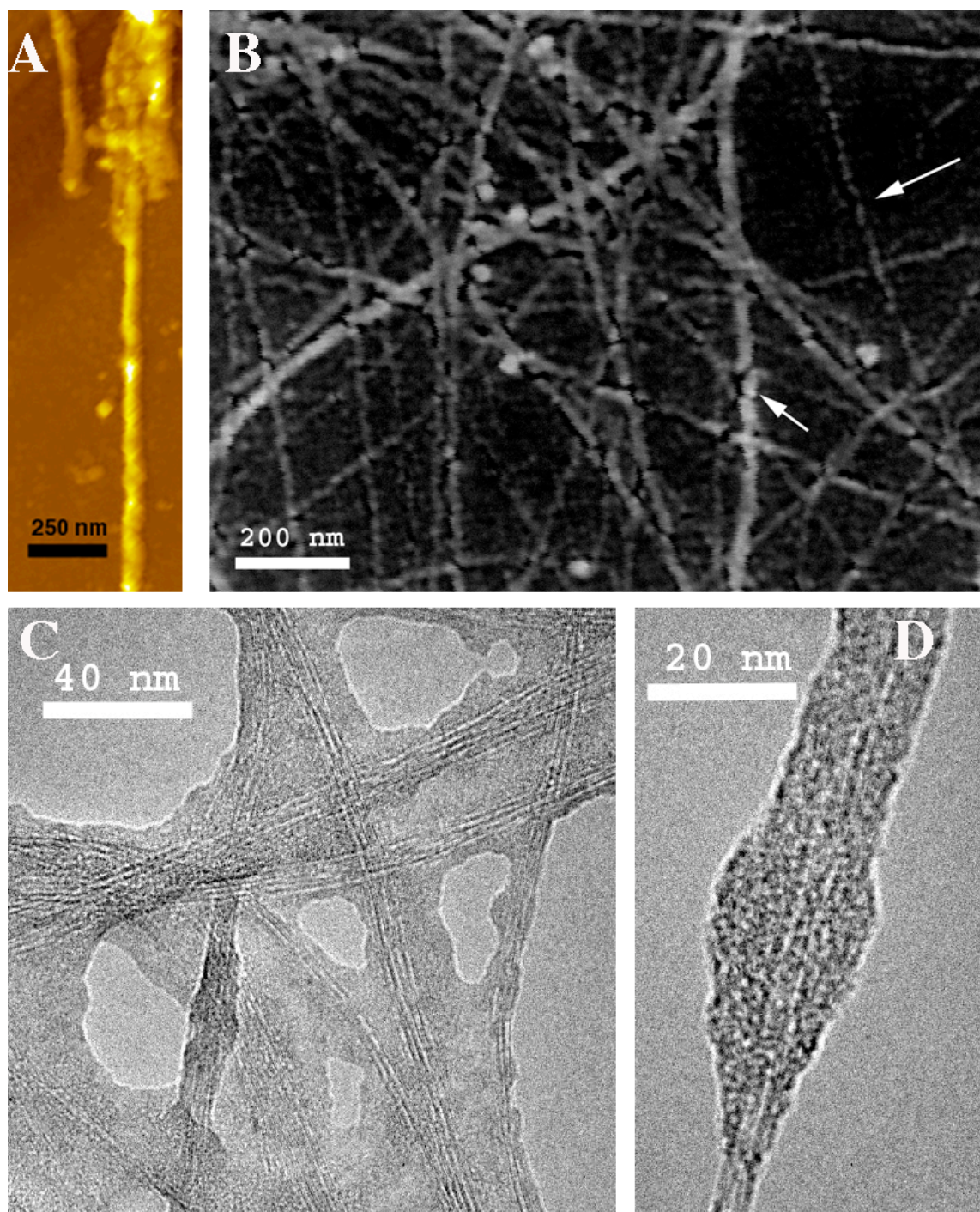


Figure 3.3. (A) Tapping mode AFM image of $C_{18}\text{-}\alpha\text{-MM-SWNTs}$ on a silicon substrate. (B) SEM image of $C_{18}\text{-}\alpha\text{-MM-SWNTs}$. The arrows indicate damaged regions of the mucin mimic coating caused by the electron beam. (C) and (D) TEM images of $C_{18}\text{-}\alpha\text{-MM-SWNTs}$, stained with 0.5% methylamine vanadate.

TEM analysis of C₁₈- α -MM-SWNTs provided a direct visualization of the mucin coating (Fig. 3.3C and 3.3D). The thickness of the coating varied from 10-25 nm under these conditions in which the sample is dehydrated under high vacuum. The coating was associated with the CNT surface shown in Figure 3.3C, and was not observed in regions of the image lacking CNTs. A single tube (or small bundle) coated with C₁₈- α -MM is shown in Figure 3.3D. The coating was not entirely uniform along the length of this SWNT, perhaps the result of electron beam (100 keV) induced-damage or collapse of the mucin polymers under high vacuum. In this regard, AFM imaging is a superior technique for visualizing mucin-coated SWNTs as they would exist in a functionally relevant aqueous environment.

Specific binding of proteins to mucin mimic-coated CNTs

On cells, mucins serve the dual role of molecular recognition and resistance to biofouling. We sought to determine if these same functions could be realized in the context of the nanotube surface. The C₁₈- α -MM coating introduces α -GalNAc residues onto the CNT surface, which could be recognized by an α -GalNAc-specific receptor such as the lectin *Helix pomatia* agglutinin (HPA) (38). To test this, we incubated C₁₈- α -MM-SWNTs with a solution of HPA conjugated with fluorescein isothiocyanate (HPA-FITC) (shown schematically in Fig. 3.4A-I). The C₁₈- α -MM-SWNTs were dialyzed to remove excess HPA-FITC then analyzed for bound lectin by fluorescence spectroscopy. As shown in trace I of Figure 3.4B, the C₁₈- α -MM-SWNTs showed significant fluorescence

attributed to bound fluorescein. HPA-FITC labeling of the $C_{18}\text{-}\alpha\text{-MM-SWNTs}$ was inhibited when 0.2 M free GalNAc was present in solution (Fig. 3.4A-III and trace III of Fig. 3.4B), confirming that fluorescent labeling was dependent on the receptor-ligand interaction.

In addition, we prepared a similar mucin mimic in which the GalNAc residues were conjugated to the polymer backbone via a β -anomeric linkage ($C_{18}\text{-}\beta\text{-MM}$). This mucin mimic was physically identical to its α -linked counterpart but should not be capable of HPA binding (39). We coated SWNTs with $C_{18}\text{-}\beta\text{-MM}$ and incubated them with HPA-FITC (shown schematically in Fig. 3.4A-II). No significant fluorescence labeling was observed (trace II in Fig. 3.4B), indicating that the lectin does not interact with the mucin mimic-coated tubes in the absence of its preferred ligand. These results demonstrate that mucin mimic-coated CNTs can engage in specific molecular recognition with protein receptors and resist non-specific protein binding.

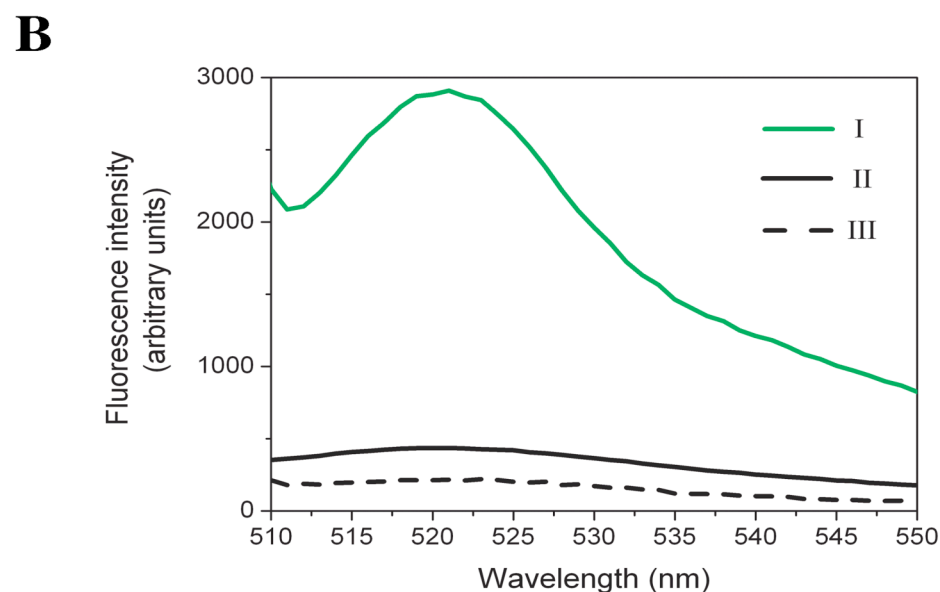
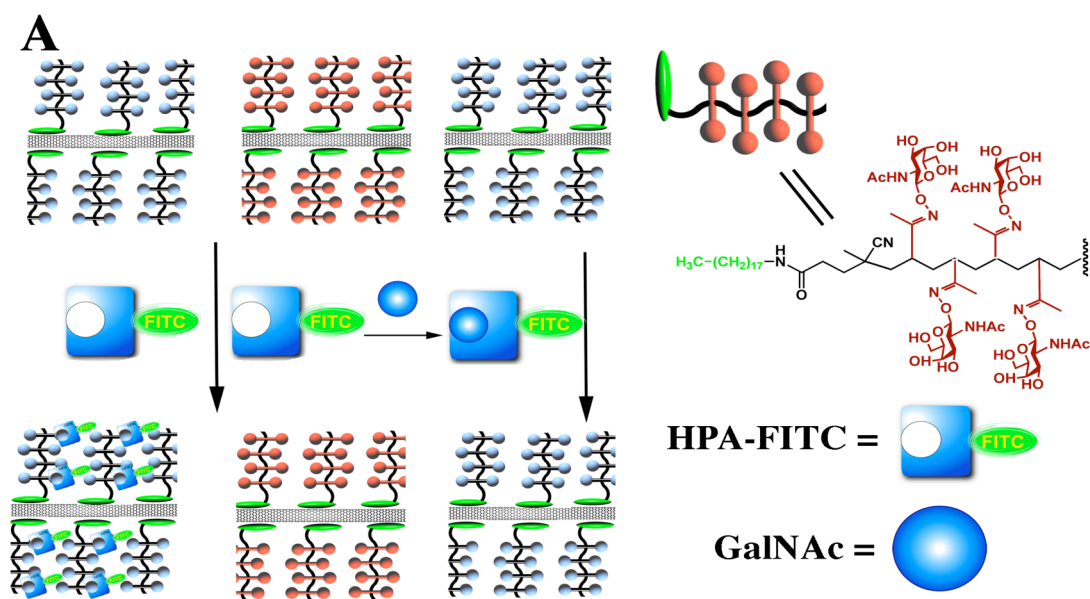


Figure 3.4. Specific binding of HPA to C_{18} - α -MM-coated nanotubes. (A) Scheme for I) specific binding of HPA to the surface of C_{18} - α -MM-SWNTs; II) lack of binding of HPA to C_{18} - β -MM-SWNTs; III) inhibition of HPA binding by soluble GalNAc. (B) Fluorescence spectra (510-550 nm) showing the specific binding of HPA to C_{18} - α -MM-SWNTs surface. Trace I, spectrum showing bound HPA-FITC on the surface of C_{18} - α -MM-SWNTs; Trace II, spectrum showing the lack of bound HPA to C_{18} - β -MM-SWNTs; Trace III, spectrum showing fluorescence associated with HPA-FITC binding in the presence of soluble GalNAc. The excitation wavelength was 492 nm. Spectra were corrected for background fluorescence by subtracting the fluorescence spectrum of C_{18} - α -MM-SWNTs or C_{18} - β -MM-SWNTs alone. These data are representative of results observed in triplicate experiments.

Interfacing mucin mimic-coated CNTs with living cells

CNTs have shown their potential applications in cell biology (18-21). These applications, however, have relied upon non-specific interaction between CNTs and cell surfaces, which precludes targeting to a particular cell type within a mixed population, or to a specific organelle within a cell. We were interested in tailoring the interface between CNTs and cells so as to more accurately reflect physiological interactions at the cell periphery. Glycans are major determinants of molecular recognition on the cell surface. They participate in diverse processes such as pathogen binding, cell trafficking, endocytosis and modulation of cell signaling (40). Glycan structures vary as a function of cell type and physiological state (41), and discrete epitopes are associated with specific organelles (42). Thus, CNTs that are functionalized with mucin mimics that can engage in glycan-receptor interactions are ideal substrates for more refined applications in cell biology.

In order to interface these functionalized CNTs with cells, we took advantage of the *Helix pomatia* agglutinin (HPA), a hexavalent lectin that is specific for α -GalNAc residues and is capable of crosslinking cells and glycoproteins (43). We reasoned that the complex of HPA with C18- α -MM-coated CNTs would possess sufficient available HPA binding sites for further complex formation with cell-surface glycoproteins (Fig. 3.5a-pathway I). Alternatively, HPA bound to cell surface glycans would present binding sites for α -GalNAc residues on C18- α -MM-coated CNTs (Fig. 3.5-pathway II). In either

scenario, binding of HPA to α -GalNAc residues would permit specific interaction of the cells and CNTs.

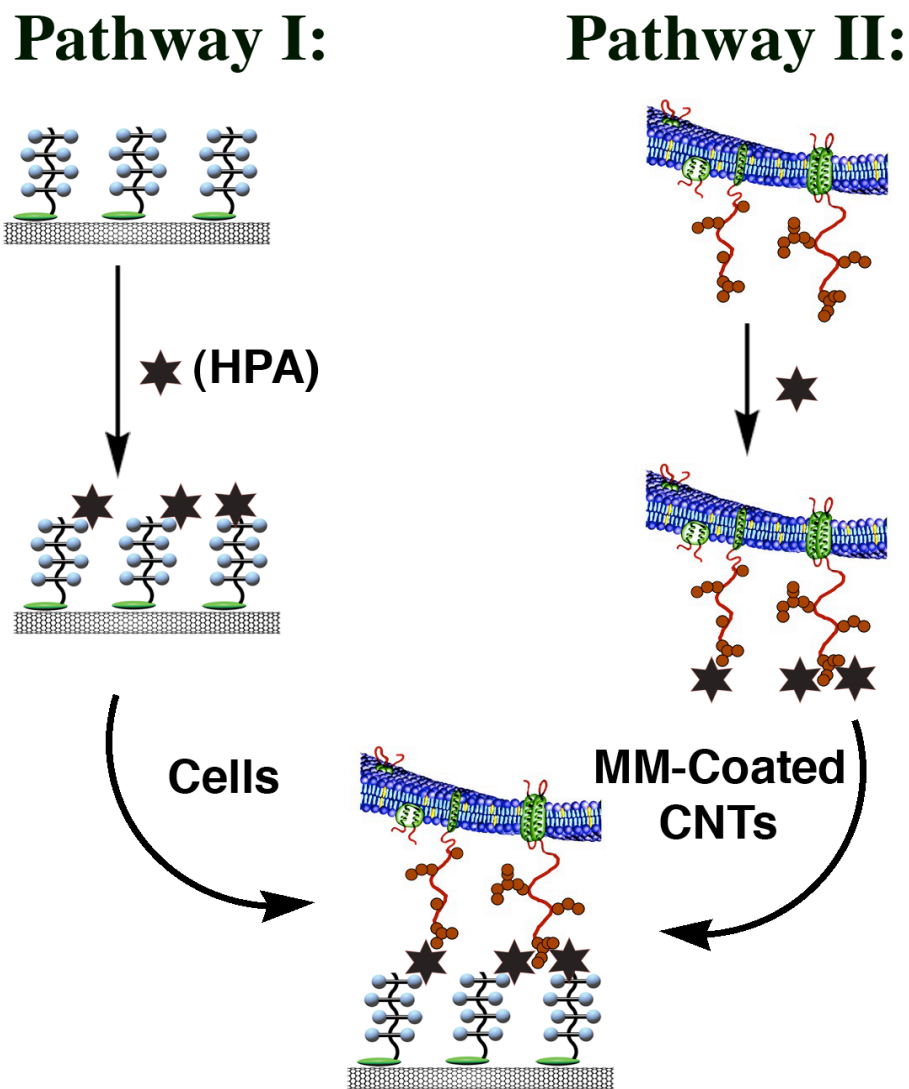


Figure 3.5. Schematic of interfacing CNTs on cell surfaces via carbohydrate-receptor binding: In pathway I, C₁₈- α -MM-coated CNTs were first bound to HPA, a hexavalent α -GalNAc binding lectin. The complex was then bound to cell surface glycoconjugates using available HPA binding sites presented on CNTs. In pathway II, HPA was first bound to cell surface glycoconjugates. The available HPA binding sites on cell surface were then bound to α -GalNAc residues on C₁₈- α -MM-coated CNTs.

To evaluate pathway I (Fig. 3.5), we required a means for detection of HPA binding to the C_{18} - α -MM-coated CNTs. This was provided by the commercial reagent fluorescein isothiocyanate-conjugated HPA (HPA-FITC). We complexed C_{18} - α -MM-coated CNTs with HPA-FITC, and the protein-modified CNTs were then incubated with Chinese hamster ovary (CHO) cells. The labeling observed by fluorescence microscopy (Fig. 3.6A) and flow cytometry analysis (Fig. 3.6B) suggested the formation of α -GalNAc-HPA complexes at both the CNT and cell surfaces. As a control, we performed the same experiment using CNTs coated with a similar polymer bearing β -linked GalNAc residues (C_{18} - β -MM), which do not bind HPA. In this case, no fluorescent labeling of cells was observed (not shown).

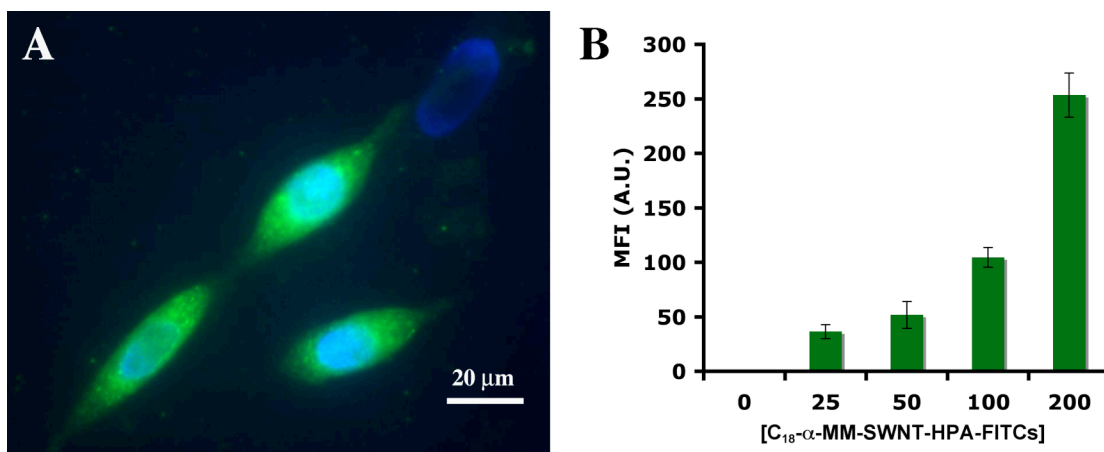


Figure 3.6. Binding of C_{18} - α -MM-coated CNTs to Chinese hamster ovary (CHO) cells via HPA crosslinks. (A) Fluorescence micrograph of CHO cells labeled with FITC-HPA-conjugated C_{18} - α -MM-coated CNTs (The cell nuclei were stained as blue with a DAPI dye). (B) Flow cytometry analysis of the cells in a treated with various doses of modified CNTs. MFI = mean fluorescence intensity. Error bars represent the standard deviation for three replicates.

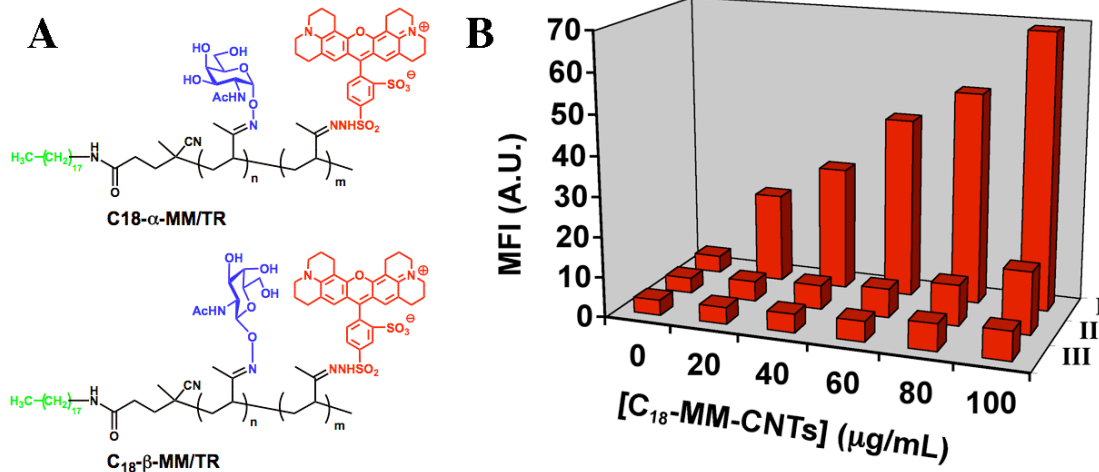


Figure 3.7. (A) The structures of C₁₈-α-MM/TR and C₁₈-β-MM/TR. (B) Flow cytometry analysis of cells in pathway II of Figure 3.5: Row I shows the specific binding of C₁₈-α-MM/TR-CNTs to CHO cells coated with HPA; Row II shows no binding of C₁₈-α-MM/TR-CNTs to cells in the absence of HPA; Row III shows that C₁₈-β-MM/TR-CNTs do not bind CHO cells coated with HPA receptors. These data are representative of results observed in triplicate experiments.

In order to evaluate pathway II (Fig. 3.5), we required a method for direct detection of C₁₈-α-MM-coated CNTs that is independent of HPA. Thus, we synthesized a C₁₈-α-MM polymer in which ~3% of the GalNAc residues were substituted with the fluorescent dye Texas Red (C₁₈-α-MM/TR, Fig. 3.7A). CHO cells were incubated with unmodified HPA to introduce α-GalNAc receptors onto the cell surface. The cells were then treated with various concentrations of C₁₈-α-MM/TR-coated CNTs and analyzed by flow cytometry. As shown in Figure 3.7B, dose-dependent labeling was observed (row I), and the labeling was dependent upon pre-complexation of the cells with HPA (row II). The control CNTs modified with C₁₈-β-MM/TR (Fig. 3.7A) showed no significant cell surface binding in the presence of HPA (Fig. 3.7B-row III). At the highest doses of C₁₈-

α -MM/TR-coated CNTs (>80 mg/mL), some non-specific fluorescent labeling of cells was observed. This may result from non-specific binding to the cell surface, or from internalization during the 1-hour incubation. However, at lower concentrations of C₁₈- α -MM/TR-coated CNTs, cell labeling was highly specific.

Cytotoxicity studies of mucin mimic-coated CNTs

Recent reports that unfunctionalized CNTs show potent cytotoxicity towards various cell types including HEK293 cells (23), HacaT cells (26), and alveolar macrophages (27) have stimulated concern regarding their potential utility in biological systems. We were therefore interested in evaluating the cytotoxicity of our glycopolymer-coated CNTs. CHO cells were cultured with C₁₈- α -MM-, C₁₈- α -MM/TR-, C₁₈- β -MM/TR-, or HPA-FITC-conjugated, C₁₈- α -MM-coated CNTs (each at 100 mg/mL) for 3 days. In control experiments, the cells were cultured with unmodified CNTs or with media alone. Viable cells were counted each day (Fig. 3.8). Cells cultured with the glycopolymer-coated CNTs were indistinguishable from cells grown in the absence of CNTs. By contrast, cells cultured with unmodified CNTs were unable to expand during the course of the experiment. Presumably, the unmodified CNTs either inhibited cell growth or induced cell death at a rate comparable to the proliferation rate. Similar results were obtained with Jurkat cells (not shown). Thus, the glycopolymer coating renders the CNTs nontoxic while simultaneously providing a means for specific cell surface binding.

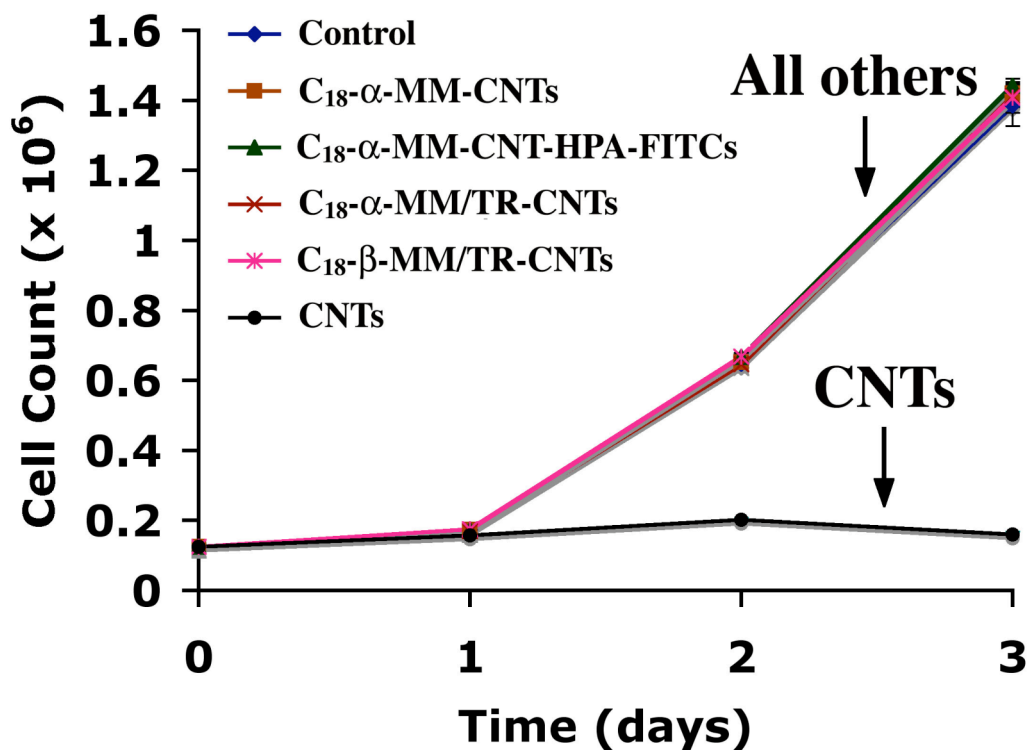


Figure 3.8. Effects of glycopolymer-coated and unmodified CNTs on the growth of CHO cells. Similar results were obtained for Jurkat cells. Error bars represent the standard deviation for three replicates.

Conclusions

In summary, we have developed a practical and general approach to engineering biomimetic surfaces on CNTs. The mucin mimics used in this study endowed the CNT surfaces with properties shared by cell surfaces, including the display of carbohydrates capable of molecular recognition. The mucin mimic synthetic process allows for

introduction of myriad functional epitopes, in addition to sugars, that could encode interactions with numerous receptor types. We have also demonstrated a strategy for interfacing biocompatible CNTs with cell surfaces by virtue of carbohydrate-receptor interactions. This strategy may offer new opportunities for probing biological processes. Experimental and theoretical studies have indicated that the environment surrounding the nanotube can influence CNT properties. Therefore, variations in a cell's local environment might be monitored by changes in the electrical, mechanical, or optical properties of CNTs.

Materials and methods

General procedure for coating mucin mimics on CNTs

High-purity SWNTs (HiPCO, >95%) were purchased from Carbon Nanotechnologies Inc., and high-purity of MWNTs (CVD, >95%) were purchased from Nanolab. In a typical preparation experiment, 1 mg of as-produced carbon nanotubes was suspended in 5 mL of aqueous C₁₈-MM solution (0.1%~0.5%). The mixture was sonicated using a water-bath sonicator for 1 h. First, insoluble material was removed by low-speed centrifugation at 3,000 x g for 30 min, and the product suspension was decanted from the insoluble material. Then the excess free mucin mimic polymers were removed by dialysis of the suspension in a polycarbonate membrane against deionized water for 24 h. The resulting C₁₈-MM-NTs (C₁₈- α -MM-SWNTs, C₁₈- β -MM-SWNTs, C₁₈- α -MM/TR-SWNTs, C₁₈- β -MM/TR-SWNTs, C₁₈- α -MM-MWNTs, C₁₈- β -MM-

MWNTs, C₁₈- α -MM/TR-MWNTs, and C₁₈- β -MM/TR-MWNTs) formed stable suspensions in aqueous solution. The concentrations of the resulting suspensions were calculated by evaporating the water and weighting the dried coated CNTs.

Control experiment I: As-produced carbon nanotubes were treated under the same conditions but without C₁₈-MMs. The resulting suspensions were not stable and the carbon nanotubes precipitated after several h.

Control experiment II: Mucin mimics without C₁₈ lipid tails were sonicated with carbon nanotubes in water for 1 h. The resulting suspensions were not stable and the carbon nanotubes precipitated after several h.

AFM, SEM, and TEM imaging

The sample solution was deposited in a 1 μ L droplet onto a silicon wafer and then allowed to dry in air. Tapping mode was used to acquire the images under ambient conditions (Molecular Imaging, Pico SPM).

SEM images of C₁₈- α -MM-SWNTs were obtained on a JEOL 6400 field emission SEM operated at 5 keV. Samples were deposited onto a silicon wafer and then allowed to dry in air.

TEM images of C₁₈- α -MM-SWNTs were obtained on a JEOL 2011 microscope operating at electron energy of 100 keV. Samples were prepared by depositing the suspension onto grids, allowing the grids to absorb for 2 min, and then staining the

material with 0.5% methylamine vanadate in H₂O (Nanovan, Nanoprobes Inc., Yaphank, NY).

Fluorescence microscopy and flow cytometry

A Zeiss Axiovert 200M inverted microscope equipped with a 63 × 1.4 NA Plan-Apochromat oil immersion lens was employed for imaging. A 175W xenon lamp housed in a Sutter DG4 illuminator linked to the microscope by an optical fiber assured shuttering and illumination. Images were acquired using a CoolSNAP HQ CCD camera (Roper Scientific). Slidebook software (Intelligent Imaging Solutions) was used to control the microscope and the camera.

Flow cytometry data were acquired using a FACScalibur flow cytometer (BD Biosciences).

HPA-FITC Binding Assays

Helix pomatia agglutinin conjugated with fluorescein isothiocyanate (HPA-FITC) was obtained from EY-Laboratories. *N*-acetylgalactosamine (GalNAc) was obtained from Sigma. A 1 mL solution of HPA-FITC (100 µg/mL) in buffer (0.10 M Tris, and 0.15 M NaCl, pH 8.0) was added to the suspensions of mucin mimic-coated nanotubes (C₁₈-α-MM-SWNTs or C₁₈-β-MM-SWNTs) in H₂O (1 mL). An additional 0.5 mL buffer was added and the reactions were incubated for 1h at rt in the dark. GalNAc inhibition of HPA binding to C₁₈-α-MM-SWNTs was tested by pre-incubating 1 mL of HPA-FITC solution in buffer (100 µg/mL) with 0.5 ml of GalNAc in buffer (200 mg/mL) for 1h at rt

in the dark. This pre-incubated solution was added to the suspension of C₁₈- α -MM-SWNTs in H₂O (1 mL), and the resulting solution was incubated for 1 h at rt in the dark, as described above. After incubation, the solutions were all subjected to dialysis against the buffer for 48 h. The dialyzed solutions were analyzed at 510-550 nm using a fluorescence microplate reader (excitation wavelength 492 nm). Spectra were corrected for background fluorescence by subtracting the fluorescence spectrum of C₁₈- α -MM-SWNTs or C₁₈- β -MM-SWNTs alone.

Interfacing mucin mimic-coated CNTs with living cells (pathway I)

A 1-mL solution of HPA-FITC (100 μ g/mL) in buffer (0.10 M Tris, and 0.15 M NaCl, pH 8.0) was added to the suspensions of mucin mimic-coated nanotubes (C₁₈- α -MM-CNTs or C₁₈- β -MM-CNTs) in H₂O (1 mL). An additional 0.5 mL of buffer was added and the reactions were incubated for 1 h at rt in the dark. After incubation, the solutions were all subjected to dialysis against the buffer for 48 h. The dialyzed solutions were analyzed at 510-550 nm using a fluorescence microplate reader (excitation wavelength 492 nm). The concentrations were calculated as described above. The characterized solutions were then used for cell surface binding experiments.

For fluorescence microscopy experiments, CHO Cells were seeded onto glass slides mounted with tissue culture wells (LAB-TEK) and allowed to adhere for 2 d. The cells were washed 3 times with PBS, and then fixed in 3% paraformaldehyde in PBS.

After three washes, cells were blocked in PBS with 1% bovine serum albumin for 20 min, followed by the addition of C₁₈-MM-CNT-HPA-FITC complex. After a 1-h incubation at rt in the dark, the cells were washed 3 times. The cells were then mounted using Vectashield with 4,6-diamidino-2-phenylindole (Vector Laboratories) and imaged by fluorescence microscopy.

For flow cytometry experiments, Cells (2×10^6) were seeded in a 10-cm dish for 3 d. The cells were lifted with 1 mM EDTA in PBS, washed, and counted. Flow cytometry analysis was performed on 500,000 cells. The cells were pelleted (3,500 rpm, 3 min) and washed twice with 200 μ L of PBS containing 1% FCS. Cells were then treated with HPA-FITC-conjugated C₁₈-MM-CNTs for 1 h at rt in the dark. After incubation, cells were pelleted, washed three times and analyzed by flow cytometry.

Interfacing mucin mimic-coated CNTs with living cells (pathway I)

In order to determine the appropriate condition for complexation of HPA and cells, cells were incubated with various dilutions of HPA-FITC and then analyzed by flow cytometry. The cells were pelleted and washed twice with 200 μ L of PBS containing 1% FCS. Cells were then treated with various concentrations of HPA-FITC for 1 h at rt in the dark. After incubation, the cells were pelleted, washed three times and analyzed using a FACScalibur flow cytometer (BD Biosciences). A concentration of HPC-FITC (400 μ g/mL) that produced robust cell surface labeling at sub-saturating

levels was chosen for the following experiments. Cells (0.5×10^6) were pelleted (3,500 rpm, 3 min) and washed twice with 200 μ L of PBS containing 1% FCS. Cells were then treated with unmodified HPA (400 μ g/mL) for 1 h at rt, followed by washing with buffer for 3 times. The cells were then incubated with C₁₈-MM/TR-CNTs for 1 h at rt in the dark. After incubation, cells were pelleted, washed three times and analyzed by flow cytometry.

Cytotoxicity assays

For CHO cells, the cells were seeded at a density of 1.25×10^5 cells/mL and incubated with C₁₈- α -MM-, C₁₈- α -MM/TR-, C₁₈- β -MM/TR-, or HPA-FITC-conjugated, C₁₈- α -MM-coated CNTs (each at 100 μ g/mL) for 3 d. In control experiments, the cells were cultured with unmodified CNTs or with media alone. Cells were washed twice with PBS and then trypsinized with 0.25% trypsin-EDTA (PBS, pH 7.4), resuspended in media and counted every 24 h.

For Jurkat cells, the cells were seeded at a density of 1.25×10^5 cells/mL and incubated with C₁₈- α -MM-, C₁₈- α -MM/TR-, C₁₈- β -MM/TR-, or HPA-FITC-conjugated, C₁₈- α -MM-coated CNTs (each at 100 μ g/mL) for 3 d. In control experiments, the cells were cultured with unmodified CNTs or with media alone. Cells were counted every 24 h.

Cell culture conditions

All cell lines were maintained in a 5% CO₂, water-saturated atmosphere at 37 °C and media were supplemented with penicillin (100 unit/mL), streptomycin (0.1 mg/mL) and 10% FCS unless otherwise indicated. CHO cells were grown in Ham F12 nutrient mixture. Jurkat cells were grown in RPMI-1640 media.

Synthesis of new compounds

All chemical reagents were of analytical grade, obtained from commercial suppliers and used without further purification. Flash chromatography was performed using Merck 60Å 230-400 mesh silica gel. Analytical TLC was performed on Analtech Uniplate silica gel plates and visualized by staining with ceric ammonium molybdate or by absorbance of UV light at 254nm. ¹H NMR, and ¹³C NMR spectra were obtained with Bruker AMX-400 or Bruker DRX-500 MHz spectrometers. ¹H and ¹³C chemical shifts (δ) are reported in parts per million (ppm) referenced to TMS (0 ppm) and were measured relative to the residual solvent peak. Coupling constants (J) are reported in hertz (Hz). High-resolution fast atom bombardment (FAB) mass spectra were obtained at the UC Berkeley Mass Spectrometry Laboratory. The concentration of the polymer solutions investigated by DLS was 0.02 wt %. The weight average molecular weights (M_w) and polydispersities (PDI) were measured by size exclusion chromatography using a Waters-Alliance Inc. model 2690 equipped with the Viscotek Triple Detector Array and four ViscoGel columns: G3000HR (exclusion limit 6x10⁴ g/mol), G4000HR (exclusion limit 4x10⁵ g/mol), G5000HR (exclusion limit 4x10⁶ g/mol) and G6000HR (exclusion

limit 4×10^7 g/mol). A flow rate of 1.0 mL/min was used and polystyrene standards were used for calibration. The weight average molecular weights of water-soluble mucin-mimic polymers were determined by size exclusion chromatography (Varian ProStar model 210) using a polysaccharide standard (PL Polysaccharide Standard Kit SAC-10) in deionized water with a flow rate of 1.0 mL/min on two PL aquagel-OH 40 columns (bead size 8 mm and measurable M_w range 10,000 – 200,000) using a UV-Vis detector (Varian ProStar Model 345).

C₁₈-Azobis(4-cyanovaleric acid) (1). To a solution of 4,4'-azobis(4-cyanovaleric acid) (590 mg, 2.11 mmol) in CH₂Cl₂ (100 mL) was added 4-(dimethylamino)pyridine (260 mg, 2.11 mmol), triethylamine (1.20 mL, 8.61 mmol), and octadecylamine (2.27 g, 8.44 mmol). The solution was stirred for 15 min and *N*-(3-dimethylaminopropyl)-*N'*-ethylcarbodiimide hydrochloride (1.62 g, 8.44 mmol) was added. The solution was stirred in the dark for 18 h under N₂, diluted with CH₂Cl₂, and washed with brine (250 mL) and water (250 mL). The organic layer was dried over Na₂SO₄, filtered and concentrated *in vacuo*. The resulting solid was purified on a silica gel column (hexanes:ethyl acetate, 2:1) to afford compound **1** (980 mg, 59%) as a white solid. mp = 102-104 °C; IR (thin film): 2916, 2848, 2026, 1614, 1520, 1398, 776 cm⁻¹; ¹H NMR (400 MHz, CDCl₃): δ 0.80 (t, 6 H, *J* = 6.3), 1.49 (t, 6 H, *J* = 6.8), 1.67-1.76 (m, 31 H), 1.78-1.81 (m, 6 H), 2.13-2.23 (m, 6 H), 2.40-2.49 (m, 18 H), 3.20-3.27 (m, 12 H), 5.74-5.77 (m, 4 H), 5.93-5.95 (m, 2 H); ¹³C NMR (100 MHz, CDCl₃): δ 14.09, 22.66, 26.91, 29.33, 29.45, 29.55, 29.67, 31.89, 39.80, 72.56, 171.64; HRMS(FAB): Calcd. for C₄₈H₉₁LiN₆O₂

$[M+Li]^+$ 783.7203, found 783.7197. Anal. Calcd. for $C_{49}H_{93}N_6O_3 \cdot H_2O$: C, 73.54; H 11.71; N, 8.75; found C, 73.72; H, 11.97; N, 8.66.

C₁₈-poly(MVK) (2). Anhydrous *p*-dioxane (0.56 mL) was introduced into a 10 mL Schlenk tube containing methyl vinyl ketone (0.56 mL, 6.73 mmol) and **1** (50 mg, 0.064 mmol) under N₂. The reaction mixture was stirred for 72 h at 95 °C after degassing by four freeze-pump-thaw cycles. The reaction mixture was allowed to cool to rt, diluted with *p*-dioxane (5 mL), and added dropwise to excess diethyl ether (1 L) with vigorous stirring. The precipitate was filtered, washed with diethyl ether and dried *in vacuo* overnight to afford **10** as a white solid (325 mg). IR (thin film): 2926, 1709, 1426, 1356, 1239, 1163, 1109, 734 cm⁻¹; GPC (THF eluent, polystyrene standard), M_w = 2.18 x 10⁵ Da, PDI = 2.20; Anal. Calcd. for (C₄H₆O)_n: C, 68.54; H, 8.63; found C, 67.98; H, 8.93.

α-Aminoxy GalNAc C₁₈-poly(MVK) (3). To a solution of **2** (3.0 mg, 0.043 mmol based on carbonyl number) in THF (3 mL) and H₂O (1 mL) was added aminoxy 2-acetamido-2-deoxy-α-D-galactopyranoside (**35**) (28 mg, 0.120 mmol) and acetic acid (5 μL). The reaction mixture was stirred at 95 °C for 24 h, allowed to cool to rt and concentrated *in vacuo*. The resulting solid was dissolved in H₂O (4 mL) and heated to reflux for 48 h. The reaction mixture was cooled to rt, dialyzed in H₂O and lyophilized to give **3** (12 mg, 87% carbonyls reacted) as a fluffy white solid. IR (KBr) 3435, 1641, 1384, 1013, 664, 576 cm⁻¹; GPC (H₂O eluent, polysaccharide standard), M_w = 30.0 x 10³ Da, PDI = 2.80; Anal. Calcd. for (C₁₂H₂₀N₂O)_n: C, 49.99; H, 6.99; N, 9.82; found: C, 47.04; H, 7.71; N, 7.82.

α -Aminoxy GalNAc-Texas Red C₁₈-poly(MVK) (4). To a solution of **2** (6 mg, 0.09 mmol based on carbonyl number) in THF (5 mL) and H₂O (2 mL) was added aminoxy 2-acetamido-2-deoxy- α -D-galactopyranoside (**35**) (40 mg, 0.170 mmol), Texas Red hydrazide (5 mg, 8 μ mol) and acetic acid (5 μ L). The reaction mixture was stirred for 24 h at 95 °C, allowed to cool to rt and concentrated *in vacuo*. The resulting solid was dissolved in H₂O (7 mL) and heated to reflux for 48 h. The reaction mixture was cooled to rt, dialyzed in H₂O and lyophilized to give **4** (21 mg, 77% of carbonyls reacted) as a fluffy dark red solid. IR (KBr) 3434, 1658, 1641, 1381, 1005, 557, 463 cm⁻¹; GPC (H₂O eluent, polysaccharide standard), M_w = 30.9 x 10³ Da, PDI = 2.56.

References

1. M. Sarikaya, C. Tamerler, A. K. Y. Jen, K. Schulten, F. Baneyx, Molecular biomimetics: nanotechnology through biology. *Nat. Mater.* **2**, 577-585 (2003).
2. G. M. Whitesides, The 'right' size in nanobiotechnology. *Nat. Biotechnol.* **21**, 1161-1165 (2003).
3. M. Bruchez, M. Moronne, P. Gin, S. Weiss, A. P. Alivisatos, Semiconductor nanocrystals as fluorescent biological labels. *Science* **281**, 2013-2016 (1998).
4. W. C. W. Chan, S. M. Nie, Quantum dot bioconjugates for ultrasensitive nonisotopic detection. *Science* **281**, 2016-2018 (1998).
5. T. A. Taton, C. A. Mirkin, R. L. Letsinger, Scanometric DNA array detection with nanoparticle probes. *Science* **289**, 1757-1760 (2000).
6. B. Dubertret *et al.*, In vivo imaging of quantum dots encapsulated in phospholipid micelles. *Science* **298**, 1759-1762 (2002).
7. X. Y. Wu *et al.*, Immunofluorescent labeling of cancer marker Her2 and other cellular targets with semiconductor quantum dots. *Nat. Biotechnol.* **21**, 41-46 (2003).
8. J. M. Nam, C. S. Thaxton, C. A. Mirkin, Nanoparticle-based bio-bar codes for the ultrasensitive detection of proteins. *Science* **301**, 1884-1886 (2003).
9. Y. Cui, Q. Q. Wei, H. K. Park, C. M. Lieber, Nanowire nanosensors for highly sensitive and selective detection of biological and chemical species. *Science* **293**, 1289-1292 (2001).
10. D. H. Reich *et al.*, Biological applications of multifunctional magnetic nanowires (invited). *J. Appl. Phys.* **93**, 7275-7280 (2003).
11. a. Bianco, K. Kostarelos, M. Prato, Applications of carbon nanotubes in drug delivery. *Curr. Opin. Chem. Biol.* **9**, 674-679 (2005).
12. Y. Lin *et al.*, Advances toward bioapplications of carbon nanotubes. *J. Mater. Chem.* **14**, 527-541 (2004).

13. J. Goldberger, R. Fan, P. D. Yang, Inorganic nanotubes: A novel platform for nanofluidics. *Acc. Chem. Res.* **39**, 239-248 (2006).
14. A. Star *et al.*, Label-free detection of DNA hybridization using carbon nanotube network field-effect transistors. *Proc. Natl. Acad. Sci. USA* **103**, 921-926 (2006).
15. R. J. Chen *et al.*, Noncovalent functionalization of carbon nanotubes for highly specific electronic biosensors. *Proc. Natl. Acad. Sci. USA* **100**, 4984-4989 (2003).
16. D. A. Heller *et al.*, Optical detection of DNA conformational polymorphism on single-walled carbon nanotubes. *Science* **311**, 508-511 (2006).
17. S. S. Wong, E. Joselevich, A. T. Woolley, C. L. Cheung, C. M. Lieber, Covalently functionalized nanotubes as nanometre-sized probes in chemistry and biology. *Nature* **394**, 52-55 (1998).
18. K. Kostarelos *et al.*, Cellular uptake of functionalized carbon nanotubes is independent of functional group and cell type. *Nat. Nanotech.* **2**, 108-113 (2007).
19. N. W. S. Kam, H. J. Dai, Carbon nanotubes as intracellular protein transporters: Generality and biological functionality. *J. Am. Chem. Soc.* **127**, 6021-6026 (2005).
20. X. Chen, A. Kis, A. Zettl, C. R. Bertozzi, A cell nanoinjector based on carbon nanotubes. *Proc. Natl. Acad. Sci. USA* **104**, 8218-8222 (2007).
21. N. W. S. Kam, M. O'Connell, J. A. Wisdom, H. J. Dai, Carbon nanotubes as multifunctional biological transporters and near-infrared agents for selective cancer cell destruction. *Proc. Natl. Acad. Sci. USA* **102**, 11600-11605 (2005).
22. M. Bottini *et al.*, Multi-walled carbon nanotubes induce T lymphocyte apoptosis. *Toxicol. Lett.* **160**, 121-126 (2006).
23. D. X. Cui, F. R. Tian, C. S. Ozkan, M. Wang, H. J. Gao, Effect of single wall carbon nanotubes on human HEK293 cells. *Toxicol. Lett.* **155**, 73-85 (2005).
24. A. Magrez *et al.*, Cellular toxicity of carbon-based nanomaterials. *Nano Lett.* **6**, 1121-1125 (2006).

25. Y. Sato *et al.*, Influence of length on cytotoxicity of multi-walled carbon nanotubes against human acute monocytic leukemia cell line THP-I in vitro and subcutaneous tissue of rats in vivo. *Mol. BioSyst.* **1**, 176-182 (2005).
26. A. A. Shvedova *et al.*, Exposure to carbon nanotube material: Assessment of nanotube cytotoxicity using human keratinocyte cells. *J. Toxicol. Environ. Health, Part A* **66**, 1909-1926 (2003).
27. G. Jia *et al.*, Cytotoxicity of carbon nanomaterials: Single-wall nanotube, multi-wall nanotube, and fullerene. *Environ. Sci. Technol.* **39**, 1378-1383 (2005).
28. G. J. Strous, J. Dekker, Mucin-Type Glycoproteins. *Crit. Rev. Biochem. Mol. Biol.* **27**, 57-92 (1992).
29. Y. Shimizu, S. Shaw, Cell-Adhesion - Mucins in the Mainstream. *Nature* **366**, 630-631 (1993).
30. J. Hilkens, M. J. L. Ligtenberg, H. L. Vos, S. V. Litvinov, Cell Membrane-Associated Mucins and Their Adhesion-Modulating Property. *Trends Biochem. Sci.* **17**, 359-363 (1992).
31. D. Rabuka *et al.*, Hierarchical assembly of model cell surfaces: Synthesis of mucin mimetic polymers and their display on supported bilayers. *J. Am. Chem. Soc.* **129**, 5462-5471 (2007).
32. R. Shogren, T. a. Gerken, N. Jentoft, Role of Glycosylation on the Conformation and Chain Dimensions of O-Linked Glycoproteins - Light-Scattering-Studies of Ovine Submaxillary Mucin. *Biochemistry* **28**, 5525-5536 (1989).
33. T. a. Gerken, K. J. Butenhof, R. Shogren, Effects of Glycosylation on the Conformation and Dynamics of O-Linked Glycoproteins - C-13 Nmr-Studies of Ovine Submaxillary Mucin. *Biochemistry* **28**, 5536-5543 (1989).
34. D. H. Live *et al.*, Probing cell-surface architecture through synthesis: An NMR-determined structural motif for tumor-associated mucins. *Proc. Natl. Acad. Sci. USA* **96**, 3489-3493 (1999).
35. L. A. Marcaurrelle, Y. S. Shin, S. Goon, C. R. Bertozzi, Synthesis of oxime-linked mucin mimics containing the tumor-related T-N and sialyl T-N antigens. *Org. Lett.* **3**, 3691-3694 (2001).

36. C. Richard, F. Balavoine, P. Schultz, T. W. Ebbesen, C. Mioskowski, Supramolecular self-assembly of lipid derivatives on carbon nanotubes. *Science* **300**, 775-778 (2003).
37. N. B. Holland, Y. X. Qiu, M. Ruegsegger, R. E. Marchant, Biomimetic engineering of non-adhesive glycocalyx-like surfaces using oligosaccharide surfactant polymers. *Nature* **392**, 799-801 (1998).
38. N. Sharon, Lectin Receptors as Lymphocyte Surface-Markers. *Adv. Immunol.* **34**, 213-298 (1983).
39. V. Piller, F. Piller, J. P. Cartron, Comparison of the Carbohydrate-Binding Specificities of 7 N-Acetyl-D-Galactosamine-Recognizing Lectins. *Eur. J. Biochem.* **191**, 461-466 (1990).
40. B. E. Collins, J. C. Paulson, Cell surface biology mediated by low affinity multivalent protein-glycan interactions. *Curr. Opin. Chem. Biol.* **8**, 617-625 (2004).
41. M. A. Hollingsworth, B. J. Swanson, Mucins in cancer: Protection and control of the cell surface. *Nat. Rev. Cancer* **4**, 45-60 (2004).
42. A. Helenius, M. Aebi, Intracellular functions of N-linked glycans. *Science* **291**, 2364-2369 (2001).
43. J. N. Lisgarten *et al.*, Crystallization of Helix pomatia agglutinin (HPA), a protein from the edible snail. *Acta. Crystallogr. D Biol. Crystallogr.* **55**, 1903-1905 (1999).

Chapter 4: Development of glycosylated dendrimers for biomimetic functionalization of carbon nanotubes*

Introduction

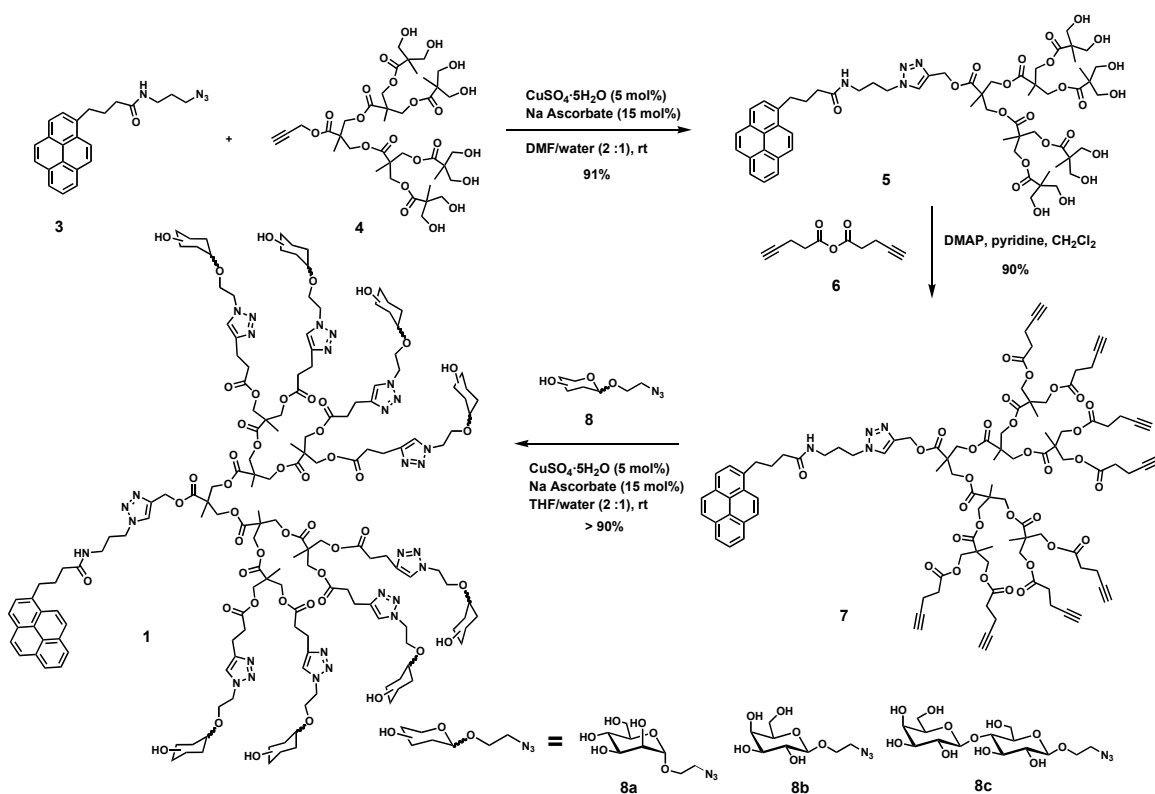
The unique structural, mechanical, electrical, and optical properties of single-walled carbon nanotubes (SWNTs) have stimulated an explosion of interest in their biological applications (1-3). Already, SWNTs have been employed for biosensing (5), imaging (6), intracellular delivery (7), and cancer cell targeting (8, 9). However, expanding the use of SWNTs in living systems will require improvements in their biocompatibility. Unmodified SWNTs are notoriously cytotoxic (10-13). Thus, surface modifications that mitigate their toxicity while simultaneously functionalizing the SWNTs for biological recognition are highly sought after (9, 14-18).

A promising avenue we have recently explored is to functionalize SWNTs with synthetic glycopolymers that mimic the structures found on vertebrate cell surfaces (17, 18). For example, we demonstrated that poly(methylvinylketone) polymers conjugated to synthetic sugars via oxime linkages could be adsorbed onto carbon nanotubes (CNTs) by virtue of a hydrophobic end-group. The coated CNTs were soluble in water, resisted non-specific protein binding and bound specifically to cells via receptor-ligand interactions (17, 18). Most importantly, the coated CNTs were nontoxic to cultured cells. These findings were tempered, however, by the irregular surfaces and nonuniform

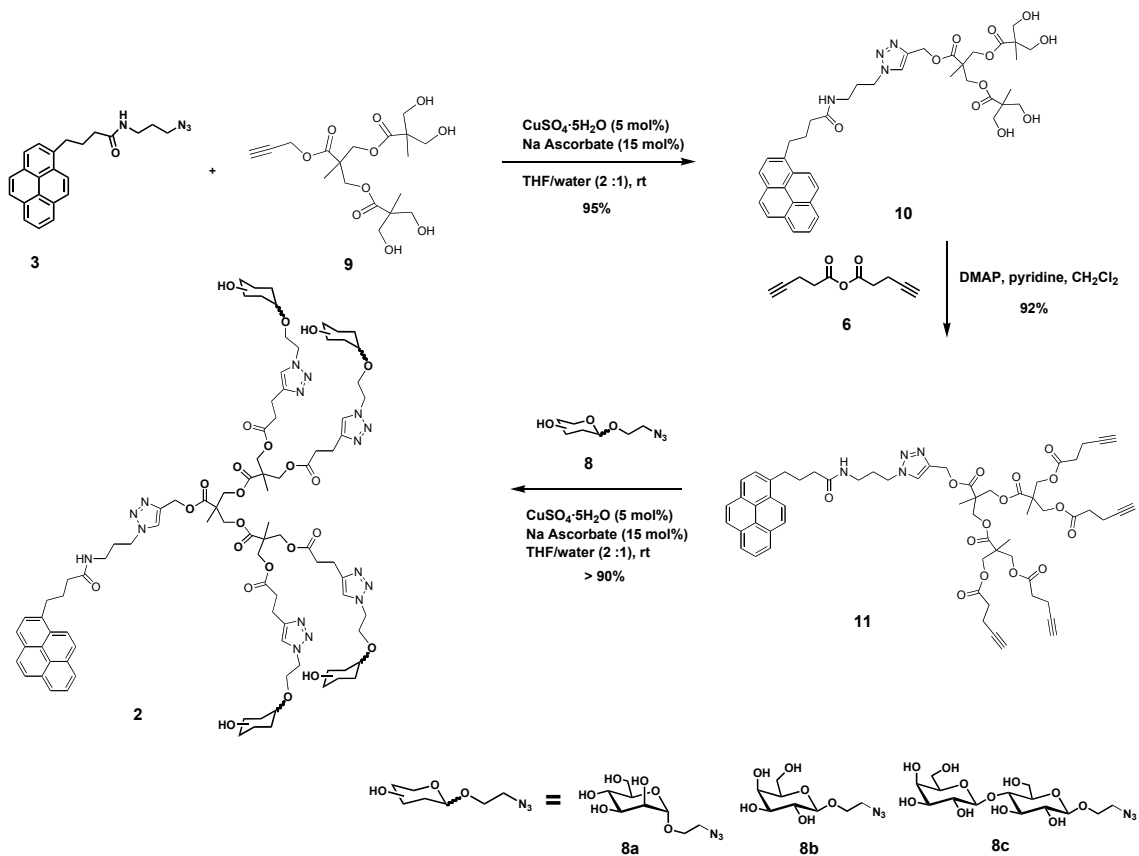
* Peng Wu, Nancy Hu, Un Chong Tam, Ola Blixt contributed to the work described in this chapter.

thickness of the CNT coatings, properties caused by the heterogeneity of the polymers which had polydispersities of ~ 1.7 (19). These unwanted features might undermine future efforts to achieve reproducible changes in their electrical and optical properties upon ligand or cell binding.

To address this problem, we turned our attention to dendrimers as an alternative biocompatible coating for CNTs. Dendrimers possess homogeneous molecular structures and have been exploited in a number of biomedical applications (20-22). Indeed, dendrimers have been recently explored to functionalize CNTs for the attachment of photoactive groups (23), for solubility improvement (24), and for metal capture (25). Their branched architectures and high peripheral functional group density make dendrimers ideal models for mimicking cell surface glycans (4, 26). Many glycodendrimers have been developed to study multivalent carbohydrate-protein interactions implicated in cell-cell recognition events (26, 27). Inspired by these examples as well as recent breakthroughs in dendrimer synthesis using click chemistry (28, 29), we developed a new class of amphiphilic bifunctional glycodendrimers based on 2,2-bis(hydroxymethyl) propionic acid (bis-MPA), a biocompatible building block. As depicted in Scheme 4.1 and Scheme 4.2 (compound **1** and **2**), the dendrimers comprised carbohydrate units displayed in the periphery and a pyrene tail capable of binding SWNT surfaces via π - π interaction. Their geometry is reminiscent of the multi-antennary *N*-linked glycans that populate vertebrate cell surfaces.



Scheme 4.1. Synthesis of generation 3 glycodendrimers. The pyrene tail was conjugated to the focal point of **4** (**4**) by click chemistry and the resulting dendrimer **5** was further coupled with pent-4-ynoic anhydride **6** to introduce additional acetylene groups to the periphery of the dendrimer. The resulting dendrimer **7** was then reacted with a 2-azidoethyl mono- or disaccharides **8a-c** using click chemistry to furnish the desired G3 glycodendrimers **1a-c**. A panel of G2 (**2a-c**) (Scheme 7.2) and G3 glycodendrimers with a variety of glycan structures was synthesized.



Scheme 4.2. Synthesis of generation 2 glycodendrimers (**2a-c**).

Results and discussions:

Design and synthesis of glycosylated dendrimers

The synthesis employed the copper(I)-catalyzed azide-alkyne cycloaddition (CuAAC) reaction, a widely-used example of click chemistry that Sharpless and Hawker have used previously to prepare diverse dendritic structures (29, 30). In our work, the CuAAC reaction allowed for chemoselective ligation of azide-functionalized pyrene and glycan moieties to the alkyne-functionalized focal point and chain ends of a dendrimeric scaffold, respectively (Scheme 4.1)). The synthetic glycans, each with an azidoethyl aglycone,(31) remained unprotected in the synthesis. Applying this methodology, we prepared a panel of G2 (**2a-c**) (Scheme 4.2) and G3 (**1a-c**) (Scheme 4.1) glycodendrimers in near quantitative yield (see reference 32 for nomenclature key). Analysis of the dendrimers by NMR, MALDI-TOF mass spectrometry and gel-permeation chromatography (GPC) indicated that the structures were monodispersed.

Functionalization of CNTs with glycosylated dendrimers

With the panel of glycodendrimers in hand, we then functionalized SWNTs by ultrasonication in aqueous solution. The SWNTs were fully solubilized during the process (Fig. 4.1A I-VI). The suspensions of glycodendrimer-functionalized SWNTs were stable for up to several months, while the unfunctionalized SWNTs precipitated very quickly (within one hour) in water (Fig. 4.1A VII). After several months, coated SWNTs precipitated slowly with the G2 dendrimer-modified SWNTs precipitating more quickly than those coated with G3 dendrimers. The precipitates were easily re-dispersed into solution by ultrasonication for less than one minute. The pyrene moiety on the

glycodendrimer was essential to solubilize the SWNTs. In control experiments, SWNTs precipitated rapidly from aqueous solutions of glycodendrimers that were identical to the above dendrimers but lacked the pyrene moiety (data not shown). We also investigated the glycodendrimer-coated SWNTs by scanning electron microscopy (SEM) and transmission electron microscopy (TEM). Both SEM (Fig. 4.1B) and TEM (Fig. 4.1C) images showed small bundles and individual SWNTs coated entirely with a uniform layer of amorphous glycodendrimer.

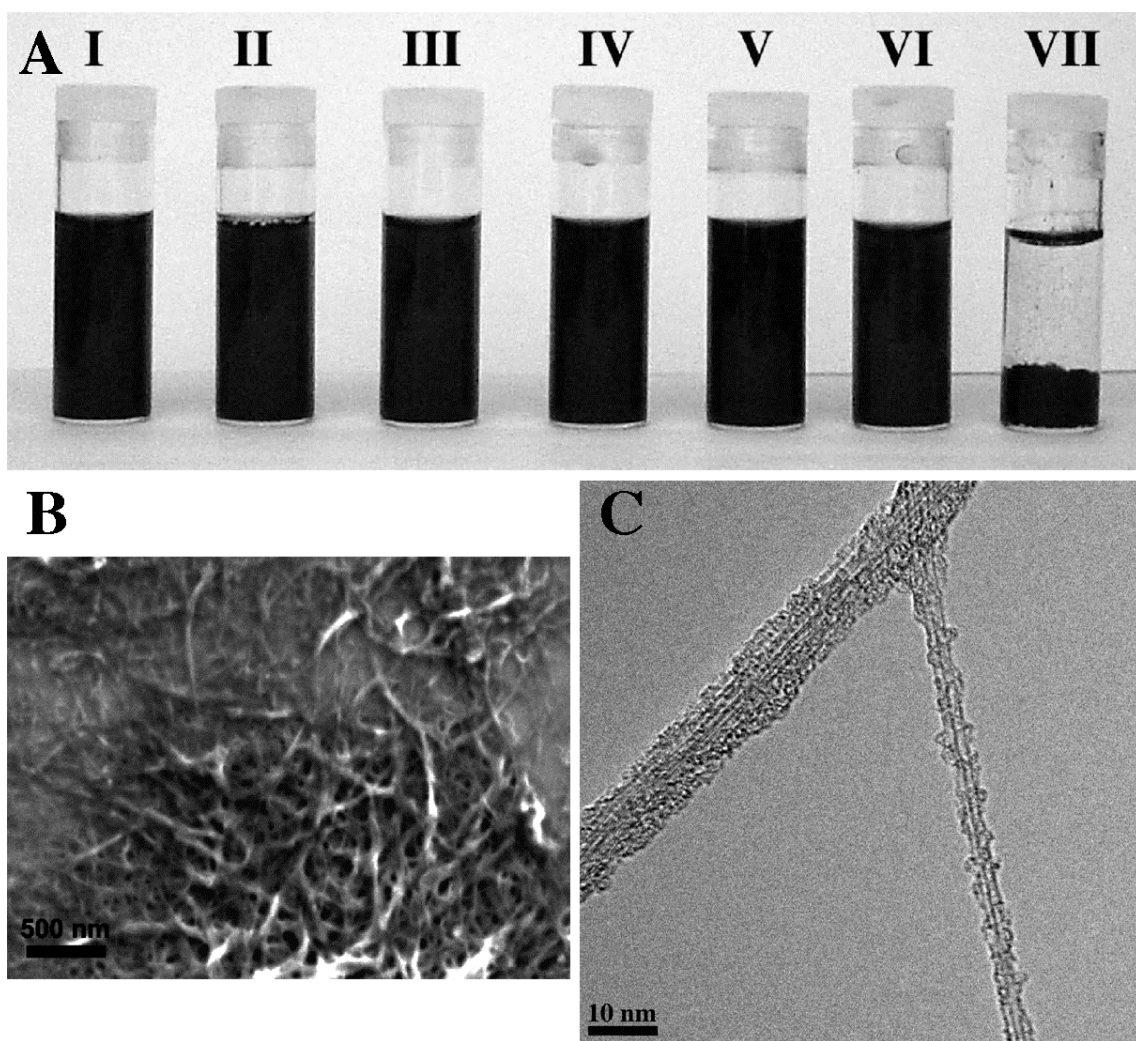


Figure 4.1. (A) Photographs of vials containing SWNT suspensions. G2Man-SWNTs (I), G2Gal-SWNTs (II), G2Lac-SWNTs (III), G3Man-SWNTs (IV), G3Gal-SWNTs (V), G3Lac-SWNTs (VI) formed stable suspensions in water for more than three months, while as-produced SWNTs (VII) precipitate in water in several hours. (B) SEM and (C) TEM images of G3Man-SWNTs. The glycodendrimer coating can be visualized as the density surrounding the SWNT.

Specific binding of proteins to glycodendrimer-coated CNTs

For applications to biosensing or cell targeting, the ability of SWNT-bound glycodendrimers to interact with specific receptors is critical. We probed this using a panel of carbohydrate-binding proteins (i.e., lectins). *Canavalia ensiformis* agglutinin (Con A), *Arachis hypogaea* agglutinin (PNA) and *Psophocarpus tetragonolobus* agglutinin (PTA) are lectins with well-documented specificity for α -mannose, lactose and β -galactose, respectively. All three are available in fluorescein isothiocyanate (FITC)-labeled forms. SWNTs coated with different glycodendrimers (G3Man-SWNTs, G3Gal-SWNTs, and G3Lac-SWNTs) were incubated with FITC-conjugated lectins for 30 minutes, and the unbound protein was removed by dialysis before analysis by fluorescent spectroscopy. The SWNT-associated fluorescence derived from FITC was quantified to evaluate the binding specificity (Fig. 4.2). To our satisfaction, significant fluorescence was observed for ConA-treated G3Man-SWNTs, while only background fluorescence was observed for PTA- or PNA-treated G3Man-SWNTs. Similarly, G3Gal-SWNTs were found to bind to FITC-conjugated PTA, but not to PNA or Con A. Since the non-reducing terminal monosaccharide in lactose is β -galactose, G3Lac-SWNTs were recognized by both PNA and PTA, but not Con A. Similar results were obtained from parallel studies using SWNTs coated with G2 glycodendrimers (data not shown). Thus, the specificities of the lectins are accurately reflected in the context of glycodendrimer-functionalized SWNTs.

To more accurately mirror the complexity of biological glycoconjugates, which typically display multiple glycan epitopes, we functionalized SWNTs with an aqueous mixture of G2Man (**2a**) and G2Lac (**2c**) at various ratios. After dialysis to remove the

free glycodendrimers, the glycodendrimer-coated SWNTs were incubated with a 1:1 (molar ratio) mixture of Texas Red-conjugated PNA and FITC-conjugated ConA. Fluorescence analysis of lectin-treated SWNTs revealed that the intensity of Texas Red emission dropped with an accompanied increase in FITC emission that matched the percentage G2Man in the SWNT coating (Fig. 4.3). This result demonstrates that multiple epitopes with discrete receptor specificities can be simultaneously recognized on the SWNT surface.

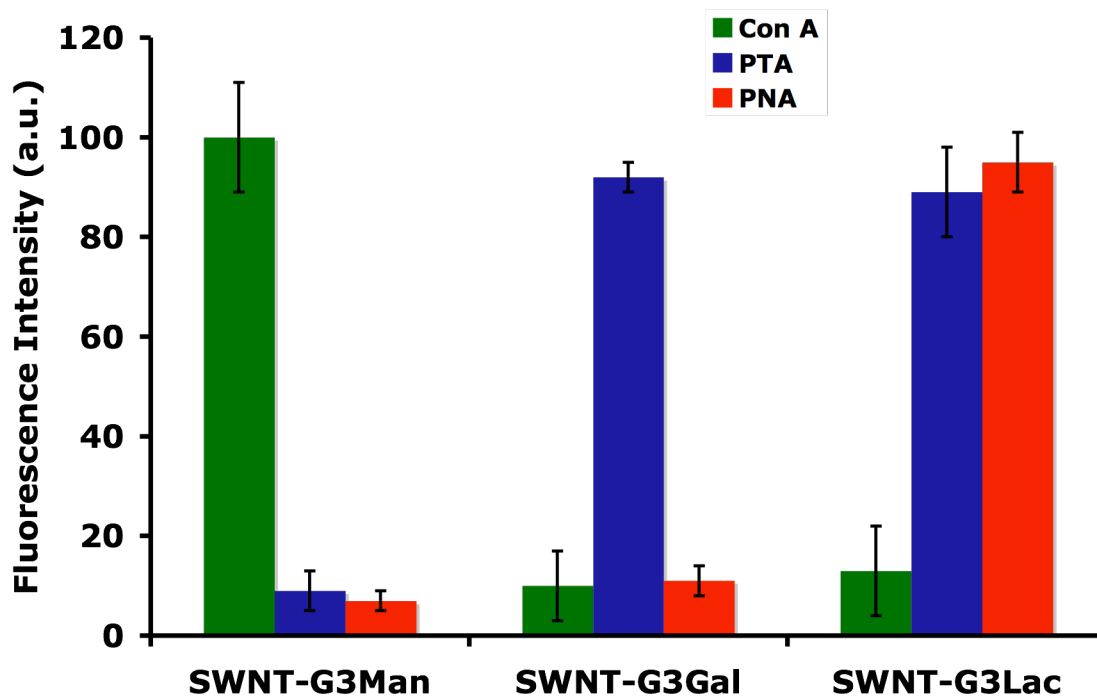


Figure 4.2. Lectin binding to glycodendrimer-coated SWNTs. Con A and PNA exhibit specific binding to G3Man-SWNTs and G3Lac-SWNTs, respectively. PTA binds to both G3Gal-SWNTs and G3Lac-SWNTs. Error bars indicate the standard deviation for 3 replicate experiments.

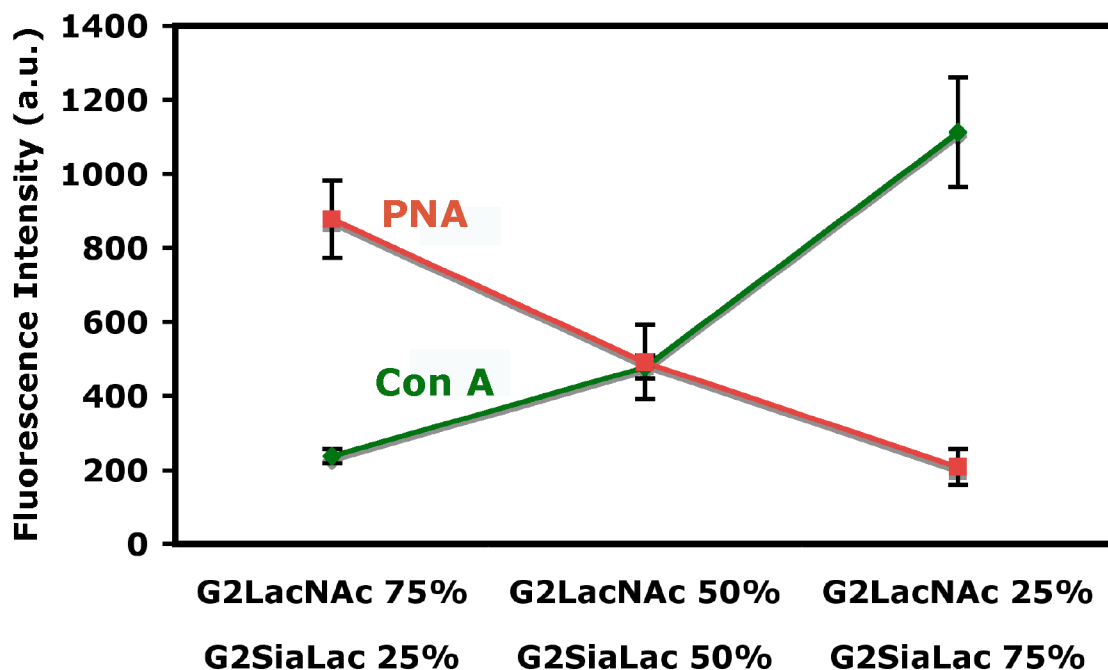


Figure 4.3. Modulation of lectin bindings to SWNTs co-functionalized with two different glycodendrimers. SWNTs coated with G2Lac and G2Man at various ratios were incubated with a 1:1 (molar ratio) mixture of Texas Red-conjugated PNA and FITC-conjugated Con A. The intensities of Texas Red and FITC emission paralleled the ratio of G2Lac and G2Man components in the SWNT coating, respectively. Error bars indicate the standard deviation for three replicate experiments.

Interfacing glycodendrimer-coated CNTs with living cells

Another interesting application of the glycodendrimer-coating strategy is to interface live cells and SWNTs for more refined applications in cell biology. We achieved this using a multivalent lectin crosslinker. As an example, we first coated G2Man-SWNTs with FITC-conjugated Con A (ConA-FITC), a tetravalent lectin capable of crosslinking cells and glycoproteins (33). We hypothesized that after binding to the surface of G2Man-SWNTs, Con A would still possess open sites for further complexation with α -mannose residues on cell surface glycoproteins. This notion was confirmed by incubating the lectin-modified SWNTs with Chinese hamster ovary (CHO) cells and detection of FITC fluorescence by microscopy. As shown in Figure 4.4, Con A labeled G2Man-SWNTs bound specifically to the cell membranes. As a control, we performed the same experiment using SWNTs coated with a G2Gal (**2c**) dendrimer, which do not bind to Con A. In this case, no fluorescent labeling of the cells was observed (data not shown). By contrast, G2Gal-SWNTs and G2Lac-SWNTs labeled the CHO cells robustly when PTA and PNA were used as crosslinkers, respectively (data not shown). Moreover, the G3 glycodendrimer-coated SWNTs (G3Man-SWNTs, G3Gal-SWNTs, and G3Lac-SWNTs) gave similar results (data not shown). Collectively, these data demonstrated that SWNTs coated with glycodendrimers could be specifically bound to cells without significant non-specific protein or cell binding.

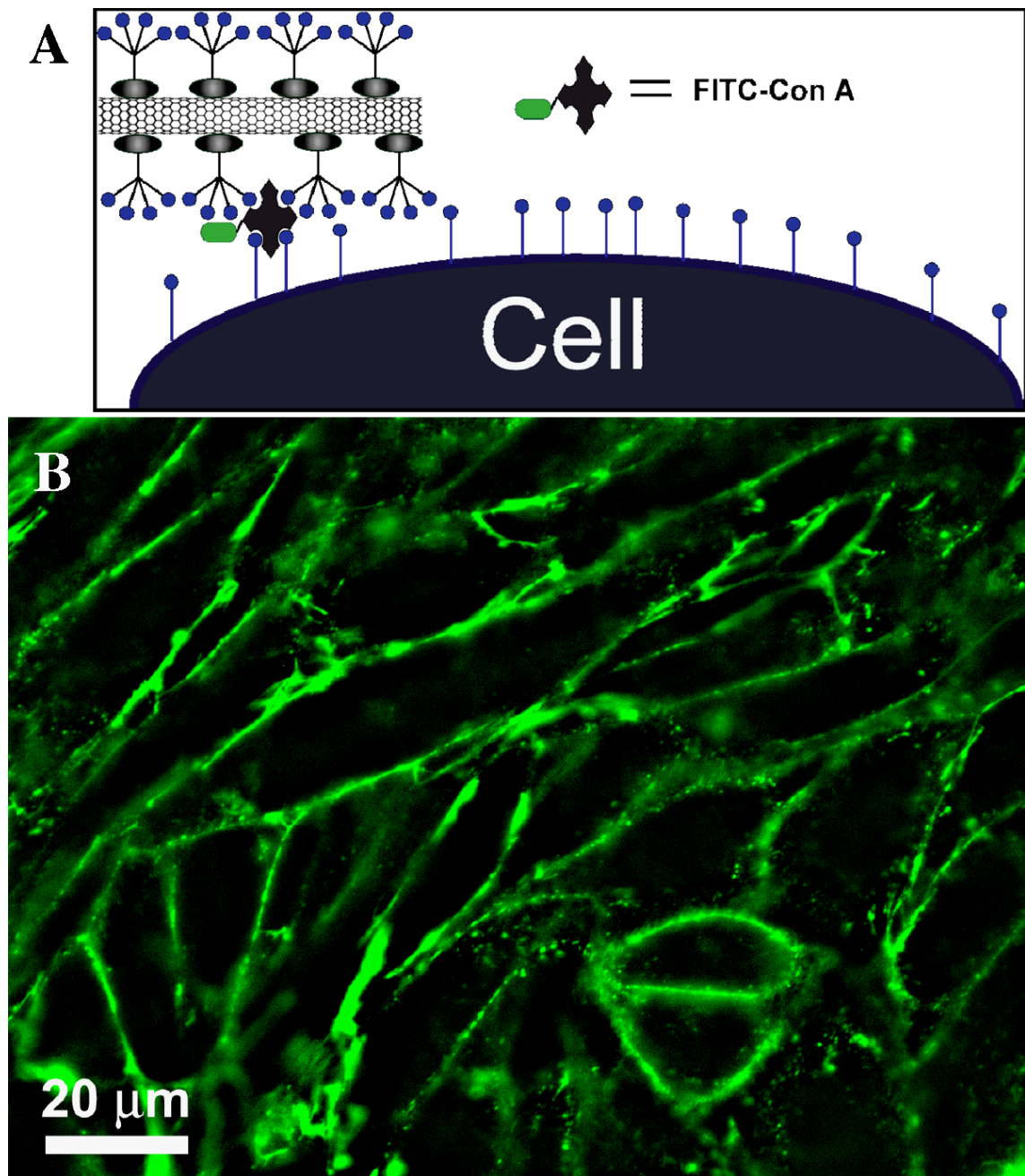


Figure 4.4. (A) The schematic representation of the interfacing between glycodendrimer-coated SWNTs with live cells. (B) Fluorescence micrograph of CHO cells labeled with the complexes of G2Man-SWNT and FITC-Con A.

Cytotoxicity studies of glycodendrimer-coated CNTs

At the outset, our goal was to develop a coating for SWNTs that would render them nontoxic to cells. To evaluate the cytotoxicity of glycodendrimer-coated SWNTs, we cultured HEK293 cells with G2Man-SWNTs, G2Gal-SWNTs, G2Lac-SWNTs, G3Man-SWNTs, G3Gal-SWNTs, and G3Lac-SWNTs (each at 100 $\mu\text{g}/\text{mL}$) for 4 days. In control experiments, the cells were cultured with unmodified SWNTs or with media alone. Viable cells (trypan blue assay) were counted each day. As shown in Figure 4.5, cells cultured with glycodendrimer-coated SWNTs proliferated at the same rate as cells grown in the absence of SWNTs. In contrast, unmodified SWNTs greatly hampered the growth of HEK293 cells. Thus, glycodendrimer-coated SWNTs did not appear to affect cell proliferation, unlike their uncoated counterparts.

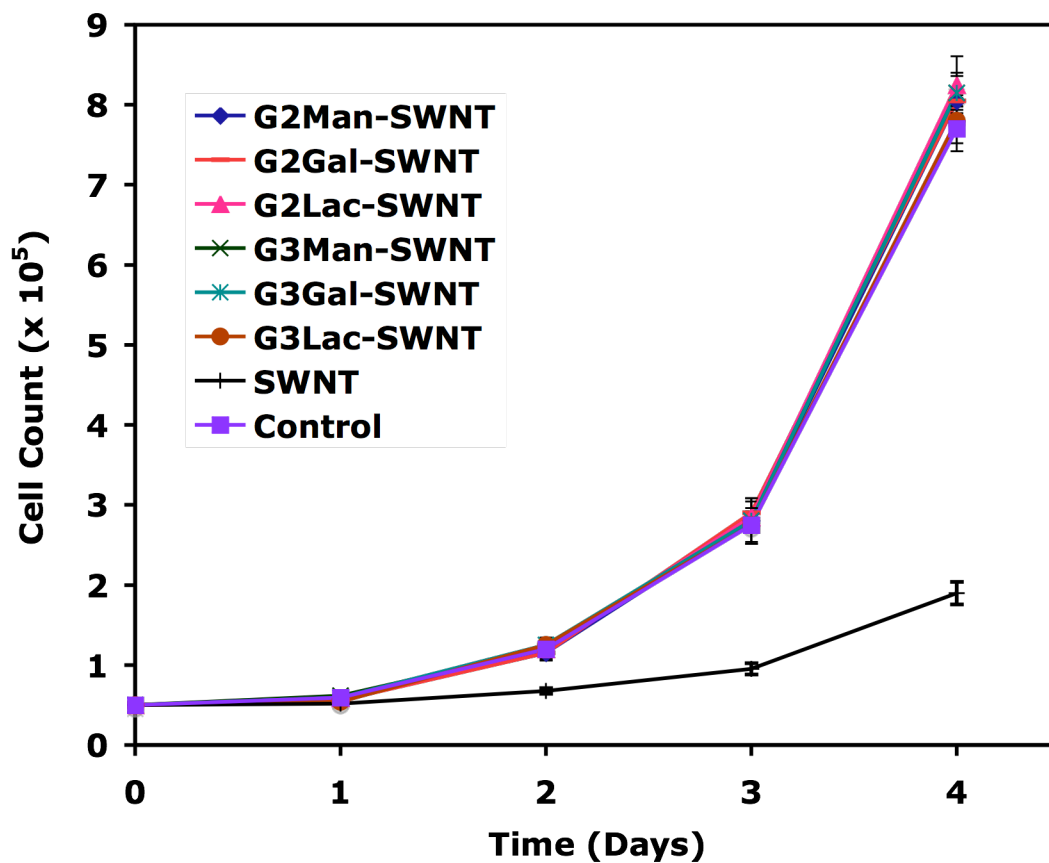


Figure 4.5. Effects of glycodendrimer-coated SWNTs on the proliferation of HEK293 cells. Cell number was measured by the Trypan blue dye exclusion method. The control cells were grown in the absence of SWNTs. The error bars represent the standard deviation for three replicates.

Conclusions

In summary, we developed a strategy for generating uniform and bioactive coatings SWNTs using glycodendrimers. The dendrimer-coated SWNTs participate in specific carbohydrate-receptor interactions and show no toxicity to cultured cells. The synthetic method used to construct the glycodendrimers can be readily extended to alternative ligand systems for other receptor interactions. Future applications include probing biological processes using SWNTs as biosensors.

Materials and methods

Synthesis of new compounds

Analytical TLC was performed on commercial Merck plates (GF254, 0.24 mm thick). Silica for flash chromatography was Merck Kieselgel 60 (230-400 mesh, ASTM). ^1H NMR and ^{13}C NMR spectra were acquired on Bruker AMX-400, or DRX-500 MHz spectrometers at rt. ^1H and ^{13}C chemical shifts (δ) are reported in parts per million (ppm) referenced to TMS (0 ppm) and were measured relative to the residual solvent peak. Coupling constants (J) are reported in hertz (Hz). High-resolution fast atom bombardment (FAB) mass spectra were obtained at the UC Berkeley Mass Spectrometry Laboratory. Size exclusion chromatography (SEC) was carried out at rt on a Waters low pressure chromatography system equipped with a Waters 410 differential refractometer and six Waters Styragel[®] columns (five HR-5 μm and one HMW-20 μm) using THF as eluant (flow rate: 1 mL/min). The molecular weights of the polymers were calculated relative to linear polystyrene standards. MALDI-TOF mass spectrometry was performed on a PerSeptive Biosystems Voyager DE mass spectrometer operating in linear mode, using dithranol in combination with silver trifluoroacetate as matrix.

***N*-(3-Azidopropyl)-4-(pyren-1-yl)butanamide (3).** 1-Pyrenebutyric acid or 7-(diethylamino)-coumarin-3-carboxylic acid (1.15 g, 4.00 mmol) was dissolved in DMF (40.0 mL). *O*-Benzotriazol-1-yl-*N,N,N',N'*-tetramethyluronium tetrafluoroborate (5.10 g, 16.0 mmol), *N*-hydroxybenzotriazole (2.20 g, 16.0 mmol), and *N*-methyldmorpholine were added sequentially at room temperature. The solution was stirred for 5 min before (3-azidopropyl) amine (0.50 g, 5.0 mmol) was added slowly. The solution was stirred for 4 h before the solvent was removed under vacuum. The residue was partitioned between EtOAc (100 mL) and 10% NaHCO₃ (50 mL) and the organic layer was washed with another portion of 10% NaHCO₃ (50 mL) and brine (50 mL). After drying over Na₂SO₄ and the removal of solvent, the crude product was purified by silica gel chromatography eluting with CH₂Cl₂ and gradually increasing the polarity by addition of EtOAc to final composition of 15%. The product was isolated as a yellow solid. Yield: 3.00 g (91%). ¹H NMR (CDCl₃, 400MHz): δ 8.24 (d, *J* = 7.2 Hz, 1H), 8.14 (d, *J* = 7.6 Hz, 2H), 8.08 (d, *J* = 2.8 Hz, 1H), 8.06-7.96 (m, 4H), 7.79 (d, *J* = 7.6 Hz, 1H) 5.68 (s, 1H), 3.32 (t, *J* = 6.0 Hz, 1H), 3.26-3.19 (m, 4H), 2.20-2.12 (m, 4H), 1.66 (m, 2H). ¹³C NMR (CDCl₃, 100 MHz): δ 172.7, 135.7, 131.4, 130.8, 129.9, 128.7, 127.4, 127.3(7), 127.3(2), 126.7, 125.9, 125.1, 124.9(28), 124.9(16) 124.8, 123.3, 114.5, 49.3, 37.1, 35.9, 32.7, 28.8, 27.3. FAB-HRMS calcd for C₂₃H₂₂N₄ONa [MNa]⁺: *m/z* 393.1691. Found: 393.1699.

Pyrene-G2-(OH)₄ (10). To a solution of **9** (*4*) (370 mg, 0.920 mmol) and *N*-(3-azidopropyl)-4-(pyren-1-yl)butanamide (350 mg, 0.950 mmol) in THF/H₂O (3:1, 3.0 mL), were added sodium ascorbate (35.0 mg, 0.176 mmol) and CuSO₄·5H₂O (15 mg, 60 μmol). The reaction mixture was then allowed to stir for 12 h at rt. The solvents were evaporated and the crude product was purified by silica gel chromatography eluting with

EtOAc and gradually increasing the polarity by addition of MeOH to final composition of 20% to give 650 mg (91%) of the target molecule as a colorless solid, which was used directly in the next step.

Pyrene-G2-(Acet)₄ (11). Pent-4-ynoic acid anhydride (**6**) (560 mg, 3.15 mmol) was added to a solution of **10** (400 mg, 0.520 mmol), pyridine (1.00 mL, 12.4 mmol), and DMAP (38 mg, 0.30 mmol) in CH₂Cl₂ (2 mL). The solution was stirred at rt overnight and the reaction progress was monitored by ¹³C NMR analysis of the anhydride resonance at ~167 ppm. The excess **6** was quenched with 0.5 mL of water with vigorous stirring, followed by dilution with 100 mL of CH₂Cl₂. The solution was washed with 10% of NaHSO₄ (3 x 60 mL), and 10% of Na₂CO₃ (3 x 100 ml). The organic phase was dried (MgSO₄), filtered, concentrated and purified by silica gel chromatography eluting with hexanes and gradually increasing the polarity by addition of EtOAc to final composition of 20% to give the target molecule as a yellow solid. Yield: 523 mg (92%). ¹H NMR (CDCl₃, 500MHz): δ 8.30 (d, *J* = 9.0 Hz, 1H), 8.17 (d, *J* = 3.0 Hz, 1H), 8.16 (d, *J* = 3.5 Hz, 1H), 8.11 (d, *J* = 8.5 Hz, 2H), 8.02 (s, 2H), 7.99 (t, *J* = 7.5 Hz, 1H), 7.86 (d, *J* = 8.5 Hz, 1H), 7.74 (s, 1H), 5.83 (br, 1H), 5.22 (s, 2H), 4.39 (t, *J* = 7.0 Hz, 2H), 4.26-4.15 (m, 12H), 3.40 (t, *J* = 7.5 Hz, 2H), 3.25 (m, 2H), 2.54 (m, 8H), 2.45 (m, 8H), 2.30 (m, 2H), 2.22 (m, 2H), 2.10 (m, 2H), 1.97 (t, *J* = 2.5 Hz, 4H), 1.23 (s, 3H), 1.20 (s, 6H). ¹³C NMR (CDCl₃): δ 173.1, 172.0, 171.8, 171.2, 142.0, 135.7, 131.4, 130.8, 129.9, 128.7, 127.43, 127.40, 127.3, 126.7, 125.9, 125.0, 124.94, 124.91, 124.8, 124.5, 123.3, 82.3, 69.2, 65.5, 65.3, 58.4, 47.7, 46.6, 46.3, 36.3, 35.9, 33.1, 32.8, 30.1, 27.3, 17.7, 17.5, 14.3. MALDI-MS Calcd for C₆₁H₆₆N₄O₁₅Na [MNa]⁺: *m/z* 1117.4. Found: 1117.6.

Pyrene-G3-(OH)₈ (5). *N*-(3-azidopropyl)-4-(pyren-1-yl)butanamide, (175 mg, 0.470 mmol) and **4 (4)** (398 mg, 0.460 mmol) were dissolved in 4 mL of DMF and the solution was cooled to 0 °C. An ice-cold solution of CuSO₄·5H₂O (8 mg, 32 μmol) in water (2 mL) followed by sodium ascorbate (25.0 mg, 126 μmol) was added to the DMF solution. The reaction mixture was stirred for 12 h at rt. The solvents were evaporated and the crude product was purified by silica gel chromatography eluting with EtOAc and gradually increasing the polarity by addition of MeOH to final composition of 20% to give 541 mg (95%) of the target molecule as a yellow solid, which was used directly in the next step.

Pyrene-G3-(Acet)₈ (7). The procedure was similar to that described for 11. The reaction was performed with 650 g (4.20 mmol) of **5**, 1.64 mL (20.2 mmol) of pyridine, 77 mg (0.63 mmol) of DMAP, and 1.12 g (6.30 mmol) of **6** to afford 900 mg (90%) of target molecule. ¹H NMR (CDCl₃, 500MHz): δ 8.30 (d, *J* = 9.0 Hz, 1H), 8.17 (d, *J* = 3.0 Hz, 1H), 8.16 (d, *J* = 3.5 Hz, 1H), 8.11 (d, *J* = 8.5 Hz, 2H), 8.03 (s, 2H), 7.99 (t, *J* = 7.5 Hz, 1H), 7.86 (d, *J* = 8.5 Hz, 1H), 7.77 (s, 1H), 5.96 (br, 1H), 5.23 (s, 2H), 4.40 (t, *J* = 6.5 Hz, 2H), 4.26-4.16 (m, 28H), 3.40 (t, *J* = 7.5 Hz, 2H), 3.26 (m, 2H), 2.54 (m, 16H), 2.46 (m, 16H), 2.32 (m, 2H), 2.23 (m, 2H), 2.10 (m, 2H), 1.98 (t, *J* = 2.5 Hz, 8H), 1.26 (s, 3H), 1.23 (s, 12H), 1.20 (s, 6H). MALDI-MS Calcd for C₁₀₁H₁₁₄N₄O₃₁Na [MNa]⁺: *m/z* 1902.7. Found: 1903.7.

General procedure for synthesis of G2 (1a-c) and G3 (2a-c) dendrimers by coupling saccharides (8a-c) with dendrimer 11 or 7. Dendrimer **11** or **7** (18 μmol) and saccharides **8a-c** (96 μmol) were dissolved in 1.2 mL of THF/H₂O (1.5:1) followed by addition of sodium ascorbate (3.0 mg, 15 μmol) and CuSO₄·5H₂O (1 mg, 4 μmol). The

reaction mixture was stirred overnight at rt. LC-MS analysis indicated that the alkyne-bearing dendrimer was completely consumed. The solvents were then evaporated. The crude product was redissolved in 0.5 mL of aqueous EDTA (0.1 M, pH = 8) and purified by size-exclusion chromatography (sephadex[®] G-25) eluting with H₂O/*n*-butanol (95:5). Lyophilization of the solvents gave the target glycodendrimer in > 92% yield.

G2Man (2a). Yield: 37 mg (97%). ¹H NMR (DMSO-d₆, 500 MHz): δ 8.38 (d, *J* = 9.5 Hz, 1H), 8.27 (m, 2H), 8.21 (m, 2H), 8.16 (s, 1H), 8.13 (d, *J* = 3.0 Hz, 2H), 8.05 (t, *J* = 7.5 Hz, 1H), 7.95 (m, 2H), 7.81 (s, 4H), 5.16 (s, 2H), 4.70 (br, 4H), 4.59 (d, *J* = 1.0, 4H), 4.54-4.43(m, 12H), 4.36 (t, *J* = 7.0, 2H), 4.16 (m, 4H), 4.07 (s, 8H), 3.91 (m, 4H), 3.75 (m, 4H), 3.60 (m, 4H), 3.53(br, 4H), 3.42-3.30 (m, 24H), 3.09 (m, 6H), 2.84 (t, *J* = 7.5 Hz, 8H), 2.65 (t, *J* = 7.5 Hz, 8H), 2.24 (t, *J* = 7.0 Hz, 2H), 2.01 (m, 2H), 1.95 (m, 2H), 1.14 (s, 3H), 1.04 (s, 6H). MALDI-MS Calcd for C₉₃H₁₂₆N₁₆O₃₉Na [MNa]⁺: *m/z* 2114.8. Found: 2115.2.

G2Gal (2b). Yield: 89 mg (93%). ¹H NMR (DMSO-d₆, 500 MHz): δ 8.36 (d, *J* = 9.5 Hz, 1H), 8.25 (m, 2H), 8.20 (m, 2H), 8.14 (s, 1H), 8.11 (d, *J* = 3.0 Hz, 2H), 8.03 (t, *J* = 8.0 Hz, 1H), 7.93 (m, 2H), 7.91 (s, 4H), 5.16 (s, 2H), 4.96 (br, 4H), 4.77 (br, 4H), 4.59 (t, *J* = 5.2, 4H), 4.52-4.33 (m, 10H), 4.15-4.02 (m, 20H), 3.84 (m, 4H), 3.62 (br, 4H), 3.50(m, 8H), 3.42-3.30 (m, 18H), 3.09 (m, 2H), 2.84 (t, *J* = 7.5 Hz, 8H), 2.65 (t, *J* = 7.5 Hz, 8H), 2.24 (t, *J* = 7.5 Hz, 2H), 2.00 (m, 2H), 1.93 (m, 2H), 1.14 (s, 3H), 1.05 (s, 6H). MALDI-MS Calcd for C₉₃H₁₂₆N₁₆O₃₉Na [MNa]⁺: *m/z* 2114.8. Found: 2114.6.

G2Lac (2c). Yield: 74 mg (96%). ¹H NMR (DMSO-d₆, 500 MHz): δ 8.38 (d, *J* = 9.5 Hz, 1H), 8.28 (m, 2H), 8.22 (m, 2H), 8.16 (s, 1H), 8.13 (d, *J* = 3.5 Hz, 2H), 8.05 (t, *J* = 7.5 Hz, 1H), 7.94 (m, 2H), 7.91 (s, 4H), 5.26 (br, 4H), 5.16 (s, 2H), 5.11 (br, 4H), 4.78

(br, 4H), 4.69-4.43 (m, 24H), 4.35 (t, $J = 7.0$, 2H), 4.29 (d, $J = 7.5$ Hz, 4H), 4.19(d, $J = 7$ Hz, 4H), 4.07-4.04 (m, 12H), 3.86 (m, 4H), 3.76 (d, $J = 11$ Hz, 4H), 3.59-3.56 (m, 8H), 3.53-3.44 (m, 12H), 3.34-3.25 (m, 26H), 3.07 (m, 2H), 3.03 (t, $J = 8.0$ Hz, 4H), 2.82 (t, $J = 7.5$ Hz, 8H), 2.63 (t, $J = 7.5$ Hz, 8H), 2.24 (t, $J = 7.0$ Hz, 2H), 2.01 (m, 2H), 1.95 (m, 2H), 1.14 (s, 3H), 1.05 (s, 6H). MALDI-MS Calcd for $C_{117}H_{166}N_{16}O_{59}Na [MNa]^+$: m/z 2763.0. Found: 2762.8.

G3Man (1a). Yield: 46 mg (90%). 1H NMR (DMSO- d_6 , 500 MHz): δ 8.38 (d, $J = 9.0$ Hz, 1H), 8.27 (m, 2H), 8.21 (m, 2H), 8.15 (s, 1H), 8.13 (d, $J = 3.0$ Hz, 2H), 8.05 (t, $J = 7.5$ Hz, 1H), 7.95 (m, 2H), 7.81 (s, 8H), 5.16 (s, 2H), 4.73 (br, 8H), 4.59 (br, 8H), 4.54-4.43(m, 24H), 4.36 (t, $J = 7.0$, 2H), 4.22-4.10 (m, 28H), 3.91 (m, 8H), 3.75 (m, 8H), 3.60 (m, 8H), 3.53(br, 8H), 3.42-3.30 (m, 34H), 3.11(t, $J = 7.0$ Hz, 8H), 3.07 (m, 2H), 2.84 (t, $J = 7.5$ Hz, 16H), 2.65 (t, $J = 7.5$ Hz, 16H), 2.24 (t, $J = 7.5$ Hz, 2H), 2.01 (m, 2H), 1.94 (m, 2H), 1.17 (s, 3H), 1.09 (s, 18H). MALDI-MS Calcd for $C_{165}H_{234}N_{28}O_{79}Na [MNa]^+$: m/z 3896.5. Found: 3896.0 (MNa^+).

G3Gal (1b). Yield: 100 mg (93%). 1H -NMR (DMSO- d_6 , 500 MHz): δ 8.36 (d, $J = 9.5$ Hz, 1H), 8.25 (m, 2H), 8.20 (m, 2H), 8.14 (s, 1H), 8.11 (d, $J = 3.0$ Hz, 2H), 8.03 (t, $J = 8.0$ Hz, 1H), 7.92 (m, 2H), 7.90 (s, 8H), 5.16 (s, 2H), 5.00 (br, 8H), 4.63 (br, 8H), 4.48 (m, 16H), 4.35 (t, $J = 6.5$, 2H), 4.15-4.10 (m, 28H), 4.03 (m, 8H), 3.82 (m, 8H), 3.62 (br, 8H), 3.50 (m, 16H), 3.38-3.25 (m, 50H), 3.06 (m, 2H), 2.82 (t, $J = 7.5$ Hz, 16H), 2.63 (t, $J = 7.5$ Hz, 16H), 2.23 (t, $J = 7.5$ Hz, 2H), 1.98 (m, 2H), 1.93 (m, 2H), 1.16 (s, 3H), 1.08 (s, 18H). MALDI-MS Calcd for $C_{165}H_{234}N_{28}O_{79}Na [MNa]^+$: m/z 3896.5. Found: 3896.2.

G3Lac (1c). Yield: 97 mg (91%). 1H NMR (DMSO- d_6 , 500 MHz): δ 8.37 (d, $J = 9.5$ Hz, 1H), 8.26 (m, 2H), 8.21 (m, 2H), 8.15 (s, 1H), 8.12 (d, $J = 3.5$ Hz, 2H), 8.05 (t, J

= 7.5Hz, 1H), 7.93 (m, 2H), 7.90 (s, 8H), 5.27 (br, 8H), 5.16 (s, 2H), 5.12 (br, 8H), 4.81 (br, 8H), 4.69-4.47 (m, 48H), 4.35 (t, $J = 6.5$, 2H), 4.29 (d, $J = 8.0$ Hz, 8H), 4.19(d, $J = 7$ Hz, 8H), 4.14-4.04 (m, 28H), 3.83 (m, 8H), 3.75 (d, $J = 11$ Hz, 8H), 3.61-3.58 (m, 16H), 3.53-3.44 (m, 24H), 3.36-3.25 (m, 50H), 3.07 (m, 2H), 3.03 (t, $J = 8.0$ Hz, 8H), 2.83 (t, $J = 7.5$ Hz, 16H), 2.63 (t, $J = 7.5$ Hz, 16H), 2.24 (t, $J = 7.0$ Hz, 2H), 2.01 (m, 2H), 1.95 (m, 2H), 1.17 (s, 3H), 1.09 (s, 18H). MALDI-MS Calcd for $C_{213}H_{314}N_{28}O_{119}Na [MNa]^+$: m/z 5192.9. Found: 5193.8.

Functionalization of SWNTs with glycosylated dendrimers

In a typical preparation experiment, 1 mg of SWCNTs (Carbon Nanotechnologies Inc) was suspended in 5 mL of aqueous glycodendrimer solution (0.1%~0.5%). The mixture was sonicated using a water-bath sonicator for 1 h. The insoluble materials were removed by centrifugation and the product suspension was decanted from insoluble material. The excess free glycodendrimers were removed by dialysis of the suspension in a polycarbonate membrane against deionized water or PBS buffer.

SEM and TEM characterization

SEM images of glycodendrimer-coated SWNTs were obtained on an FEI Sirion XL 30 SEM operated at 5 keV. TEM images of glycodendrimer-coated SWNTs were obtained on a JEOL 2011 microscope operating at electron energy of 100 keV.

Lectin Binding Assays

Lectins, *Canavalia ensiformis* agglutinin (Con A) conjugated with fluorescein isothiocyanate (Con A-FITC), *Arachis hypogaea* agglutinin conjugated with fluorescein isothiocyanate (PNA-FITC), and *Psophocarpus tetragonolobus* agglutinin conjugated with fluorescein isothiocyanate (PTA -FITC), were obtained from EY-Laboratories. In a typical experiment, a 1-mL solution of lectin-FITC conjugates (100 $\mu\text{g/mL}$) in PBS buffer containing 1 mM CaCl_2 was added to the suspensions of glycodendrimer-coated SWNTs (1 mL). The reactions were incubated for 1 h at rt in the dark. After incubation, the solutions were all subjected to dialysis against the buffer for 48 h. The dialyzed solutions were analyzed at 517 nm using a fluorescence microplate reader (excitation wavelength 492 nm). Fluorescence intensities were corrected for background fluorescence by subtracting the fluorescence intensities of glycodendrimer-coated SWNTs alone.

Cell culture conditions

All cell lines were maintained in a 5% CO_2 , water-saturated atmosphere at 37 °C and media were supplemented with penicillin (100 unit/mL), streptomycin (0.1 mg/mL) and 10% FCS unless otherwise indicated. CHO cells were grown in Ham F12 nutrient mixture. HEK 293 cells were grown in DMEM media.

Cell binding of glycodendrimer-coated SWNTs

CHO Cells were seeded onto glass slides mounted with tissue culture wells (LAB-TEK) and allowed to adhere for 2 d. The cells were washed 3 times with PBS, and then

fixed in 3% paraformaldehyde in PBS. After three washes, cells were blocked in PBS with 1% bovine serum albumin for 20 min, followed by the addition of glycodendrimer-coated SWNTs complexed with appropriate lectin-FITC conjugates as described above. After a 1-h incubation at rt in the dark, the cells were washed 3 times. The cells were then mounted using Vectashield with 4,6-diamidino-2-phenylindole (Vector Laboratories). A Zeiss Axiovert 200M inverted microscope equipped with a 63 × 1.4 NA Plan-Apochromat oil immersion lens was employed for imaging. A 175W xenon lamp housed in a Sutter DG4 illuminator linked to the microscope by an optical fiber assured shuttering and illumination. Images were acquired using a CoolSNAP HQ CCD camera (Roper Scientific). Slidebook software (Intelligent Imaging Solutions) was used to control the microscope and the camera.

Cytotoxicity assays

HEK 293 Cells were incubated with glycodendrimer-coated SWNTs (each at 50 $\mu\text{g}/\text{mL}$) for 4 d. In control experiments, the cells were cultured with unmodified SWNTs or with media alone. Cells were washed twice with PBS and then trypsinized with 0.25% trypsin-EDTA (PBS, pH 7.4), resuspended in media. The viable cells were counted every day using the Trypan blue dye exclusion method.

References

1. Y. Lin *et al.*, Advances toward bioapplications of carbon nanotubes. *J. Mater. Chem.* **14**, 527-541 (2004).
2. D. Tasis, N. Tagmatarchis, A. Bianco, M. Prato, Chemistry of carbon nanotubes. *Chem. Rev.* **106**, 1105-1136 (2006).
3. R. S. Kane, A. D. Stroock, Nanobiotechnology: Protein-nanomaterial interactions. *Biotechnol. Prog.* **23**, 316-319 (2007).
4. P. Wu *et al.*, Multivalent, bifunctional dendrimers prepared by click chemistry. *Chem. Commun.*, 5775-5777 (2005).
5. A. Star *et al.*, Label-free detection of DNA hybridization using carbon nanotube network field-effect transistors. *Proc. Natl. Acad. Sci. USA* **103**, 921-926 (2006).
6. S. S. Wong, E. Joselevich, A. T. Woolley, C. L. Cheung, C. M. Lieber, Covalently functionalized nanotubes as nanometre-sized probes in chemistry and biology. *Nature* **394**, 52-55 (1998).
7. K. Kostarelos *et al.*, Cellular uptake of functionalized carbon nanotubes is independent of functional group and cell type. *Nat. Nanotech.* **2**, 108-113 (2007).
8. N. W. S. Kam, M. O'Connell, J. A. Wisdom, H. J. Dai, Carbon nanotubes as multifunctional biological transporters and near-infrared agents for selective cancer cell destruction. *Proc. Natl. Acad. Sci. USA* **102**, 11600-11605 (2005).
9. Z. Liu *et al.*, In vivo biodistribution and highly efficient tumour targeting of carbon nanotubes in mice. *Nat. Nanotech.* **2**, 47-52 (2007).
10. V. L. Colvin, The potential environmental impact of engineered nanomaterials. *Nat. Biotechnol.* **21**, 1166-1170 (2003).
11. D. X. Cui, F. R. Tian, C. S. Ozkan, M. Wang, H. J. Gao, Effect of single wall carbon nanotubes on human HEK293 cells. *Toxicol. Lett.* **155**, 73-85 (2005).
12. G. Jia *et al.*, Cytotoxicity of carbon nanomaterials: Single-wall nanotube, multi-wall nanotube, and fullerene. *Environ. Sci. Technol.* **39**, 1378-1383 (2005).
13. A. Magrez *et al.*, Cellular toxicity of carbon-based nanomaterials. *Nano Lett.* **6**, 1121-1125 (2006).
14. M. S. Arnold, M. O. Guler, M. C. Hersam, S. I. Stupp, Encapsulation of carbon nanotubes by self-assembling peptide amphiphiles. *Langmuir* **21**, 4705-4709 (2005).

15. C. M. Sayes *et al.*, Functionalization density dependence of single-walled carbon nanotubes cytotoxicity in vitro. *Toxicol. Lett.* **161**, 135-142 (2006).
16. H. Dumortier *et al.*, Functionalized carbon nanotubes are non-cytotoxic and preserve the functionality of primary immune cells. *Nano Lett.* **6**, 1522-1528 (2006).
17. X. Chen, G. S. Lee, A. Zettl, C. R. Bertozzi, Biomimetic engineering of carbon nanotubes by using cell surface mucin mimics. *Angew. Chem. Int. Ed.* **43**, 6111-6116 (2004).
18. X. Chen *et al.*, Interfacing carbon nanotubes with living cells. *J. Am. Chem. Soc.* **128**, 6292-6293 (2006).
19. D. Rabuka *et al.*, Hierarchical assembly of model cell surfaces: Synthesis of mucin mimetic polymers and their display on supported bilayers. *J. Am. Chem. Soc.* **129**, 5462-5471 (2007).
20. C. C. Lee, J. A. MacKay, J. M. J. Frechet, F. C. Szoka, Designing dendrimers for biological applications. *Nat. Biotechnol.* **23**, 1517-1526 (2005).
21. Y. Kim, S. C. Zimmerman, Applications of dendrimers in bio-organic chemistry. *Curr. Opin. Chem. Biol.* **2**, 733-742 (1998).
22. S. Svenson, D. a. Tomalia, Commentary - Dendrimers in biomedical applications - reflections on the field. *Adv. Drug Deliv. Rev.* **57**, 2106-2129 (2005).
23. S. Campidelli *et al.*, Dendrimer-functionalized single-wall carbon nanotubes: Synthesis, characterization, and photoinduced electron transfer. *J. Am. Chem. Soc.* **128**, 12544-12552 (2006).
24. Y. P. Sun *et al.*, Soluble dendron-functionalized carbon nanotubes: Preparation, characterization, and properties. *Chem. Mater.* **13**, 2864-2869 (2001).
25. M. Holzinger *et al.*, Functionalization of single-walled carbon nanotubes with (R-)oxycarbonyl nitrenes. *J. Am. Chem. Soc.* **125**, 8566-8580 (2003).
26. W. B. Turnbull, J. F. Stoddart, Design and synthesis of glycodendrimers. *Rev. Mol. Biotechnol.* **90**, 231-255 (2002).
27. M. J. Cloninger, Biological applications of dendrimers. *Curr. Opin. Chem. Biol.* **6**, 742-748 (2002).
28. H. C. Kolb, M. G. Finn, K. B. Sharpless, Click chemistry: Diverse chemical function from a few good reactions. *Angew. Chem. Int. Ed.* **40**, 2004-2021 (2001).

29. P. Wu *et al.*, Efficiency and fidelity in a click-chemistry route to triazole dendrimers by the copper(I)-catalyzed ligation of azides and alkynes. *Angew. Chem. Int. Ed.* **43**, 3928-3932 (2004).
30. C. J. Hawker, K. L. Wooley, The convergence of synthetic organic and polymer chemistries. *Science* **309**, 1200-1205 (2005).
31. F. Fazio, M. C. Bryan, O. Blixt, J. C. Paulson, C. H. Wong, Synthesis of sugar arrays in microtiter plate. *J. Am. Chem. Soc.* **124**, 14397-14402 (2002).
32. Glycodendrimer Nomenclature: Man denotes α -D-mannopyranoside, Gal denotes β -D-galactopyranoside, Lac denotes 1,4-(β -D-galactopyranosyl)- β -D-glucopyranoside, G2 denotes generation 2 and G3 denotes generation 3. G2Man, G2Gal, G2Lac, G3Man, G3Gal, and G3Lac denote the corresponding glycodendrimers.
33. G. N. Reeke, J. W. Becker, G. M. Edelman, Covalent and 3-Dimensional Structure of Concanavalin-a .4. Atomic Coordinates, Hydrogen-Bonding, and Quaternary Structure. *J. Biol. Chem.* **250**, 1525-1547 (1975).

Chapter 5: Label-free detection of glycan-lectin interactions using carbon nanotube network field-effect transistors^{*}

Introduction

Lectins are proteins or glycoproteins that bind to glycans (a generic term for any carbohydrate or assembly of carbohydrates) with high specificity (1). Glycans, a major determinant of molecular recognition on cell surface, participate in diverse processes such as pathogen binding, cell trafficking, endocytosis, and modulation of cell signaling (2). Most of these processes involve specific interactions between glycans and lectins. Therefore, the detection of glycan-lectin interactions is of central importance. Several optical detection strategies using fluorescent dye-labeled glycans (3), glycan microarrays (4), glycan-quantum dot conjugates (5), and glycan-modified gold nanoparticles (6, 7) have been developed to probe lectin binding. On the other hand, label-free electronic detection using nanomaterials such as single-walled carbon nanotubes (SWNTs) offers sensitivity, selectivity, and low-cost for biosensing (8), yet has not been exploited to study glycan-lectin interactions. Field-effect transistors (FETs) fabricated using SWNTs as conducting channels (SWNT-FETs) have been well developed (9). Indeed, they have

^{*} Peng Wu and Brian Kessler contributed to the work described in this chapter.

already been explored for electronic detection of biomolecules such as DNA (10), antibodies (11), and antigens (12). The detection scheme has been to immobilize DNA or proteins on SWNT surface as recognition receptors that are specific for their ligands. The subsequent specific receptor-ligand binding was detected by monitoring the changes in the device characteristics.

We have recently developed a glycosylated dendrimer for coating carbon nanotubes (CNTs) with glycans (13). This dendrimer comprised glycans displayed in the periphery and a pyrene tail that bound to SWNT surface via π - π interaction. Here we report a label-free electronic detection method for investigating glycan-lectin interactions using single-walled carbon nanotube network field-effect transistors (SWNTN-FETs) functionalized with glycodendrimers (Fig. 5.1). The glycodendrimers with various glycans could assemble on nanotube surface in SWNTN-FET devices and preserve lectin-binding specificity. The generality and selectivity of this method was demonstrated by detecting various lectins.

Results and discussions

Functionalization of SWNTN-FETs with glycodendrimers

SWNTN-FET devices were fabricated using SWNTs grown on the Si wafer surface by chemical vapor deposition technique. Electrical leads were patterned on top of SWNTs using standard photolithography. Each device consisted of a random network of SWNTs patterned into interdigitated electrodes with 10- μm separation (Fig. 5.2). Transistor characteristics such as G - V_g transfer curves, i.e., source-drain conductance (G) as a function of an applied gate voltage were measured using a custom electronic test fixture.

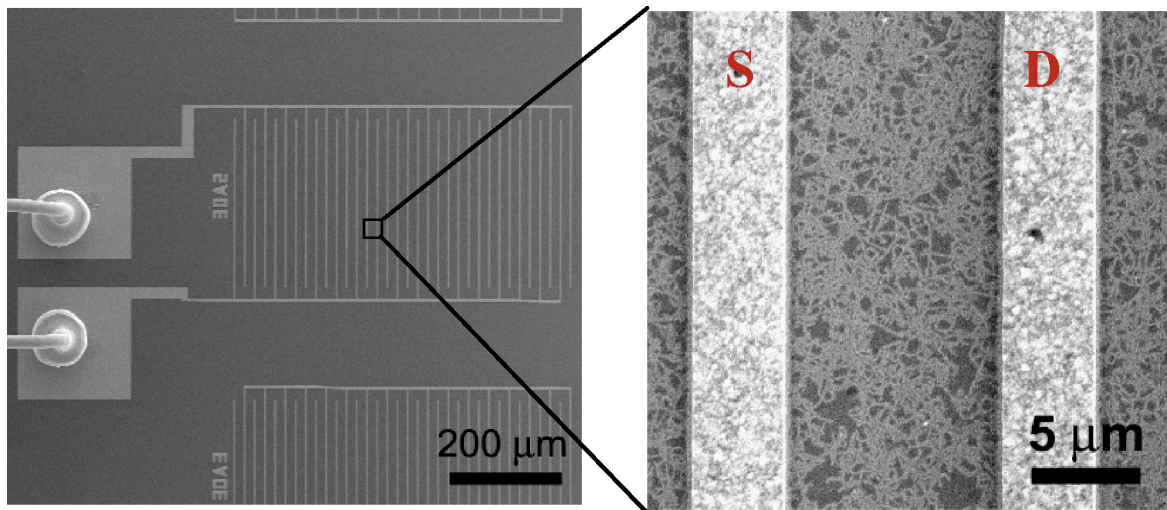


Figure 5.2. Scanning electron microscopy image of the SWNTN-FET devices. The distance between source (S) and drain (D) interdigitated metal electrodes is 10 μm .

In order to detect glycan-lectin interactions, we chose to immobilize glycans on SWNTN-FET sensors by coating the side walls of SWNTs using glycodendrimers. The merit of using glycodendrimers in SWNT-FET sensors is the well-defined size and molecular structure. Mimicking the branched structure of cell-surface glycans, the dendrimer scaffold extended the coated glycans well above the nanotube surface, making them the first entity to interact with lectins. Furthermore, the distance of lectin binding sites from nanotube surface can be readily tuned by choosing different generations of glycodendrimers. Generation 2 (G2) and generation 3 (G3) glycodendrimers (14) used in this study have the sizes of 1-3 nm, a reasonable distance for electron transfer.

We have previously shown the coating of SWNTs with glycodendrimers in aqueous solution (13). In this work, we applied this coating strategy to a FET device setting. SWNTN-FET devices were incubated with 100 μM of glycodendrimers in aqueous solution for 30 min, followed by thorough washing to remove excess glycodendrimers. The G - V_g characteristics are known to be sensitive to the environment surrounding the nanotubes such as molecular adsorption (15, 16). Functionalization of the devices with glycodendrimers resulted in a shift of G - V_g curves toward more negative gate voltage values (Fig. 5.3A). This was presumably due to the negative charge transfer or electron doping from the pyrene tails of glycodendrimers to the SWNT conducting channel, which was in agreement with the reported effects of aromatic compounds (17-19). This shift was observed for all glycodendrimers with different glycan structures, which further confirmed that pyrene formed π stacking interactions

with SWNT surface. In a control experiment, SWNTN-FETs were incubated with the aqueous solution without glycodendrimers. In this case, no shift of G - V_g curve was observed (data not shown).

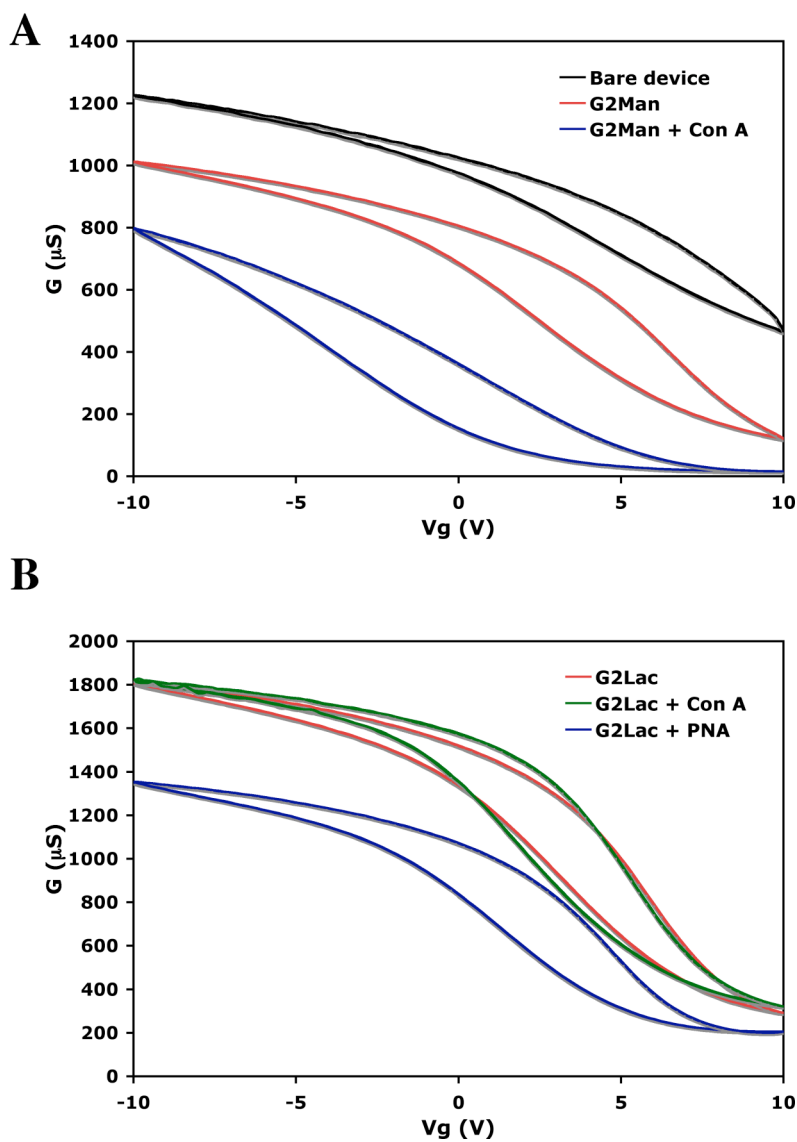


Figure 5.3. (A) The G - V_g curves of SWNTN-FETs before (bare device) and after functionalized with G2Man, as well as subsequent Con A binding. (B) The G - V_g curves of SWNTN-FETs functionalized with G2Lac, and subsequently incubated with Con A and PNA, respectively.

Lectin detection on SWNTN-FETs

We then demonstrated the electronic detection by using SWNT-FETs functionalized with G2Man and G2Lac (14) to detect *Canavalia ensiformis* agglutinin (Con A) and *Arachis hypogaea* agglutinin (PNA). Con A and PNA are lectins with well-documented specificity for α -mannose and lactose, respectively. The coated devices were incubated with lectins (about 0.1 μ M) in PBS buffer for 30 min, followed by thorough washing to remove excess lectins. As shown in Figure 5.3A, the G - V_g curve of G2Man-coated SWNTN-FETs further shifted towards more negative gate voltage values (reduction of conductance) upon Con A binding. Similarly, incubation with PNA reduced the conductance of G2Lac-coated SWNT-FETs (data not shown). The lectins with concentration as low as 0.1 μ M could be easily detected, which indicated the high sensitivity of the devices.

To test the selectivity of this detection, we incubated G2Lac-coated devices with Con A that does not recognize lactose. As shown in Figure 5.3B, incubation with Con A did not affect the conductance of G2Lac functionalized SWNTN-FETs. After removing the Con A solution, the devices were then incubated with PNA. The conductance of the devices was reduced upon PNA binding, indicating that there was no Con A binding on G2Lac-coated devices. Similarly, PNA did not change the G - V_g curve of G2Man-coated SWNTN-FETs (data not shown). These results have two important implications. First, the glycodendrimer functionalization prevented non-specific protein binding to the

devices. Second, the devices were selective for the lectins that recognized the immobilized glycans.

The synthetic process of glycodendrimers allows for the introduction of myriad glycan structures, making it a general detection method for all lectins. To demonstrate its generality, we used a panel of dendrimers with various glycans including G2Lac, G2LacNAc and G2SiaLac to functionalize the devices. Accordingly, *Psophocarpus tetragonolobus* agglutinin (PTA galactose), *Erythrina cristagalli* (ECA), and *Sambucus nigra* (SNA), which recognizes β -galactose, *N*-acetyl lactosamine, and α -2,6-sialo-galactose respectively were detected by the functionalized SWNTN-FETs.

The sensitivity of this method depends on two factors: the glycan density and the distance of glycans from CNT surface. Multivalent display of glycan ligands is important in glycan-lectin interactions because the affinities of glycan ligands in the monovalent state are generally very low (20). Therefore, higher glycan density on CNT surface would increase the detection sensitivity. On the other hand, the sensitivity would decrease when the distance between glycans and nanotube surface increases. To test the effects of these two factors, we compared G3 dendrimers-functionalized SWNTN-FET devices with G2 ones. G3 dendrimers have higher density of ligand display, while making the lectin binding sites farther away from nanotube surface. Similar sensitivity was observed for both G2 and G3 glycodendrimers. Thus, the sizes and ligand densities of G2 and G3 glycodendrimers are well suited for studying glycan-lectin interactions in SWNTN-FET devices. We are currently synthesizing glycodendrimers with higher

generations. It would be interesting to find out the upper limit of electron transfer distance qualitatively.

Conclusions

In summary, we have developed a label-free detection strategy for studying glycan-lectin interactions using SWNTN-FETs functionalized with glycodendrimers. Various lectins have been successfully detected using this method. The high selectivity, fast response, and relatively simple fabrication of SWNTN-FETs, combined with the well-defined structure and easy accessibility of a whole array of glycodendrimers make this method a practical and general tool for studying glycan-lectin interactions. Furthermore, this method might be well suited for developing biosensors for the detection of pathogens such as viruses and bacteria (21).

Materials and methods

Fabrication of SWNTN-FETs

The SWNT-FETs were kindly provided by Nanomix Inc. (Emeryville, CA). Devices were fabricated by using SWNTs grown by means of chemical vapor deposition at 900°C using dispersed iron nanoparticles as growth promoter and a methane/hydrogen gas mixture on doped Si 100-mm wafers with SiO₂ at its surface. Electrical leads were patterned on top of the nanotubes from evaporated Ti-Au (30- and 120-nm-thick, respectively) films by using standard photolithography techniques. Each wafer consists

of about 1,000 dies with 2.54 mm x 2.54-mm dimensions. On each die, a random network of SWNTs is patterned into several devices (210 μm x 270 μm) that consist of interdigitated electrodes with 10- μm separation. Nanotubes outside the device area were removed by using oxygen plasma to electrically isolate each device.

Data acquisition

The chips with multiple SWNTN-FET devices were wire-bonded and packaged in a 40-pin CERDIP and tested by using a custom electronic test fixture, which measures an array of up to 12 separate sensors from each Si chip. The housing of the test fixture consists of a modified shielded I/O board (SCB-68; National Instruments) with a 40-pin ZIF socket. The I/O board was linked to a PC with a data acquisition card (PCI-6014; National Instruments). Programming to manage data acquisition was performed in LABVIEW (National Instruments). An analog output voltage was used to sweep the gate of the SWNTN-FETs. Device characteristics such as source-drain voltage and current were calculated in LABVIEW from voltage measurements across sense resistors. Continuous $I-V_g$ measurements were taken with a gate voltage triangle wave sweep at frequency of 3 Hz from -10 V to +10 V.

Functionalization of SWNTN-FETs with glycodendrimers

The SWNTN-FET device chips were incubated in 5 μM solutions of glycodendrimers in PBS buffer for 30 min in a humid chamber. The chips were then

washed thoroughly with PBS buffer for 3 times to remove excess glycodendrimers, followed by blown dry with nitrogen before electronic measurements.

Lectin binding on functionalized SWNTN-FETs

The devices functionalized with glycodendrimers were incubated with 5 μM solutions of lectins in PBS buffer for 30 min in a humid chamber. The chips were then washed thoroughly with PBS buffer for 3 times to remove excess glycodendrimers, followed by blown dry with nitrogen before electronic measurements.

References

1. H. Lis, N. Sharon, Lectins: Carbohydrate-specific proteins that mediate cellular recognition. *Chem. Rev.* **98**, 637-674 (1998).
2. B. E. Collins, J. C. Paulson, Cell surface biology mediated by low affinity multivalent protein-glycan interactions. *Curr. Opin. Chem. Biol.* **8**, 617-625 (2004).
3. D. N. Wang, S. Y. Liu, B. J. Trummer, C. Deng, A. L. Wang, Carbohydrate microarrays for the recognition of cross-reactive molecular markers of microbes and host cells. *Nat. Biotechnol.* **20**, 275-281 (2002).
4. J. C. Paulson, O. Blixt, B. E. Collins, Sweet spots in functional glycomics. *Nature Chemical Biology* **2**, 238-248 (2006).
5. P. Babu, S. Sinha, A. Surolia, Sugar-quantum dot conjugates for a selective and sensitive detection of lectins. *Bioconjugate Chemistry* **18**, 146-151 (2007).
6. J. M. de la Fuente, P. Eaton, A. G. Barrientos, M. Menendez, S. Penades, Thermodynamic evidence for Ca²⁺-mediated self-aggregation of Lewis X gold glyconanoparticles. A model for cell adhesion via carbohydrate-carbohydrate interaction. *J. Am. Chem. Soc.* **127**, 6192-6197 (2005).
7. H. Otsuka, Y. Akiyama, Y. Nagasaki, K. Kataoka, Quantitative and reversible lectin-induced association of gold nanoparticles modified with alpha-lactosyl-omega-mercapto-poly(ethylene glycol). *J. Am. Chem. Soc.* **123**, 8226-8230 (2001).
8. G. Gruner, Carbon nanotube transistors for biosensing applications. *Anal. Bioanal. Chem.* **384**, 322-335 (2006).
9. P. Avouris, Molecular electronics with carbon nanotubes. *Acc. Chem. Res.* **35**, 1026-1034 (2002).
10. A. Star *et al.*, Label-free detection of DNA hybridization using carbon nanotube network field-effect transistors. *Proc. Natl. Acad. Sci. USA* **103**, 921-926 (2006).
11. R. J. Chen *et al.*, Noncovalent functionalization of carbon nanotubes for highly specific electronic biosensors. *Proc. Natl. Acad. Sci. USA* **100**, 4984-4989 (2003).

12. C. Li *et al.*, Complementary detection of prostate-specific antigen using In(2)O(3) nanowires and carbon nanotubes. *J. Am. Chem. Soc.* **127**, 12484-12485 (2005).
13. P. Wu *et al.*, Biocompatible carbon nanotubes generated by functionalization with glycodendrimers. *submitted*.
14. Glycodendrimer Nomenclature: Man denotes α -D-mannopyranoside, Gal denotes β -D-galactopyranoside, Lac denotes 1,4-(β -D-galactopyranosyl)- β -D-glucopyranoside, G2 denotes generation 2 and G3 denotes generation 3. G2Man, G2Gal, G2Lac, G3Man, G3Gal, and G3Lac denote the corresponding glycodendrimers.
15. P. G. Collins, K. Bradley, M. Ishigami, A. Zettl, Extreme oxygen sensitivity of electronic properties of carbon nanotubes. *Science* **287**, 1801-1804 (2000).
16. J. Kong *et al.*, Nanotube molecular wires as chemical sensors. *Science* **287**, 622-625 (2000).
17. S. Gotovac *et al.*, Effect of nanoscale curvature of single-walled carbon nanotubes on adsorption of polycyclic aromatic hydrocarbons. *Nano Lett.* **7**, 583-587 (2007).
18. A. Star, T. R. Han, J. C. P. Gabriel, K. Bradley, G. Gruner, Interaction of aromatic compounds with carbon nanotubes: Correlation to the Hammett parameter of the substituent and measured carbon nanotube FET response. *Nano Lett.* **3**, 1421-1423 (2003).
19. Y. Zhang, S. L. Yuan, W. W. Zhou, J. J. Xu, Y. Li, Spectroscopic evidence and molecular simulation investigation of the pi-pi interaction between pyrene molecules and carbon nanotubes. *J. Nanosci. Nanotech.* **7**, 2366-2375 (2007).
20. P. R. Crocker, T. Feizi, Carbohydrate recognition systems: Functional triads in cell-cell interactions. *Current Opinion in Structural Biology* **6**, 679-691 (1996).
21. Z. H. Shen *et al.*, Nonlabeled quartz crystal microbalance biosensor for bacterial detection using carbohydrate and lectin recognitions. *Anal. Chem.* **79**, 2312-2319 (2007).

Chapter 6: Boron nitride nanotubes are noncytotoxic and can be functionalized for interaction with proteins and cells*

Introduction

Carbon nanotubes (CNTs) have been widely explored for use in biological applications including biosensing (1), imaging (2), intracellular delivering (3, 4), and cancer cell targeting (5). However, their inherent cytotoxicity has imposed severe limitations on their use in living systems and in therapeutic composites (6-9). The cytotoxicity of CNTs can be reduced by biocompatible surface functionalization (5, 10-12), but the possibility of *in situ* desorption brings considerable risk to their use in living organisms. Here we report that boron nitride nanotubes (BNNTs), isosteres of CNTs with unique physical properties, are inherently noncytotoxic. Furthermore, BNNTs can be surface functionalized with biological epitopes that mediate protein and cell binding. Finally, we show that BNNTs can deliver DNA oligomers to the interior of cells with no apparent toxicity. This work suggests that BNNTs may be superior to CNTs as biological probes and nanomedicines.

* Peng Wu, Michael Rousseas, David Okawa, and Zev Gartner contributed to the work described in this chapter.

Results and discussions

Synthesis of BNNTs

Boron nitride is isoelectronic to carbon and has a hexagonal structure analogous to that of graphite. The existence of BNNTs was predicted theoretically in 1994 (13, 14), and they were synthesized shortly thereafter (15). In addition to their structural similarity, BNNTs and CNTs have similar mechanical properties and thermal conductivity (16, 17). However, BNNTs are distinct in several key aspects. First, BNNTs are wide band gap semiconductors whose electrical properties are independent of geometry, while CNTs may be metal or semiconducting depending on chirality and diameter. Second, BNNTs are more chemically inert and structurally stable than CNTs. This latter property prompted us to investigate the effects of BNNTs in biological systems where the toxicity of CNTs is troublesome.

Pristine multi-walled BNNTs were synthesized by a chemical vapor deposition process adapted from a previously reported method (18). Slight modifications of experimental procedures were made to produce highly pure BNNTs in order to fulfill the requirement for cellular studies. Scanning electron microscopy (SEM) and transmission electron microscopy (TEM) investigations revealed high-purity and high-quality multi-walled BNNTs with an outer diameter of ~20 to 30 nm and a length of up to 10 μm (Fig. 6.1).

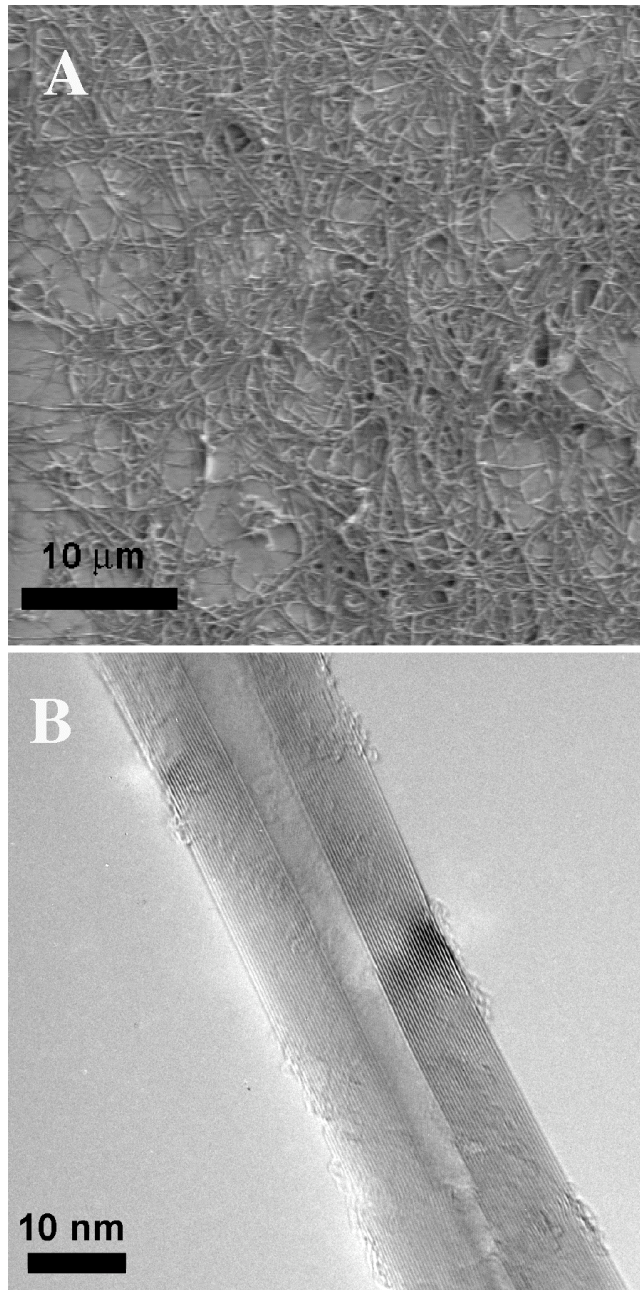


Figure 6.1. Structural characterization of pristine multi-walled BNNTs with high purity and high quality. **(A)** The SEM image of BNNTs. **(B)** High resolution TEM image of a BNNT.

Cytotoxicity studies of BNNTs

HEK 293 cells were cultured with BNNTs (at 100 $\mu\text{g}/\text{mL}$) for 4 days. For comparison, the cells were cultured similarly with two types of commercially available multi-walled CNTs (MWCNTs) with diameters and lengths similar to those of BNNTs, purchased from MER corp. (AZ, USA) and NanoLab (MA, USA). In control experiments, the cells were cultured with CNTs or with media alone. Cells were counted every day (Fig. 6.2). Cells cultured with BNNTs were indistinguishable from cells grown with media alone. In sharp contrast, cells cultured with either type of MWCNTs were unable to expand during the course of the experiment. Similar results were obtained with CHO cells (not shown).

CNTs have been shown to induce HEK 293 cell apoptosis (7). We therefore tested the viability of cells cultured with BNNTs using the Annexin V-FITC/propidium iodide (PI) assay for apoptosis. HEK 293 cells incubated with BNNTs showed no increased staining with Annexin V-FITC or PI up to 4 days compared with cells grown in media alone (Fig. 6.3). Thus, BNNTs did not appear to inhibit cell growth or induce apoptotic pathways in the cells. These results indicated that BNNTs were noncytotoxic and should be well suited for biological applications.

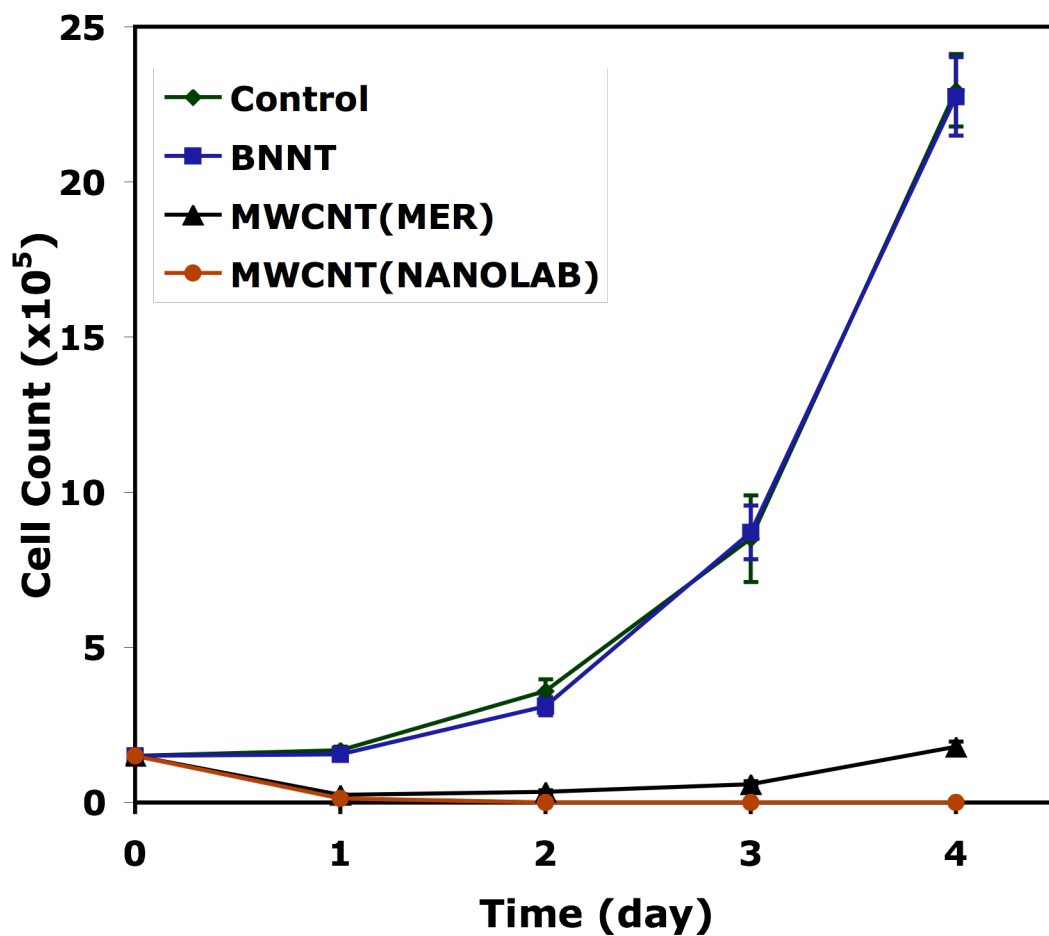


Figure 6.2. BNNTs do not inhibit cell proliferation. HEK293 cells were cultured with BNNTs (at 100 $\mu\text{g}/\text{mL}$) for 4 d. In control experiments, the cells were cultured with CNTs or with media alone. Cells numbers were counted each day. Error bars represent the standard deviation for three replicates.

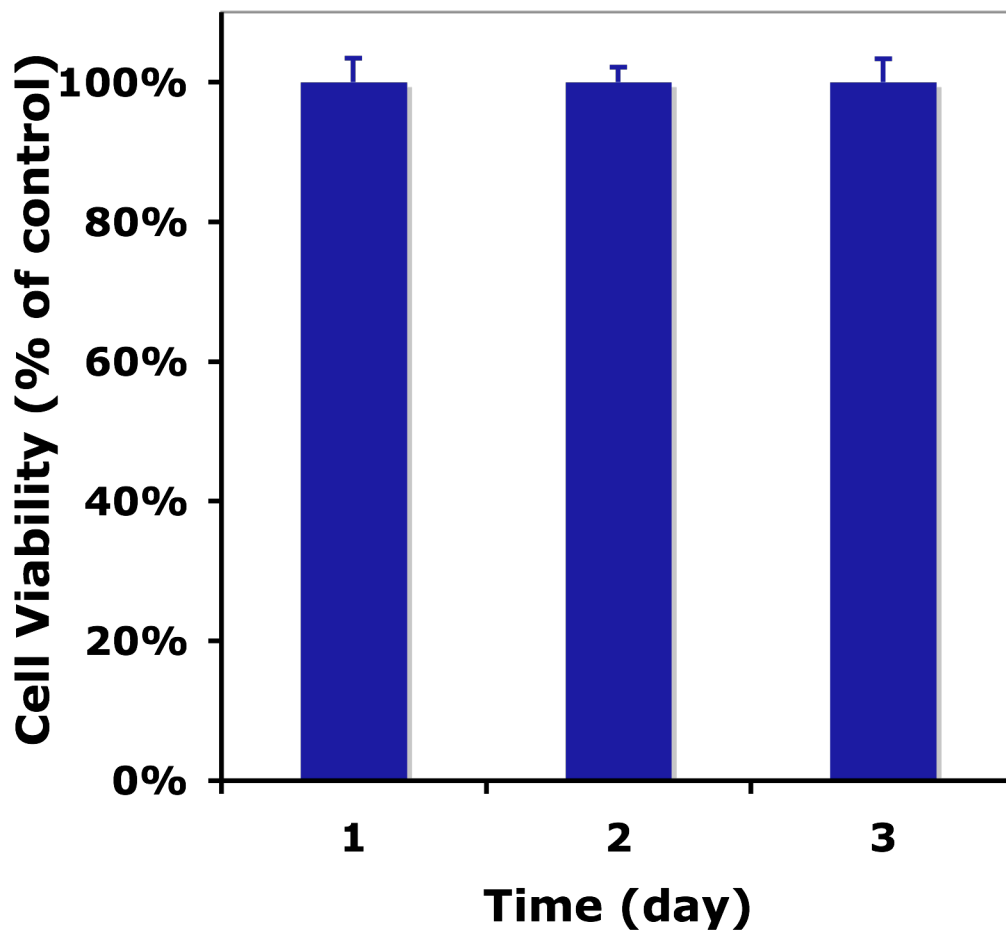


Figure 6.3. BNNTs have no effect on cell viability. HEK 293 cells were cultured with BNNTs or with media alone. Cell viability was assessed by flow cytometry (annexin V staining combined with propidium iodide incorporation) each day. Cell viability is expressed as the percentage of viability measured for control. The control represents cells cultured with media alone. The error bars represent the standard deviation for three replicates.

Biomimetic functionalization of BNNTs with glycodendrimers

Similar to CNTs, BNNTs are not soluble in aqueous media, a limitation that must be overcome for biological implementation. Although some methods for solubilizing BNNTs have been reported (19, 20), general functionalization strategies for interfacing BNNTs with biomolecules and cells are lacking. We therefore explored the use of amphipathic dendritic structures similar to those we recently reported as coatings for CNTs (21). As shown in Figure 6.4, the dendrimers comprise synthetic carbohydrate ligands at the chain ends that enable specific binding to receptors in solution. A pyrene group at the dendrimer focal point allowed adsorption to CNT surfaces through π -stacking and hydrophobic interactions. We hypothesized that these dendrimers might also interact with the isoelectronic BNNT surface, permitting specific binding to carbohydrate-binding proteins.

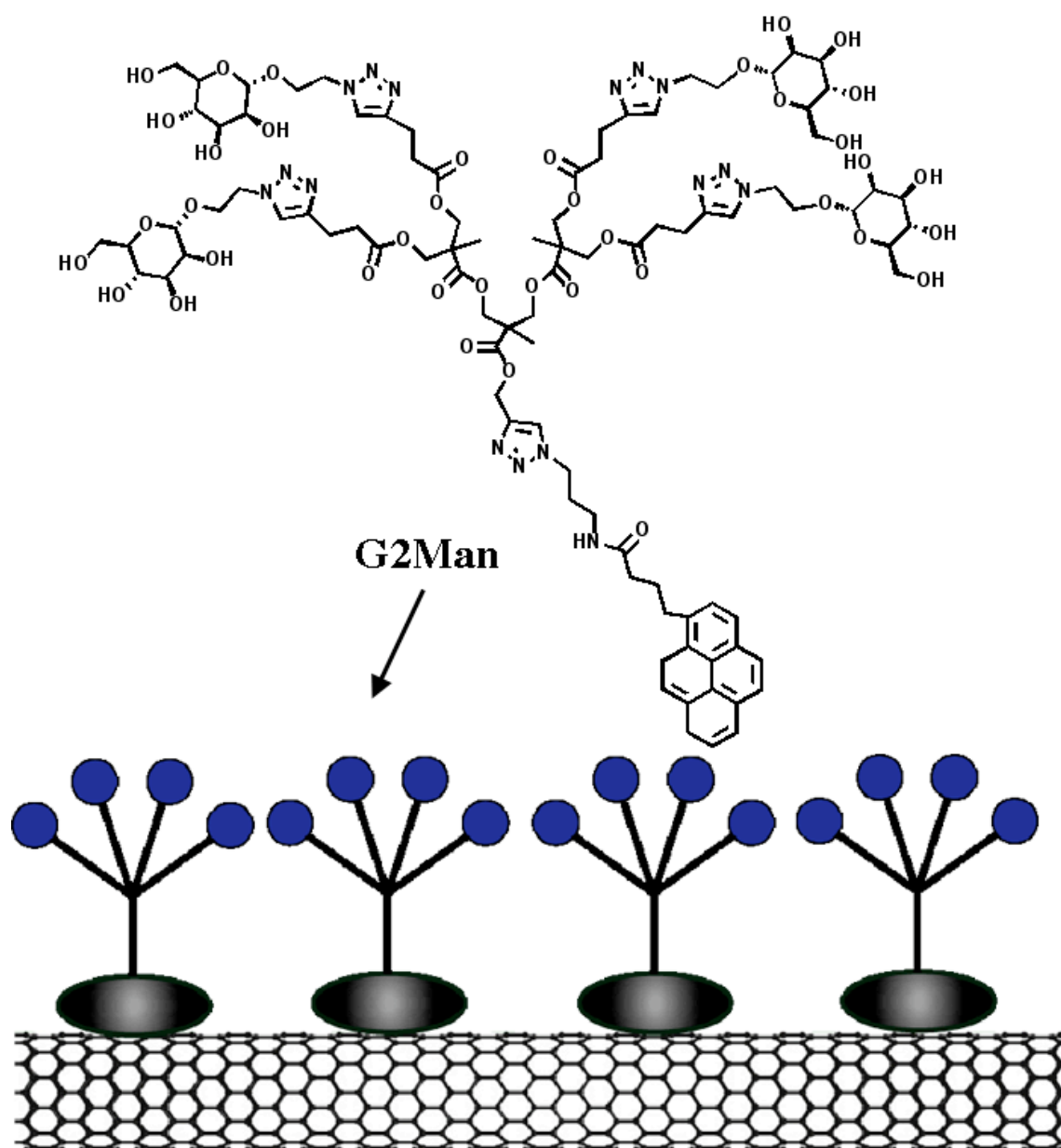


Figure 6.4. The Structure of G2Man. The glycodendrimers assemble on BNNT surface in aqueous media through hydrophobic interaction between the pyrene tails and BNNT surface. The resulting coated BNNTs (G2Man-BNNTs) were soluble in water.

A panel of glycodendrimers from generation 2 (G2) to generation 3 (G3) displaying various glycans were synthesized (21); data from studies using the G2 dendrimer with α -mannose moieties (G2Man, Fig. 6.4) are shown in Figure 6.5 and Figure 6.6. The G2Man-coated BNNTs were stable in aqueous solution for more than one month, while the unfunctionalized BNNTs precipitated very quickly (within one hour) in water (Fig. 6.5). TEM images showing BNNTs coated profusely with amorphous carbohydrates confirmed the presence of the glycodendrimer coating (Fig. 6.6). Similar results were obtained with other glycodendrimers.

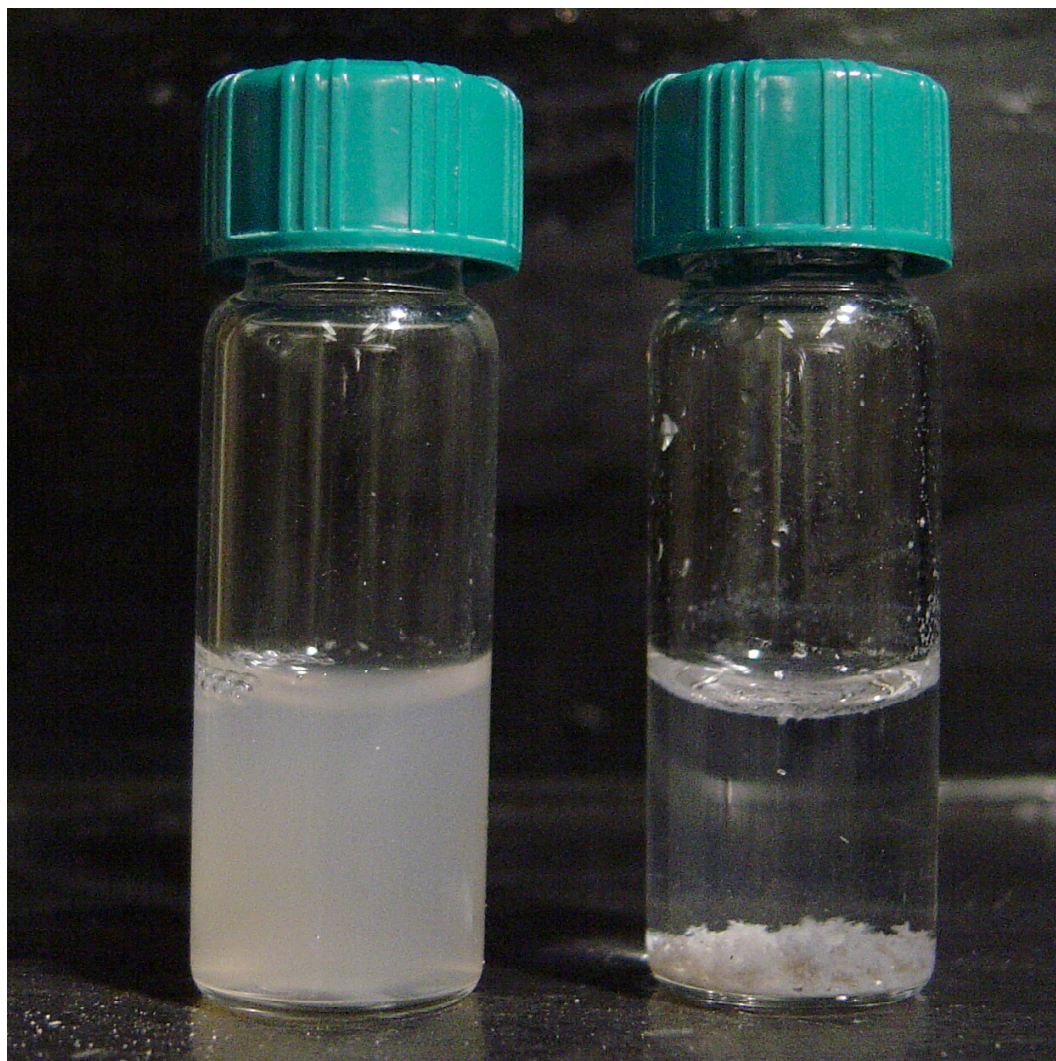


Figure 6.5. Photographs of vials containing BNNT suspensions. G2Man-BNNTs (I) formed stable suspensions in water for more than one month, while pristine BNNTs (II) precipitate in water in an hours.

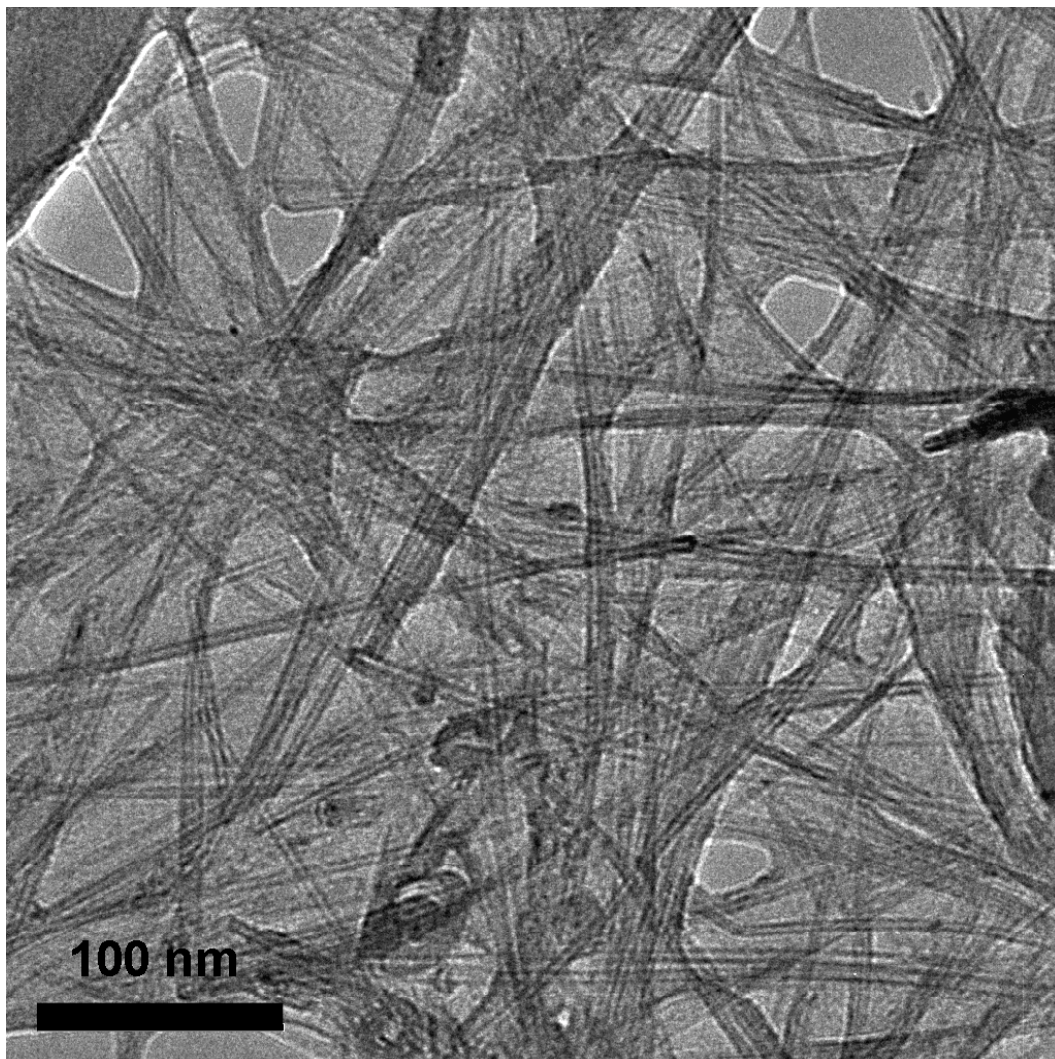


Figure 6.6. The TEM image of G2Man-BNNTs.

Cell surface glycans serve the dual role of specific molecular recognition via carbohydrate-binding proteins (lectins) and resistance to biofouling (22). We evaluated whether the glycodendrimer coating we created on the BNNTs would mimic these functions. To test specific binding, we coated BNNTs with G2Man that can be recognized by α -mannose-specific receptor *Canavalia ensiformis* agglutinin (Con A). G2Man-coated BNNTs were incubated with FITC-conjugated Con A for 30 minutes and the unbound lectin were removed by dialysis before analysis by fluorescent spectroscopy (Fig. 6.7). Significant fluorescence was associated with Con A-bound G2Man-BNNTs, while only background fluorescence was observed for the same BNNTs incubated with *helix pomatia* agglutinin (HPA), a GalNAc-specific lectin that does not recognize mannose. Thus, glycodendrimer-functionalized BNNTs can bind to proteins via ligand-receptor interactions while resisting non-specific protein binding.

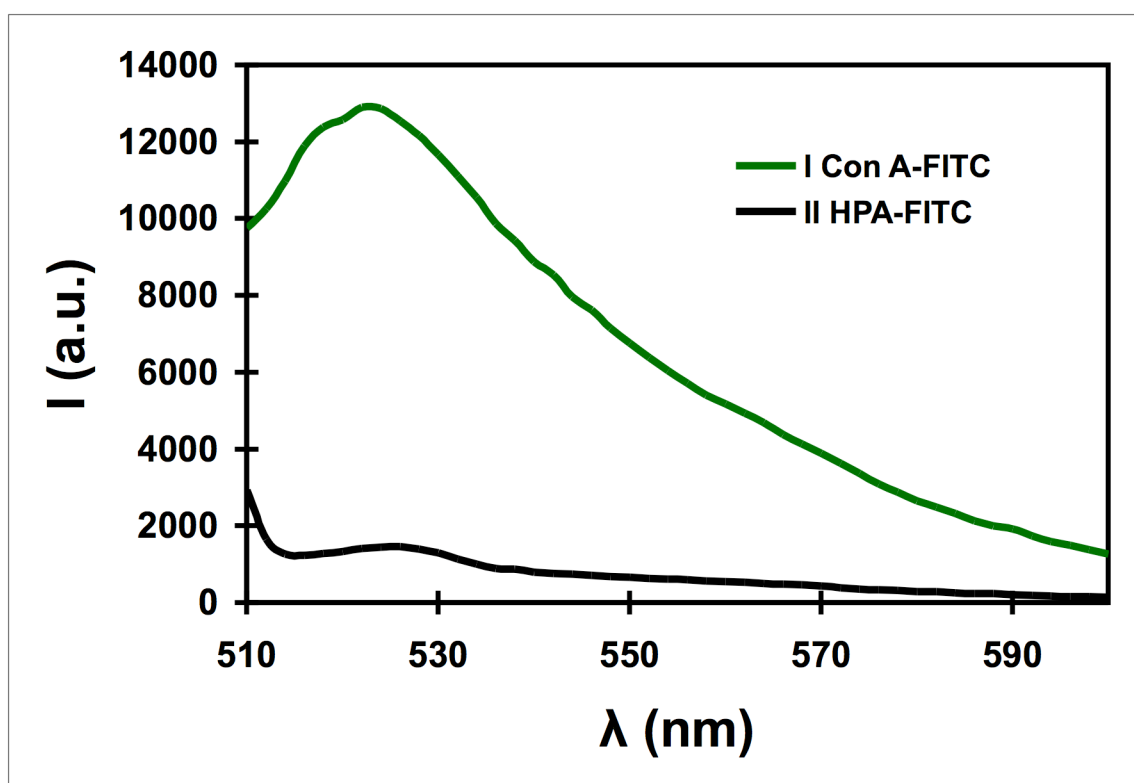


Figure 6.7. Specific binding of ConA to G2Man-BNNTs (green curve). The black curve showed HPA did not bind to G2Man-BNNTs non-specifically. The excitation wavelength was 492 nm. Spectra were corrected for background fluorescence by subtracting the fluorescence spectrum of G2Man-BNNTs alone. These data are representative of the results observed in triplicate experiments.

We used the glycodendrimer coating to specifically bind BNNTs directly to cell surfaces, which was an even more rigorous test of their noncytotoxicity. We first coated G2Man-BNNTs with FITC-conjugated Con A (Con A-FITC), a tetravalent α -mannose-specific lectin that was previously showed to be capable of crosslinking G2Man-coated CNTs to cells surface glycoproteins (21). The lectin-modified BNNTs were then incubated with Chinese hamster ovary (CHO) cells. Fluorescence microscopy analysis revealed robust cell surface fluorescence from FITC (Fig. 6.8). As a control experiment, BNNTs coated with a similar G2 dendrimer bearing galactose residues (G2Gal), which do not bind to Con A, showed no fluorescent labeling of the cells (data not shown). More importantly, we did not see any cellular toxicity even when BNNTs were directly bound to the cell surface.

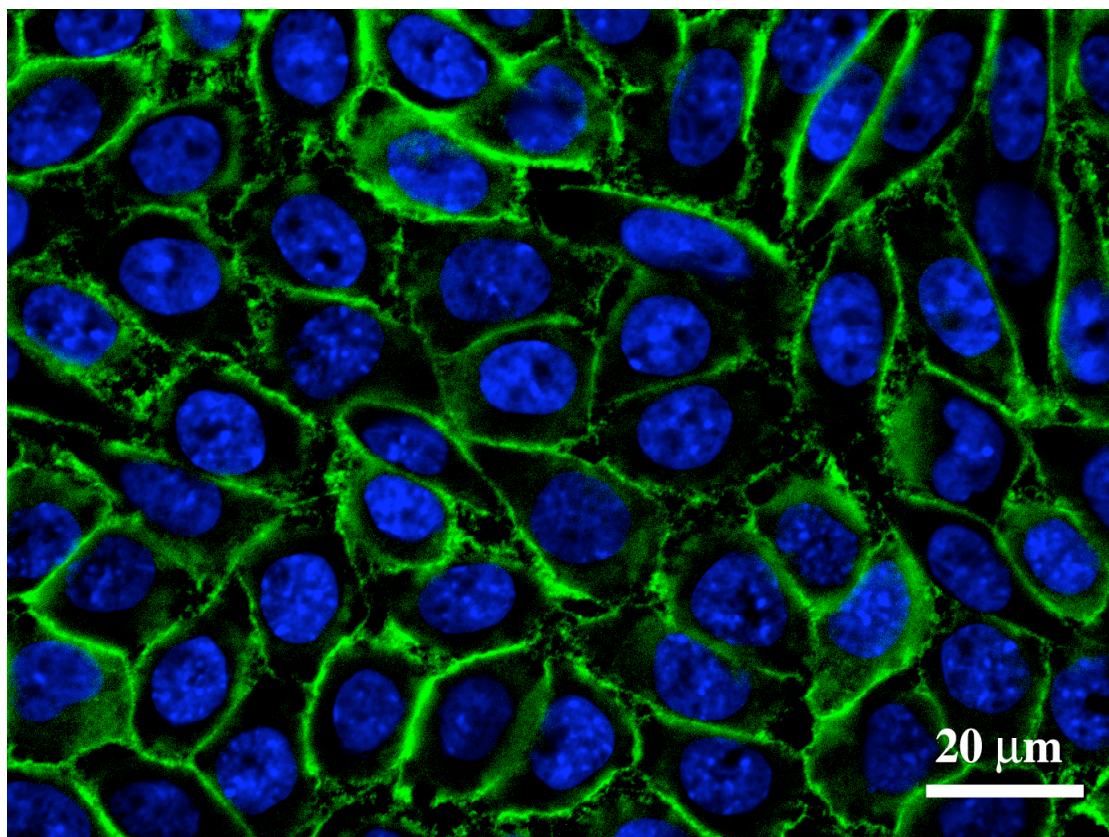


Figure 6.8. Cell surface binding of G2Man-BNNTs. FITC conjugated Con A served as cross-linkers and the FITC conjugated on Con A provided a means for detection of BNNTs bound to cell surface. The fluorescence image showed the labeling of FITC-Con A-G2Man-BNNT conjugates on CHO cell surface (green). The cell nuclei were stained as blue with a DAPI dye.

BNNTs as molecular transporters

One of the most exciting applications of CNTs is to serve as a molecular transporter to deliver biological molecules such as proteins and DNA into living cells (4, 5). Given their similar dimensions, we anticipated that BNNTs might serve similar functions but without any unwanted toxic side effects. We explored their use as cell delivery agents using single-stranded DNA (ssDNA) as cargo. We loaded a synthetic 20-mer DNA oligomer conjugated to FITC onto the surface of BNNTs by passive adsorption, as previously achieved with CNTs (23). BNNTs were sonicated with the FITC-labeled ssDNA (FITC-DNA) in aqueous solution, and the resulting suspension was stable in water and physiological buffers for at least several days. CHO cells were then incubated with the FITC-DNA-BNNTs for 12 hours. Fluorescence microscopy revealed that FITC-DNA-BNNTs were internalized by the cells in a manner dependent on the carrier BNNT (Fig. 6.9). In a control experiment, cells treated with FITC-DNA alone, without a BNNT carrier, showed no significant fluorescence above background (not shown).

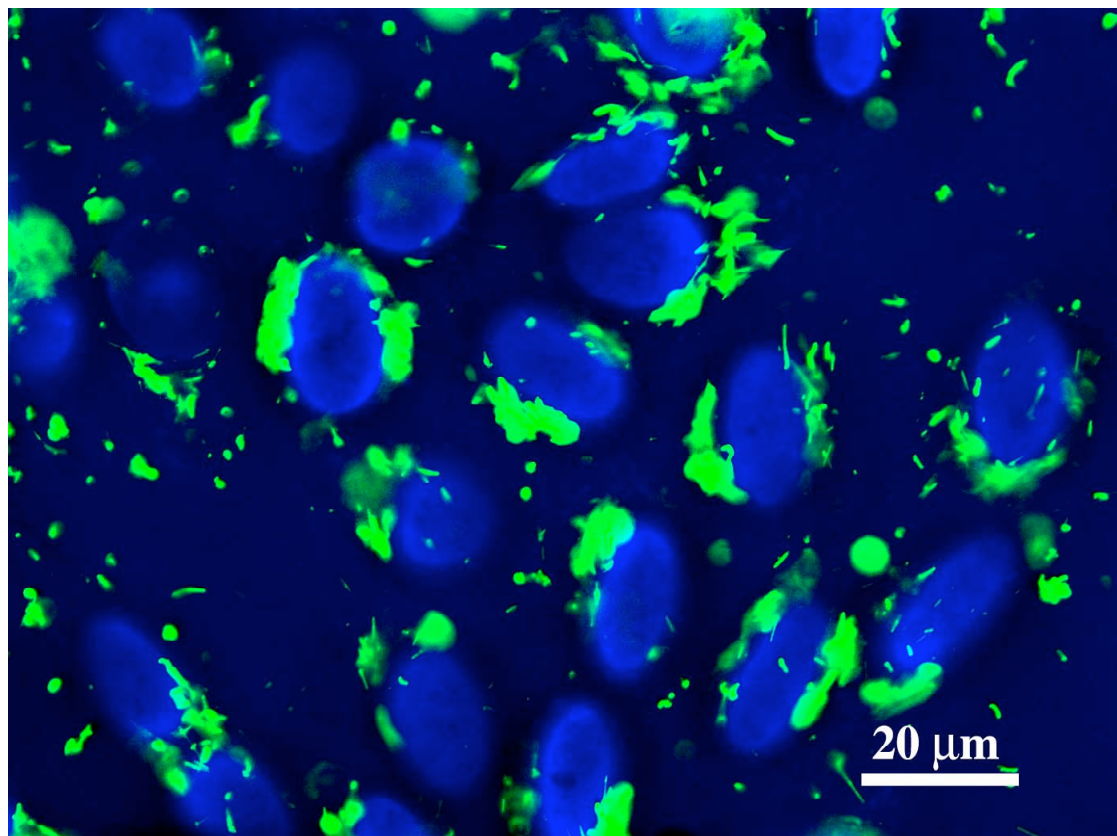


Figure 6.9. Intracellular delivery of ssDNA using BNNTs as transporters. BNNTs were coated with FITC labeled ssDNA via π - π stacking. CHO cells were incubated with FITC-DNA-BNNTs for over night. The fluorescence image showed the internalization of FITC-DNA-BNNTs. The cell nuclei were blue-stained with a DAPI dye.

Conclusions

In summary, we have showed that BNNTs are not cytotoxic, suggesting that their use in therapeutic or diagnostic applications should be seriously considered. Furthermore, we demonstrated that BNNTs could be surface functionalized with bioactive conjugates by non-covalent adsorption. This simple process enabled the surface display of glycodendrimers, which is capable of interacting with proteins and cells. The method should facilitate applications of BNNTs in biosensing and bioimaging without the limitation imposed by cytotoxicity. More generally, the observed properties of BNNTs should increase enthusiasm for their application in nanomedicine.

Materials and methods

Synthesis of BNNTs

The highly pure boron nitride nanotubes were synthesized by a chemical vapor deposition process. Briefly, a hollow cylinder of pyrolytic boron nitride was filled with equal molar quantities of MgO and B. Small holes were drilled into the sides of cylinder and one end of the tube was capped off. A small amount (approx. 20 SCCM) of nitrogen gas was flowed into the cylinder from the other end via a thin alumina tube. The assembly was placed in a flowing ammonia atmosphere and heated in a tube furnace to 1200 °C. After 20 minutes, the cylinder was removed from the furnace, and a fine coating of pure white film was scraped off the exterior of the cylinder, near the small

exhaust holes. Scanning and transmission electron microscopy reveal the film to be composed almost entirely of multi-walled boron nitride nanotubes.

SEM and TEM characterization

SEM images were obtained on an FEI Sirion XL 30 SEM operated at 5 keV. TEM images were obtained on a JEOL 2011 microscope operating at electron energy of 100 keV.

Functionalization of BNNTs with glycodendrimers

In a typical preparation experiment, 0.5 mg of BNNTs were suspended in 5 ml aqueous glycodendrimer solution (0.1%~0.5% in water). The mixture was sonicated using a water-bath sonicator for 1 hr. First, insoluble materials were removed by centrifugation at 1,000 x g for 30 min. Then the excess free glycodendrimers were removed by dialysis against PBS buffer for 24 hours.

Functionalization of BNNTs with DNA

BNNTs were sonicated in a solution of a fluorescently labeled 20-mer oligonucleotide (FITC-ATCGATCGATCGATCTATCG; purchased from Integrated DNA Technologies, IA) for 15 min (DNA concentration 20 μ M). The mixture was centrifuged at 1,000 x g for 30 min, and the resulting suspension was decanted from insoluble materials.

Lectin Binding Assays

Lectins, *Canavalia ensiformis* agglutinin (Con A) conjugated with fluorescein isothiocyanate (Con A-FITC), and *Helix Pomatia* agglutinin conjugated with fluorescein isothiocyanate (HPA-FITC) were obtained from EY-Laboratories. In a typical experiment, a 1 mL solution of lectin-FITC conjugates (100 µg/mL) in PBS buffer containing 1 mM Ca²⁺ was added to the suspensions of glycodendrimer-coated BNNTs (1 mL). The reactions were incubated for 1 h at rt in the dark. After incubation, the solutions were all subjected to dialysis against the buffer for 48 h. The dialyzed solutions were analyzed at 517 nm using a fluorescence microplate reader (excitation wavelength 492 nm). Fluorescence intensities were corrected for background fluorescence by subtracting the fluorescence intensities of glycodendrimer-coated BNNTs alone.

Cell culture conditions

All cell lines were maintained in a 5% CO₂, water-saturated atmosphere at 37 °C and media were supplemented with penicillin (100 unit/mL), streptomycin (0.1 mg/mL) and 10% FCS unless otherwise indicated. CHO cells were grown in Ham F12 nutrient mixture. HEK 293 cells were grown in DMEM media.

Cell binding of glycodendrimer-coated BNNTs

CHO Cells were seeded onto glass slides mounted with tissue culture wells (LAB-TEK) and allowed to adhere for 2 d. The cells were washed 3 times with PBS, and then

fixed in 3% paraformaldehyde in PBS. After three washes, cells were blocked in PBS with 1% bovine serum albumin for 20 min, followed by the addition of glycodendrimer-coated BNNTs complexed with appropriate lectin-FITC conjugates as described above. After a 1-h incubation at rt in the dark, the cells were washed 3 times. The cells were then mounted using Vectashield with 4,6-diamidino-2-phenylindole (Vector Laboratories). A Zeiss Axiovert 200M inverted microscope equipped with a 63 × 1.4 NA Plan-Apochromat oil immersion lens was employed for imaging. A 175W xenon lamp housed in a Sutter DG4 illuminator linked to the microscope by an optical fiber assured shuttering and illumination. Images were acquired using a CoolSNAP HQ CCD camera (Roper Scientific). Slidebook software (Intelligent Imaging Solutions) was used to control the microscope and the camera.

Cytotoxicity assays

HEK 293 Cells were incubated with BNNTs (100 µg/mL) for 4 d. In control experiments, the cells were cultured with MWCNTs purchased from MER corp. (AZ, USA) and NanoLab (MA, USA) or with media alone. Cells were washed twice with PBS and then trypsinized with 0.25% trypsin-EDTA (PBS, pH 7.4), resuspended in media. The viable cells were counted every day using Trypan blue dye exclusion method.

In parallel, the viability of HEK 293 cells grown with BNNTs was studied by Annexin V-FITC/PI assay using annexin V-FITC apoptosis detection kit obtained from BD Biosciences. Cells were cultured with BNNTs (100 µg/mL) for 4 d. In control

experiments, the cells were cultured media alone. Each day, the cells were washed twice with cold PBS and then resuspended in 1X binding buffer. 100 μ L of the cell suspension was then transferred to a 5 mL culture tube and 5 μ L of Annexin V-FITC and 5 μ L of PI were added. The solution was gently vortexed and incubated for 15 min at rt in the dark. After incubation, 400 μ L of 1X binding buffer was added to each tube. The cells were then analyzed by flow cytometry.

References

1. A. Star *et al.*, Label-free detection of DNA hybridization using carbon nanotube network field-effect transistors. *Proc. Natl. Acad. Sci. USA* **103**, 921-926 (2006).
2. S. S. Wong, E. Joselevich, A. T. Woolley, C. L. Cheung, C. M. Lieber, Covalently functionalized nanotubes as nanometre-sized probes in chemistry and biology. *Nature* **394**, 52-55 (1998).
3. X. Chen, A. Kis, A. Zettl, C. R. Bertozzi, A cell nanoinjector based on carbon nanotubes. *Proc. Natl. Acad. Sci. USA* **104**, 8218-8222 (2007).
4. K. Kostarelos *et al.*, Cellular uptake of functionalized carbon nanotubes is independent of functional group and cell type. *Nat. Nanotech.* **2**, 108-113 (2007).
5. N. W. S. Kam, M. O'Connell, J. A. Wisdom, H. J. Dai, Carbon nanotubes as multifunctional biological transporters and near-infrared agents for selective cancer cell destruction. *Proc. Natl. Acad. Sci. USA* **102**, 11600-11605 (2005).
6. M. Bottini *et al.*, Multi-walled carbon nanotubes induce T lymphocyte apoptosis. *Toxicol. Lett.* **160**, 121-126 (2006).
7. D. X. Cui, F. R. Tian, C. S. Ozkan, M. Wang, H. J. Gao, Effect of single wall carbon nanotubes on human HEK293 cells. *Toxicol. Lett.* **155**, 73-85 (2005).
8. A. Magrez *et al.*, Cellular toxicity of carbon-based nanomaterials. *Nano Lett.* **6**, 1121-1125 (2006).
9. Y. Sato *et al.*, Influence of length on cytotoxicity of multi-walled carbon nanotubes against human acute monocytic leukemia cell line THP-I in vitro and subcutaneous tissue of rats in vivo. *Mol. BioSyst.* **1**, 176-182 (2005).
10. X. Chen *et al.*, Interfacing carbon nanotubes with living cells. *J. Am. Chem. Soc.* **128**, 6292-6293 (2006).
11. C. M. Sayes *et al.*, Functionalization density dependence of single-walled carbon nanotubes cytotoxicity in vitro. *Toxicol. Lett.* **161**, 135-142 (2006).
12. H. Dumortier *et al.*, Functionalized carbon nanotubes are non-cytotoxic and preserve the functionality of primary immune cells. *Nano Lett.* **6**, 1522-1528 (2006).

13. X. Blase, A. Rubio, S. G. Louie, M. L. Cohen, Stability and Band-Gap Constancy of Boron-Nitride Nanotubes. *Europhy. Lett.* **28**, 335-340 (1994).
14. A. Rubio, J. L. Corkill, M. L. Cohen, Theory of Graphitic Boron-Nitride Nanotubes. *Phys. Rev. B* **49**, 5081-5084 (1994).
15. N. G. Chopra *et al.*, Boron-Nitride Nanotubes. *Science* **269**, 966-967 (1995).
16. E. Hernandez, C. Goze, P. Bernier, A. Rubio, Elastic properties of C and BxCyNz composite nanotubes. *Phys. Rev. Lett.* **80**, 4502-4505 (1998).
17. C. W. Chang, W. Q. Han, A. Zettl, Thermal conductivity of B-C-N and BN nanotubes. *Appl. Phys. Lett.* **86**, 173102-173102 (2005).
18. C. Tang, Y. Bando, T. Sato, K. Kurashima, A novel precursor for synthesis of pure boron nitride nanotubes. *Chem. Commun.*, 1290-1291 (2002).
19. S. Pal, S. R. C. Vivekchand, A. Govindaraj, C. N. R. Rao, Functionalization and solubilization of BN nanotubes by interaction with Lewis bases. *J. Mater. Chem.* **17**, 450-452 (2007).
20. S. Y. Xie *et al.*, Solubilization of boron nitride nanotubes. *Chem. Commun.*, 3670-3672 (2005).
21. P. Wu *et al.*, Biocompatible carbon nanotubes generated by functionalization with glycodendrimers. *submitted*.
22. B. E. Collins, J. C. Paulson, Cell surface biology mediated by low affinity multivalent protein-glycan interactions. *Curr. Opin. Chem. Biol.* **8**, 617-625 (2004).
23. M. Zheng *et al.*, DNA-assisted dispersion and separation of carbon nanotubes. *Nat. Mater.* **2**, 338-342 (2003).

Chapter 7: A metabolic oligosaccharide engineering approach towards boron neutron capture therapy

Introduction

Boron neutron capture therapy (BNCT) is a binary cancer treatment based on the nuclear reaction that occurs when ^{10}B is irradiated with low energy thermal neutrons to generate an α -particle and a lithium-7 ion bearing approximately 2.4 MeV of energy (1, 2). These high linear energy transfer particles are confined in a radius of about 10 μm or the equivalent of approximately one cell diameter, thus affording selective removal of cancer cells. For BNCT to be successful, a sufficient quantity of boron atoms must be selectively delivered to cancer cells while the boron concentration in normal cells should be kept low to minimize the damage to normal tissue. Although a number of delivery strategies including conjugation of boron drugs to monoclonal antibodies, epidermal growth factors, and liposomes have been investigated with various degrees of success (3), selective delivery of boron atoms to tumor cells remains one of the major challenges.

Cancers cells usually exhibit abnormal cell surface glycosylation in the form of overexpressed naturally occurring oligosaccharides as well as glycoforms that are normally expressed only during fetal development (4-7). Many tumor-associated carbohydrate antigens possess the monosaccharide sialic acid, and indeed, the overexpression of sialic acid has been correlated with the malignant and metastatic phenotypes in epithelial-derived cancers from gastric, colon, pancreatic, liver, lung,

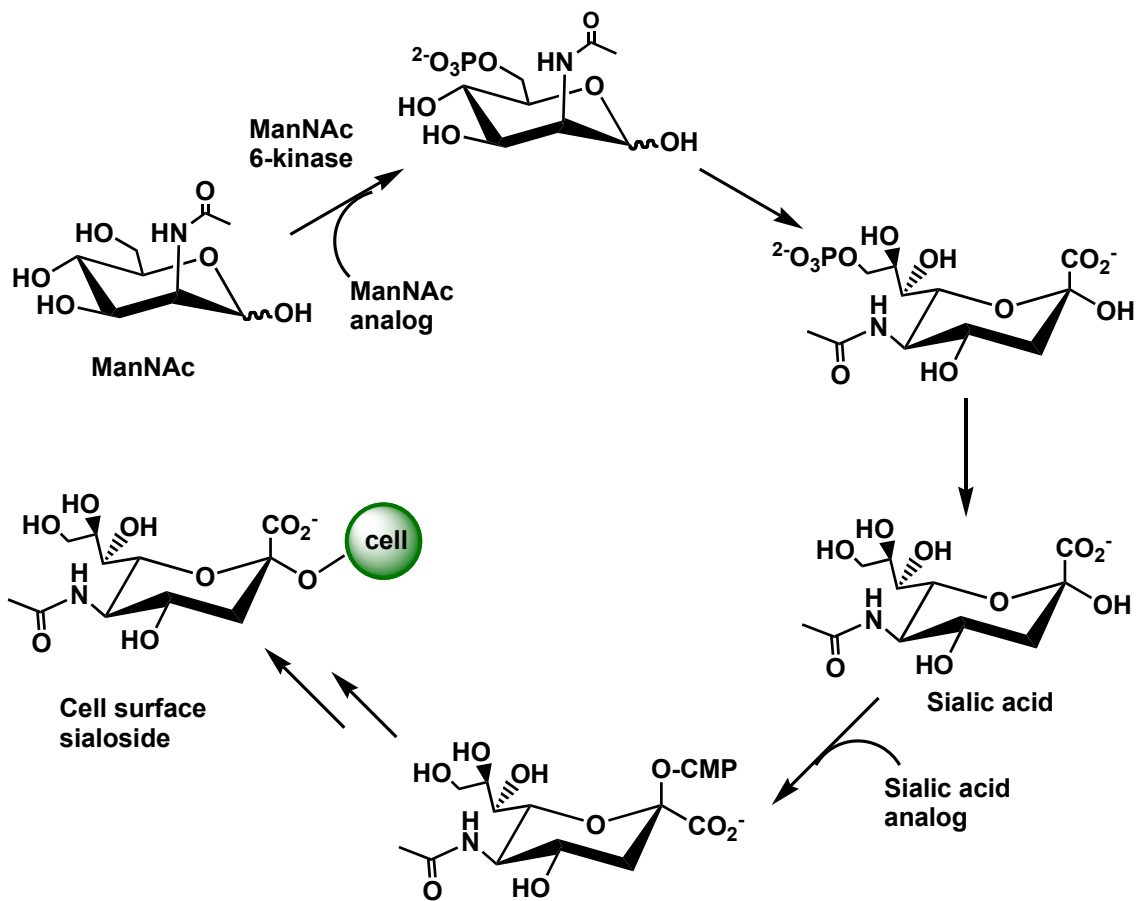
prostate, and breast tissue, and in several types of leukemia (8-12). The collective display of multiple sialylated antigens on a tumor cell can result in the presentation of up to 10^9 sialic acid residues per cell (13), and can account for the broad distribution of the high sialic acid phenotype across many different types of cancers. Therapeutic strategies that target cells on the basis of sialic acid expression may therefore find broad utility in cancer therapy.

Here we report a metabolic oligosaccharide engineering approach towards selective delivery of boron-containing reagents to tumor cells that exploits the intrinsic differences in sialic acid expression. This approach capitalizes on the substrate promiscuity of the enzymes in the sialoside biosynthetic pathway, which may allow the delivery of unnatural sialic acids that bear boron agents into cellular glycans.

Results and discussions

Design and synthesis of carboranyl sialic acid

The unnatural substrate tolerance in the biosynthesis of sialoadies has been demonstrated by the cellular metabolism of *N*-acetylmannosamine (ManNAc) analogs (14, 15) and sialic acid analogs (16-18) into cell surface sialoglycoconjugates (Scheme 7.1). Various unnatural functional groups such as bioorthogonal chemical reporters have been introduced into cellular glycans using this technique (19). On the other hand, therapeutic applications of metabolic engineering have not been well explored.

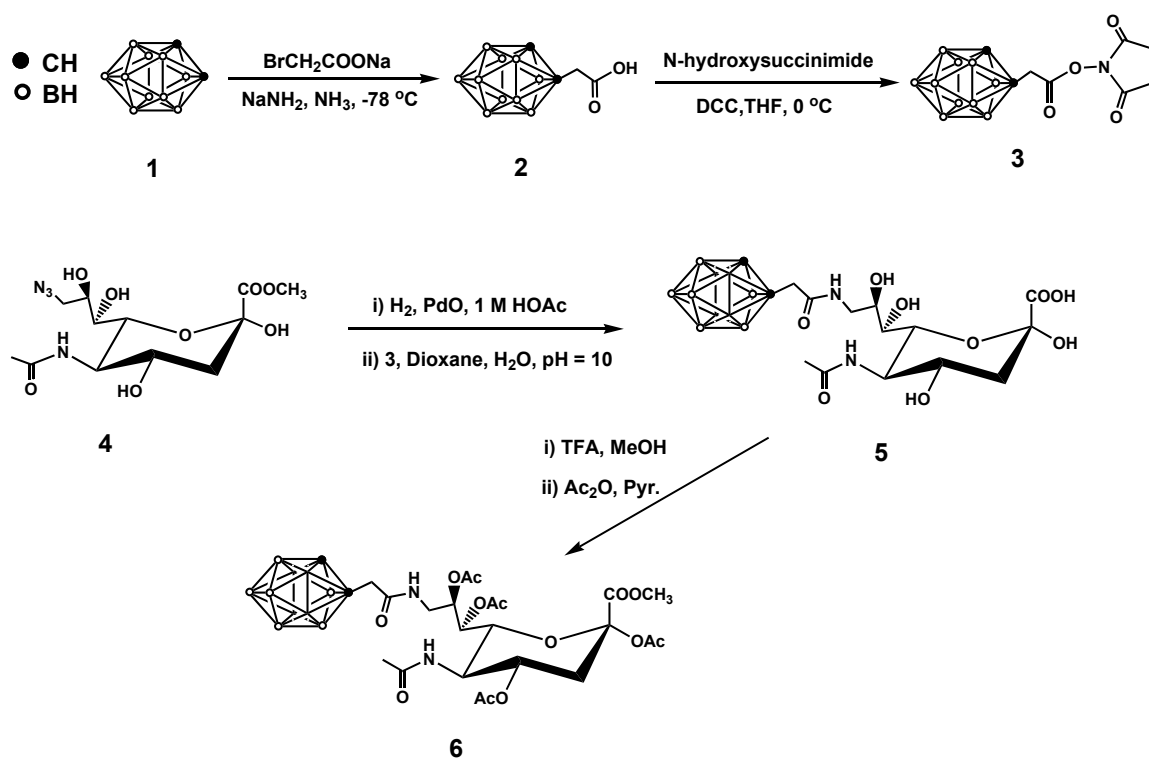


Scheme 7.1. Unnatural ManNAc and sialic acid can be metabolized by cell into cell surface sialosides. The scheme shows the conversion of ManNAc to cell surface sialic acid and points of interception with unnatural substrates.

It was shown that a rate-determine step in the de novo biosynthesis of unnatural sialic acids was the phosphorylation of ManNAc at the 6-OH by ManNAc 6-kinase (20). Accordingly, sialic acid analogs have been shown to be more efficient delivery vehicles and are able to deliver more bulky groups as well (16, 17), probably because of bypassing the bottleneck enzyme. For example, increasing the length or steric bulk of the N-acyl side chain of unnatural ManNAc decreased cell surface expression of the corresponding sialic acids (20), while sialic acid analogs permitted the delivery of bulky groups such as aryl azide (17, 18). Therefore, we selected sialic acid analogs as the delivery vehicle for *o*-carborane (B₁₀H₁₂C₂) (compound **1**, Scheme 7.2), a commonly used BNCT agent moiety (21).

One of the criteria of a successful BNCT treatment is the relatively high amount of boron concentration required in tumor sites (about 10⁹ boron atoms per cell) (1). The ideal BNCT compounds would carry multiple boron atoms on each molecule. *o*-Carborane contains 10 boron atoms and is easily incorporated into organic structures (21). In addition, the size of carborane, which is approximately 50% larger than the space occupied by the three-dimensional sweep of a phenyl group (22), should be compatible with aryl azide. We reasoned that the carboran-containing sialic acid analog should be metabolized into cellular glycoconjugates, given the successful incorporation of sialic acid analogs containing a C-9 aryl azide (18). Carborane was installed at the C-9 position of *N*-acetylneuraminic acid (NeuAc) to give 9-carboranyl-NeuAc (compound **5**; Scheme 7.2). To further improve the metabolic efficiency, compound **5** was then

protected as its methyl ester, followed by protecting the hydroxy groups to provide peracetylated sialic acid analog **6**. We hypothesized that carborane expression levels on cells treated with compound **5** or **6** would mirror intrinsic sialic acid expression levels, enabling selective delivery of boron atoms to tumor cells with higher sialic acid levels.



Scheme 7.2. Synthesis of 9-carboranyl-NeuAc and its protected derivative.

Evaluation of carboranyl sialic acid analogs in cells

To determine whether cells could use 9-carboranyl-NeuAc in place of NeuAc, we performed a competition assay with peracetylated *N*-azidoacetylmannosamine (Ac₄ManNAz). It has been shown that Ac₄ManNAz is metabolized by cells through sialic acid biosynthetic pathway to form *N*-azidoacetylneuraminic acid (SiaNAz), which is then appended to glycoconjugates that are ultimately expressed on the cell surface (15). Azides on cell surface can be further elaborated in a chemoselective fashion by Staudinger ligation, thereby introducing detectable probes onto the cell. For example, cell surface azides can be labeled with a phosphine reagent conjugated to the FLAG peptide (phosphine-FLAG) (23). Treatment of cells with a FITC-labeled anti-FLAG antibody enables the analysis of cell surface azide expression by flow cytometry. If carboranyl sialic acid analogs enter sialic acid biosynthesis pathway, they would compete for the enzymes in the pathway with Ac₄ManNAz, therefore decreasing cell surface fluorescence.

Ac₄ManNAz was incubated with Jurkat cells in the presence of increasing concentration of compound **5**. The cells were then subjected to the Staudinger ligation and treated with FITC anti-FLAG prior flow cytometric analysis. As expected, compound **5** suppressed cell surface azide expression in a dose dependent manner (Fig. 7.1). Compound **5** addition (20 mM) decreased cell surface fluorescence by 70%, indicating that carboranyl sialic acid was incorporated into cell surface glycoconjugates. By comparison, the addition of natural sialic acid had a similar inhibition effect (80%

decrease by 20 mM), further supporting the hypothesis that the same cellular enzymes acted on SiaNAz, compound **5**, and sialic acid.

To improve the metabolic efficiency of our carborane-containing analog, thus decreasing the dose requirement for BNCT treatment application, we investigated the protected derivative. It has been shown previously that protection of polar functional groups on sugars increased their cellular uptake by permitting passive diffusion through membranes (17, 24-26). For example, the fully protected azido sialic acids could be utilized by cells up to 20-fold more efficiently than their unprotected counterparts (17). Therefore, compound **6**, the fully protected derivative of **5**, was tested for incorporation into cell surface glycoconjugates via a similar competition assay. As shown in Figure 7.2, compound **6** achieved 70% inhibition at 100 μ M, which was about 20-fold more efficient than compound **5**.

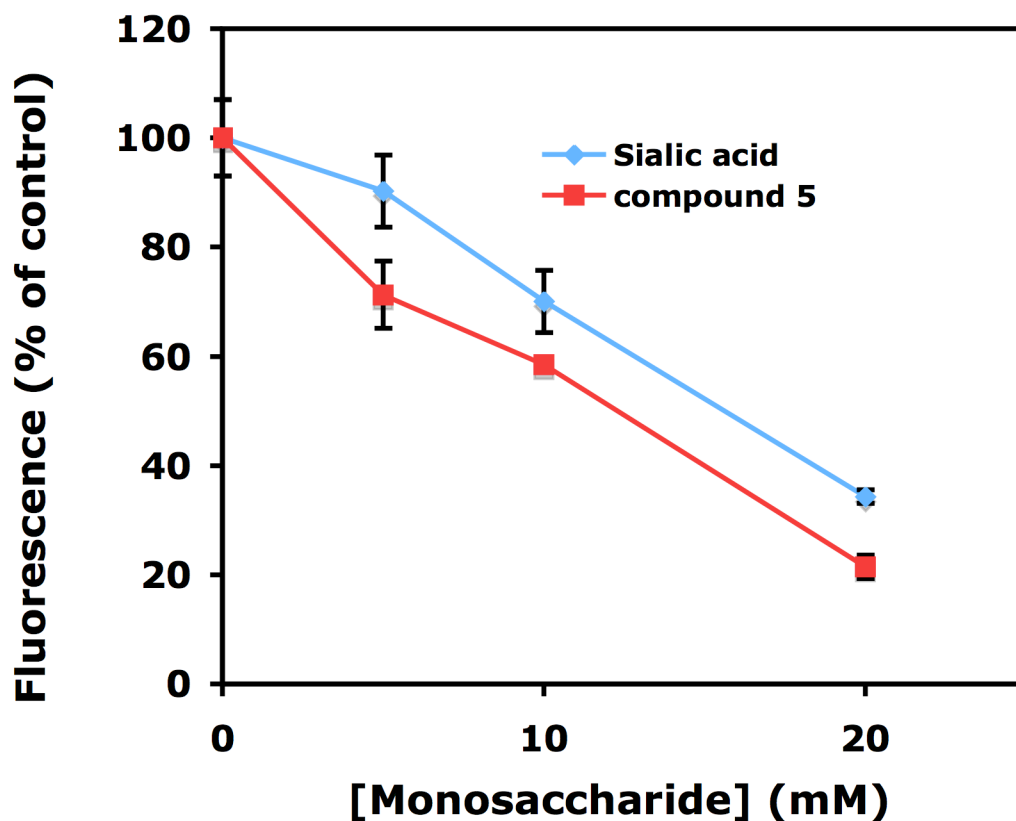


Figure 7.1. Metabolism of Ac₄ManNAz was inhibited with compound 5 and natural sialic acid. Jurkat cells were incubated with Ac₄ManNAz (20 μM) and various amounts of compound 5 and sialic acid for three days. Cells were then treated with phosphine-FLAG (0.25 mM) for 1 h at rt. followed by FITC anti-FLAG and analyzed by flow cytometry. The fluorescence signal is reported as a percent of the control (the fluorescence signal from cells incubated with 20 μM Ac₄ManNAz alone). Error bars represent the standard deviation for triplicate experiments.

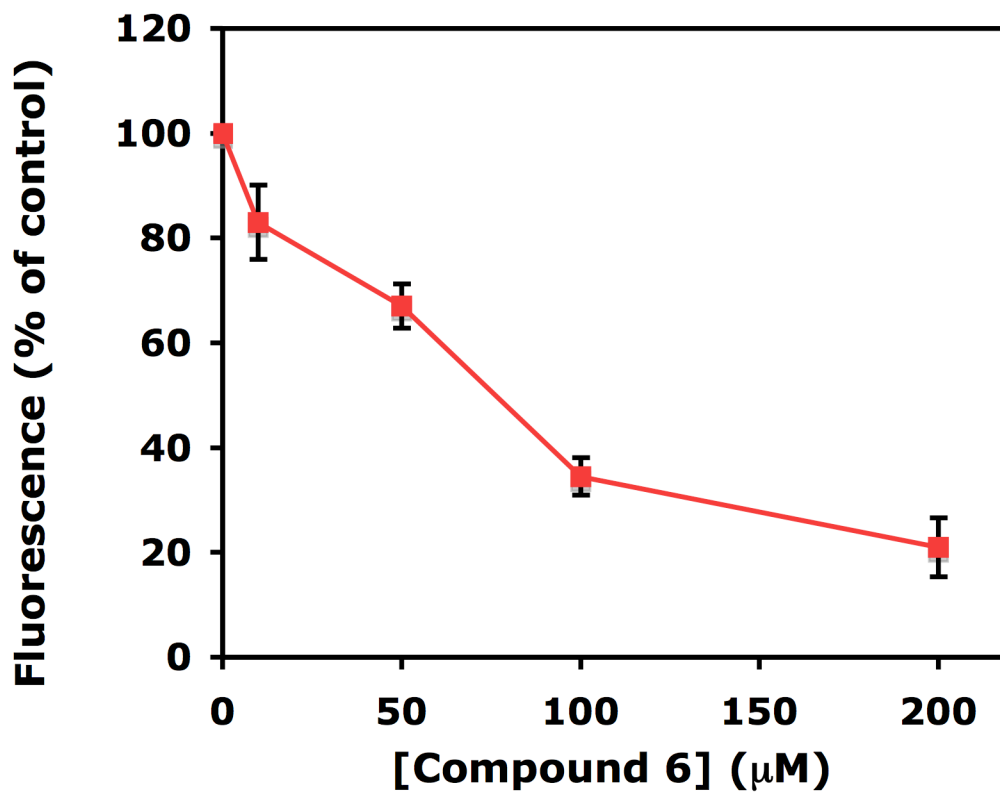


Figure 7.2. Metabolism of Ac₄ManNAz was inhibited with compound 6 with 20 fold higher efficiency than its unprotected counterpart. Error bars represent the standard deviation for triplicate experiments.

Conclusions

In summary, we have synthesized the carborane-containing sialic acid analogs and demonstrated their incorporation into cellular glycoconjugates. The results show that sialic acid derivatives are promising vehicles for the delivery of boron agents. Further evaluations of this strategy towards BNCT treatment are needed and are currently undergoing in our laboratory.

Materials and methods

Synthesis of new compounds

All chemical reagents were of analytical grade, obtained from commercial suppliers and used without further purification. Flash chromatography was performed using Merck 60Å 230-400 mesh silica gel. Analytical TLC was performed on Analtech Uniplat silica gel plates and visualized by staining with ceric ammonium molybdate or by absorbance of UV light at 254nm. ¹H NMR, and ¹³C NMR spectra were obtained with Bruker AMX-400 or Bruker DRX-500 MHz spectrometers. ¹H and ¹³C chemical shifts (δ) are reported in parts per million (ppm) referenced to TMS (0 ppm) and were measured relative to the residual solvent peak. Mass spectra were obtained at the UC Berkeley Mass Spectrometry Laboratory.

2-Carboranylethanoic acid *N*-hydroxysuccinimide ester (3). 2-Carboranylethanoic acid (27) (**2**) (650 mg, 3.2 mmol), *N*-hydroxysuccinimide (403 mg, 3.5 mmol), and dicyclohexylcarbodiimide (722 mg, 3.5 mmol) were dissolved in

anhydrous THF (15 mL) at 4 °C. The reaction was warmed up to rt and stirred overnight. The resulting reaction mixture was filtered to remove the precipitates. The solution was then concentrated and purified by silica gel chromatography eluting with MeOH:CH₂Cl₂ (1:20) to give the product (700 mg, 73%). R_f = 0.65 (MeOH:CH₂Cl₂ = 1:20). ¹H NMR (CDCl₃, 500 MHz) δ 4.37 (s, 1 H), 3.54 (s, 2H), 2.85 (s, 4 H), 2.78-1.58 (m, 10 H). ¹³C NMR (CDCl₃, 125 MHz) δ 168.5, 162.6, 66.2, 59.5, 39.1, 25.7. ESI-MS calcd for C₈H₁₆B₁₀NO₄ [M-H]⁻: *m/z* 298.3; found 298.3.

5-Acetamido-9-(2-carboranlethanolyl)-3,5,9-trideoxy-D-glyceo-D-galacto-2-nonulosonic acid (5). To a solution of 9-azido sialic acid (**4**) (83 mg, 0.25 mmol) in water (2.75 mL) was added PdO (8.35 mg) and stirred under H₂ atmosphere with pH maintained at about 1 by addition of 1M HCl. After 12 h, the reaction was filtered to remove PdO solid. To the filtrate was added dioxane (4.2 mL), and **3** (100 mg, 0.33 mmol), and the pH was adjusted to about 9.0 by addition of 1M NaOH. The mixture was stirred for 2 d. The solvent was evaporated and the residue was purified by silica gel column chromatography eluted with MeOH:CH₂Cl₂ (1:20 to 1:3) to give the product (66 mg, 64%). R_f = 0.40 (MeOH:CH₂Cl₂ = 1:4). ESI-MS calcd for C₁₅H₃₂B₁₀N₂O₉ [M-H]⁻: *m/z* 492.4; found 492.4.

2,4,7,8-Tetra-O-acetyl-5-Acetamido-9-(2-carboranlethanolyl)-3,5,9-trideoxy-D-glyceo-D-galacto-2-nonulosonic acid-1-methyl ester (6). To a solution of **5** (50 mg, 0.10 mmol) in anhydrous MeOH (2 mL) was added TFA (catalytic, 3 drops) and stirred under N₂ atmosphere at rt overnight. The solvent was then evaporated. To the resulting

residue was added pyridine (2 mL), and acetic anhydride (1 mL). The mixture was stirred at rt overnight. The solvent was evaporated and the residue was purified by reversed-phase HPLC eluted with a gradient of CH₃CN (10%-75%) and H₂O to give the product (22 mg, 32%). ESI-MS calcd for C₂₄H₄₃B₁₀N₂O₁₃ [M+H]⁺: *m/z* 676.4; found 676.4.

Cell culture conditions

Jurkat cells were grown in RPMI-1640 media supplemented with penicillin (100 unit/mL), streptomycin (0.1 mg/mL), and 10% FCS and maintained in a 5% CO₂, water-saturated atmosphere at 37 °C.

Competition assay

Cells were seeded at a density of about 1.5 x 10⁵ cells/mL and incubated for 3 d with the compounds indicated. After growth with the presence of the appropriate monosaccharides, cells were distributed into a 96-well tissue culture plate. The cells were pelleted (3500 rpm, 3min) and washed twice with 200 µL of PBS containing 1% FCS (labeling buffer). The cells were then treated with phosphine-FLAG (0.25 mM in labeling buffer) for 1h at rt. After incubation, the cells were pelleted, washed three times with cold labeling buffer and re-suspended in the labeling buffer containing FITC anti-FLAG (1:900 dilution). After incubation for 30 min at 4 °C, the cells were pelleted, washed twice with cold labeling buffer, and analyzed by flow cytometry.

References

1. M. F. Hawthorne, New horizons for therapy based on the boron neutron capture reaction. *Mol. Med. Today* **4**, 174-181 (1998).
2. R. F. Barth *et al.*, Boron neutron capture therapy of brain tumors: an emerging therapeutic modality. *Neurosurgery* **44**, 433-450; discussion 450-431 (1999).
3. W. Chen, S. C. Mehta, D. R. Lu, Selective boron drug delivery to brain tumors for boron neutron capture therapy. *Adv. Drug Deliv. Rev.* **26**, 231-247 (1997).
4. J. M. Yang *et al.*, Alterations of O-Glycan Biosynthesis in Human Colon-Cancer Tissues. *Glycobiology* **4**, 873-884 (1994).
5. T. Jorgensen *et al.*, Up-Regulation of the Oligosaccharide Sialyl Lewis(X) - a New Prognostic Parameter in Metastatic Prostate-Cancer. *Cancer Res.* **55**, 1817-1819 (1995).
6. M. Fukuda, Possible roles of tumor-associated carbohydrate antigens. *Cancer Res.* **56**, 2237-2244 (1996).
7. S. Hakomori, Y. M. Zhang, Glycosphingolipid antigens and cancer therapy. *Chem. Biol.* **4**, 97-104 (1997).
8. G. Yogeewaran, B. S. Stein, H. Sebastian, Altered Cell-Surface Organization of Gangliosides and Sialyl-Glycoproteins of Mouse Metastatic Melanoma Variant Lines Selected In vivo for Enhanced Lung Implantation. *Cancer Res.* **38**, 1336-1344 (1978).
9. J. Roth *et al.*, Reexpression of Poly(Sialic Acid) Units of the Neural Cell-Adhesion Molecule in Wilms Tumor. *Proc. Natl. Acad. Sci. USA* **85**, 2999-3003 (1988).
10. S. Sell, Cancer-Associated Carbohydrates Identified by Monoclonal-Antibodies. *Human Pathol.* **21**, 1003-1019 (1990).
11. E. P. Scheidegger, P. M. Lackie, J. Papay, J. Roth, In-Vitro and in-Vivo Growth of Clonal Sublines of Human Small-Cell Lung-Carcinoma Is Modulated by Polysialic Acid of the Neural Cell-Adhesion Molecule. *Lab. Invest.* **70**, 95-106 (1994).

12. R. Takano, E. Muchmore, J. W. Dennis, Sialylation and Malignant Potential in Tumor-Cell Glycosylation Mutants. *Glycobiology* **4**, 665-674 (1994).
13. G. W. Jourdian, L. Dean, S. Roseman, Sialic Acids .11. Periodate-Resorcinol Method for Quantitative Estimation of Free Sialic Acids and Their Glycosides. *J. Biol. Chem.* **246**, 430-& (1971).
14. L. K. Mahal, K. J. Yarema, C. R. Bertozzi, Engineering chemical reactivity on cell surfaces through oligosaccharide biosynthesis. *Science* **276**, 1125-1128 (1997).
15. E. Saxon, C. R. Bertozzi, Cell surface engineering by a modified Staudinger reaction. *Science* **287**, 2007-2010 (2000).
16. C. Oetke *et al.*, Versatile biosynthetic engineering of sialic acid in living cells using synthetic sialic acid analogues. *J. Biol. Chem.* **277**, 6688-6695 (2002).
17. S. J. Luchansky, S. Goon, C. R. Bertozzi, Expanding the diversity of unnatural cell-surface sialic acids. *Chembiochem* **5**, 371-374 (2004).
18. S. Han, B. E. Collins, P. Bengtson, J. C. Paulson, Homomultimeric complexes of CD22 in B cells revealed by protein-glycan cross-linking. *Nature Chem. Biol.* **1**, 93-97 (2005).
19. J. A. Prescher, C. R. Bertozzi, Chemistry in living systems. *Nature Chem. Biol.* **1**, 13-21 (2005).
20. C. L. Jacobs *et al.*, Substrate specificity of the sialic acid biosynthetic pathway. *Biochemistry* **40**, 12864-12874 (2001).
21. A. H. Soloway *et al.*, The chemistry of neutron capture therapy. *Chem. Rev.* **98**, 1515-1562 (1998).
22. A. J. Lunato *et al.*, Synthesis of 5-(carboranylalkylmercapto)-2'-deoxyuridines and 3-(carboranylalkyl)thymidines and their evaluation as substrates for human thymidine kinases 1 and 2. *J. Med. Chem.* **42**, 3378-3389 (1999).
23. E. Saxon *et al.*, Investigating cellular metabolism of synthetic azidosugars with the Staudinger ligation. *J. Am. Chem. Soc.* **124**, 14893-14902 (2002).

24. C. L. Jacobs *et al.*, Metabolic labeling of glycoproteins with chemical tags through unnatural sialic acid biosynthesis. *Meth. Enzymol.* **327**, 260-275 (2000).
25. S. J. Luchansky *et al.*, Constructing azide-labeled cell surfaces using polysaccharide biosynthetic pathways. *Meth. Enzymol.* **362**, 249-272 (2003).
26. A. K. Sarkar, T. A. Fritz, W. H. Taylor, J. D. Esko, Disaccharide Uptake and Priming in Animal-Cells - Inhibition of Sialyl-Lewis-X by Acetylated Gal-Beta-1-]4glcnac-Beta-O-Naphthalenemethanol. *Proc. Natl. Acad. Sci. USA* **92**, 3323-3327 (1995).
27. R. C. Haushalter, W. M. Butler, R. W. Rudolph, The Preparation and Characterization of Several Meso-Tetracarboranylporphyrins. *J. Am. Chem. Soc.* **103**, 2620-2627 (1981).